KTH ROYAL INSTITUTE
OF TECHNOLOGY

Doctoral Thesis in Electrical Engineering

High-speed jets and related phenomena at Earth's bow shock and magnetosheath

SAVVAS RAPTIS

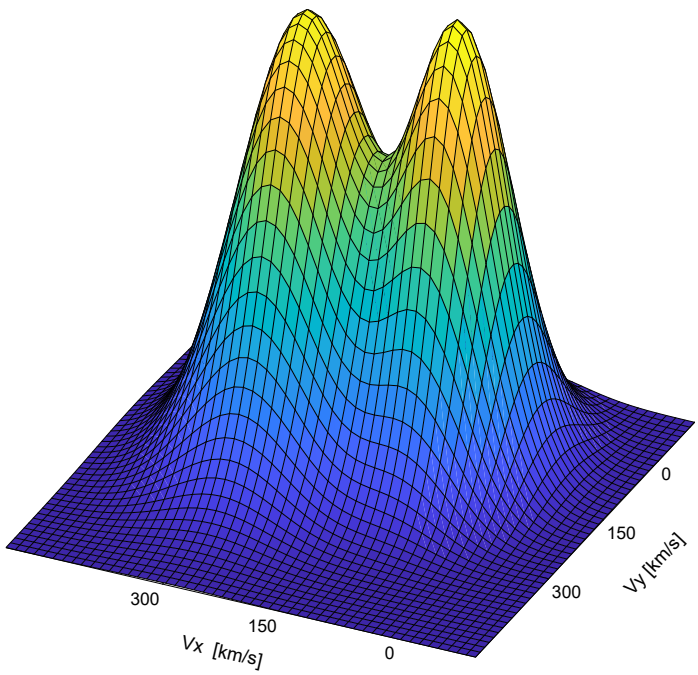

Stockholm, Sweden 2022

High-speed jets and related phenomena at Earth's bow shock and magnetosheath

SAVVAS RAPTIS

Academic Dissertation which, with due permission of the KTH Royal Institute of Technology, is submitted for public defence for the Degree of Doctor of Philosophy on Wednesday the 23rd November 2022, at 1:00 p.m. in F3, Lindstedtsvägen 26, Stockholm

Doctoral Thesis in Electrical Engineering
KTH Royal Institute of Technology
Stockholm, Sweden 2022

ISBN 978-91-8040-390-0
TRITA-EECS-AVL-2022:67

Printed by: Universitetsservice US-AB, Sweden 2022

Abstract

Magnetosheath high-speed jets are transient and localized dynamic pressure enhancements downstream of Earth's bow shock. Their formation has been associated with several mechanisms, including solar transient events and the dynamical evolution of the bow shock. After their formation, jets interact with the background magnetosheath population, exciting various waves and accelerating particles. When they reach the magnetosphere, they can penetrate the magnetopause, drive surface waves, and cause magnetopause reconnection. Their effects to the inner geospace environment can be seen through substorm activity and ground magnetometer measurements. In this thesis, a series of papers on the formation, evolution and statistical properties of jets is presented. Most of the work is done using NASA's Magnetosphere Multiscale (MMS) mission, while other missions like THEMIS and upstream solar wind monitors (e.g., ACE and Wind) are also used. For our analysis, we also make complementary use of neural networks and computer simulations. Our investigation initially showed the importance of classifying jets based on the shock orientation and interplanetary magnetic field (IMF), resulting in an open-access database of magnetosheath jets using MMS. This dataset was then used to derive statistical properties for each class of magnetosheath jets (Paper I). The jets were also classified using neural networks (Paper II), while a comparison between their statistical properties and computer simulated jets was performed (Paper III). Another aspect we investigated through multi-point measurements is the excitation of waves due to the interaction of jets with the magnetosheath (Paper IV). We then focused on the formation and evolution of jets close to the Earth's bow shock. We showed direct *in-situ* evidence that shock reformation and the evolution of upstream waves can generate downstream high-speed jets (Paper V). By evaluating the properties of jets on a kinetic level, we demonstrated that jets exhibit complex velocity distribution functions (VDFs) throughout their lifetime. Deriving partial plasma moments to isolate the jet from the background population, we revealed the limitations of studying these phenomena from a single-fluid perspective and how the derived partial plasma moments are related to the upstream solar wind and its foreshock structures (Paper VI).

Keywords: magnetosheath, solar wind, bow shock, plasma, collisionless shocks

Sammanfattning

Plasmajetar i magnetoskiktet är transienta och lokaliserade förhöjningar av det dynamiska trycket nedströms om jordens bogchock. Flera olika generationsmekanismer har föreslagits, t ex transienta strukturer i solvinden eller dynamisk omformning av bogchocken. Efter att de har genererats vid bogchocken växelverkar de med bakgrundsplasmat i magnetoskiktet, där de exciterar plasmavågor och accelererar partiklar. När de når magnetopausen kan de korsa den, driva ytvågor, eller initiera magnetisk omkoppling. Plasmajetars effekt på rymdmiljön nära Jorden manifesterar sig genom substormar och markbaserade mätningar av jordens magnetfält. Denna avhandling innehåller att antal artiklar om genereringen, utvecklingen och de statistiska egenskaperna hos plasmajetar. Huvuddelen av arbetet är baserad på mätningar från NASAs MMS-satelliter, tillsammans med kompletterande data från andra satellitmissioner, som THEMIS och solavindsmonitorer (t ex ACE och Wind). För dataanalysen använder vi också neurala nätverk och plasmasimuleringar. Våra första resultat visade på vikten av att klassificera jetar baserat på relationen mellan bogchockens orientering och riktningen på det interplanetära magnetfältet. Denna klassificering resulterade i en offentligt tillgänglig databas, innehållande MMS-observationer av plasmajetar. Detta dataset användes för att bestämma jetarnas statistiska egenskaper för de olika klasserna (Artikel I), vilket följdes upp med en klassificering baserade på neurala nätverk (Artikel II), vilket jämfördes med plasmasimuleringar (Artikel III). En ytterligare egenskap hos plasmajetar, excitation av plasmavågor, undersöktes med flerpunktsmätningar (Artikel IV). Därefter fokuserade vi på genereringen och evolutionen av jetar nära jordens bogchock. Vi visar att direkta *in situ*-mätningar tyder på att dynamisk omformning av bogchocken och vågor uppströms om den kan generera plasmajetar i magnetoskiktet (Artikel V). Genom att studera jetars plasmakinetiska egenskaper visar vi också att deras distributionsfunktioner uppvisat ett komplext beteende under jetarnas livstid. Beräkningar av partiella plasmamoment för att isolera jetarna från bakgrundsplasmat visar på begränsningarna i att betrakta dessa fenomen som en enkel fluid, och hur momenten är relaterade till solvinden uppströms om bogchocken (Artikel VI).

Acknowledgements

My biggest gratitude goes to Tomas Karlsson for being an inspiring supervisor and mentor. Apart from vastly influencing my scientific views and research output, I feel that by experiencing your approach to tackling problems and setbacks, I became a more complete and mature person, and for that, I will always be grateful. During times of uncertainty, your ability to be kind and firm at the same time has been at the very least admirable. You are one of the very few people I genuinely look up to, and having a supervisor like you was truly a privilege.

A great appreciation also goes to the rest of SPP staff. A special thanks to Andris Vaivads for being extremely helpful with his insightful comments, and for visibly demonstrating his confusion when I spoke nonsense. Per Arne Lindqvist also helped me crucially, with the use of MMS data, and by being a genuinely great person to interact with. Furthermore, a big thanks to Anita Kullen for her feedback and for providing truly pleasant interactions, especially by sharing her life stories during conference lunch/dinners. Also, a big thanks to Panagiotis Tolias for his extended and very helpful review of my work. I also acknowledge Nickolay Ivchenko, and Svetlana Ratynskaia for their comments and unusual yet refreshing directness.

Overall, I am glad that during these years I had the chance to work with so many people and groups around the world. Ferdinand Plaschke, Sigiava-Aminalragia Giamini, Mina Palmroth, Jonas Suni, Andreas Johlander, Primoz Kajdic, and Christos Katsavrias are just a few of the people I have worked with and enjoyed it to the fullest. Furthermore, the ISSI team I have been part of the last few years, led by Heli Hietala and Ferdinand, *"Foreshocks Across The Heliosphere: System Specific Or Universal Physical Processes?"* has been an enormously helpful environment. Working alone can be efficient, but it is not fun. So, a big thanks to all of you for the nice time we had discussing interesting topics together. I hope that with many of you, this was just the beginning of a long road we will travel together. At this point, I also want to acknowledge my "past supervisors" from my undergraduate years in Greece, Ingmar Sandberg, and Ioannis Daglis for being the ones introducing me to space physics research, and for still sharing useful advices, up to this day.

A huge thanks to all the people in IRF-Uppsala that greatly assisted me with their support, and a special thanks to Yuri Khotyaintsev and Daniel Graham for helping me countless times. Their willingness to provide feedback and code support whenever needed was vital for the completion of my work, and I feel deeply grateful about it. Also thanks to all the PhD/Postdocs of IRFU (to name a few, Ahmad, Elias, Konrad, Ida, Louis, + more) that we shared part of our academic life in Sweden together through courses, meetings, and great discussions! Also, a big thanks to the "magnetosheath jet team" (Adrian, Eva, Florian, Jonas, Laura, Luis, and Nikol) for forming this wonderful community together.

Moving on to the past and present SPP colleagues. Gabriel, thank you for being a great photographer, and an equally skillful expert at folding tents! Aljona, pratar du Svenska? Georgi, looking forward to visiting you in UK! Emil, we have to take that skipper license within the next decade. Federico, thanks for sharing strong (and correct) opinions on which pizza place is actually good, and whether owning fake plants should get criminalized. Ladislas, thanks for reminding me to get απόδειξη from the μαστίχα bottles I bring from Greece. Henriette, we still need to find some exotic birds on our next conference/meeting. Also, a big thanks to Konstantinos for being my consistent (when not held hostage) lunch buddy. Are we still counting the dates? Lorenz, thanks for making me temporarily a bowling-god (was it 5 strikes in a row?). Sabrina, I have to acknowledge your impressive continuous sneeze from the office next door. A special thanks to Martin for being all these years my office mate, a precise calculator in time of need, a plant protector, and a ping-pong nemesis. The last part was recently handled over to Sushen that managed to include ping-pong in his numerous weekly activities. Judit, thanks for being such an organized person that I was able to tell when the time was ∼08.00 and ∼16.00 without looking at the clock (you've been staying more lately, so I added the tildes).

I would also like to acknowledge my friends from my home country, my friends Eleftheria, Giannis, Maria, Marios, Nikos, Telis (+many more), my undergraduate pals Dimos, Kallia, and Konstantinos and my friend Petros. I also need to mention these from my life in Belgium, my friends Alex, Manos, Lydia, and Pedro and my KU Leuven buddies, Adam and Florian.

Finally, my deepest appreciation goes to my family back in Greece. My parents Eleftheria and Vasilis, and my brother Omiros. While thousands of kilometers away, you have been, and you continue to be, an enormous support throughout my life. Last, to Anastasia, all these years you have been the brightest star of my night sky. Thank you for keeping me grounded while motivating me to keep aiming higher.

Contents

List of papers

The thesis is based on the papers listed below. In the text, they are referenced by their listed number.

I *Classifying Magnetosheath Jets Using MMS: Statistical Properties*
S. Raptis, T. Karlsson, F. Plaschke, A. Kullen, & P.-A. Lindqvist
Journal of Geophysical Research: Space Physics 125.11 (2020): e2019JA027754.

II *Classification of Magnetosheath Jets Using Neural Networks and High Resolution OMNI (HRO) Data*
S. Raptis, S. Aminalragia-Giamini, T. Karlsson, & M. Lindberg
Frontiers in Astronomy and Space Sciences 7 (2020): 24

III *Magnetosheath Jet Evolution as a Function of Lifetime: Global Hybrid-Vlasov Simulations Compared to MMS Observations*
M. Palmroth, **S. Raptis**, J. Suni, T. Karlsson, L. Turc, A. Johlander U. Ganse, Y. Pfau-Kempf, X. Bianco-Cano, M. Akhavan-Tafti, M. Battarbee, M. Dubart, M. Grandin, V. Tarvus, & A. Osmane
Annales Geophysicae Vol. 39. No. 2. (2021)

IV *On the Generation of Pi2 Pulsations Due to Plasma Flow Patterns Around Magnetosheath Jets*
C. Katsavrias, **S. Raptis**, I. A. Daglis, T. Karlsson, M. Georgiou, & G. Balasis
Geophysical Research Letters 48.15 (2021): e2021GL093611

V *Downstream High-speed Plasma Jet Generation as a Direct Consequence of Shock Reformation*
S. Raptis, T. Karlsson, A. Vaivads, C. Pollock, F. Plaschke, A. Johlander, H. Trollvik, & P.-A. Lindqvist
Nature communications 13.1 (2022): 1-10

VI *On Magnetosheath Jet Kinetic Structure and Plasma Properties*
S. Raptis, T. Karlsson, A. Vaivads, M. Lindberg, A. Johlander, & H. Trollvik
Geophysical Research Letters – Accepted

Papers not included in the thesis

Other contributions by the author not included in the thesis.

Current Sheet Statistics in the Magnetosheath
E. Yordanova, Z. Vörös, **S. Raptis**, & T. Karlsson
Frontiers in Astronomy and Space Sciences 7 (2020): 2

Helium in the Earth's Foreshock: a Global Vlasiator Survey
M. Battarbee, X. Blanco-Cano, L. Turc, P. Kajdič, A. Johlander, V. Tarvus, S. Fuselier, K. Trattner, M. Alho, T. Brito, U. Gense, Y. Pfau-Kempf, M. Akhavan-Tafti, T. Karlsson, **S. Raptis**,M. Dubart, M. Grandin, J. Suni, & M. Palmroth
Annales Geophysicae Vol. 38. No. 5 (2020)

Causes of Jets in the Quasi-perpendicular Magnetosheath
P. Kajdič, **S. Raptis**, X. Blanco-Cano, & T. Karlsson
Geophysical Research Letters 48.13 (2021): e2021GL093173

Classifying the Magnetosheath Behind the Quasi-parallel and Quasi-perpendicular Bow Shock by Local Measurements
T. Karlsson, **S. Raptis**, H. Trollvik, & H. Nilsson
Journal of Geophysical Research: Space Physics 126.9 (2021): e2021JA029269.

Solar Energetic Particle Event Occurrence Prediction Using Solar Flare Soft X-ray Measurements with Machine Learning
S. Aminalragia-Giamini, **S. Raptis**, A. Anastasiadis, A. Tsigkanos, I. Sandberg, A. Papaioannou, C. Papadimitriou, P. Jiggens, A. Aran, & I.A. Daglis
Journal of Space Weather and Space Climate 11 (2021): 59.

Electron Kinetic Entropy Across Quasi-perpendicular Shocks
M. Lindberg, A. Vaivads, **S. Raptis**, P.-A. Lindqvist, B. L. Giles, & D. J. Gershman
Entropy 24.6 (2022): 745.

Dynamics of Earth's Bow Shock Under Near-radial Interplanetary Magnetic Field Conditions
C. Pollock, L-J. Chen, S. Schwartz, S. Wang, L. A. Avanov, J. L. Burch, D. J. Gershman, B. L. Giles, **S. Raptis**, & C. T. Russel
Physics of Plasmas – Accepted

Solar Wind Magnetic Holes Can Cross the Bow Shock and Enter the Magnetosheath
T. Karlsson, H. Trollvik, **S. Raptis**, H. Nillson, & H. Madanian
Annales Geophysicae - Under Review

Acronyms

List of commonly used acronyms:

AI	Artificial Intelligence
ANN	Artificial Neural Network
ARTEMIS	Acceleration, Reconnection, Turbulence and Electrodynamics of the Moon's Interaction with the Sun
BS	Bow Shock
CNN	Convolutional Neural Network
EDP	Electric Double Probe
FAC	Field-Alligned Coordinates
FGM	Fluxgate Magnetometer
FPI	Fast Plasma Investigation
GSE	Geocentric Solar Ecliptic
HFA	Hot Flow Anomaly
HSS	High-Speed Stream
IMG	Interplanetary Magnetic Field
MH	Magnetic Holes
MHD	Magnetohydrodynamics
ML	Machine Learning
MMS	Magnetosphere Multiscale
MP	Magnetopause
MSE	Mean Squared Error
MSH	Magnetosheath
MSP	Magnetosphere
NASA	National Aeronautics and Space Administration
SHFA	Spontaneous Hot Flow Anomaly
SITL	Scientist In The Loop
SLAMS	Short Large Amplitude Magnetic Structure
SIR	Stream Interaction region
SW	Solar Wind
THEMIS	Time History of Events and Macroscale Interactions during Substorms
VDF	Velocity Distribution Function
ULF	Ultra-Low Frequency
UTC	Coordinated Universal Time

List of figures

List of tables

Chapter 1

Introduction

The current consensus on the composition of the Universe shows that ordinary matter is just a tiny fraction (roughly $\sim 5\%$) of the whole cosmos [Abdullah et al., 2020]. The rest is filled with dark energy and dark matter. Understanding the origin and properties of these exotic components of the Universe is fascinating, but most of the information must be inferred indirectly via models or through theoretical research. Ordinary matter, on the other hand, has been studied for hundreds of years through direct local (*in-situ*) measurements. While most people are familiar with the typical states of gas, liquid and solid, the Universe is dominated by a more peculiar form, called *plasma*, which makes up around 99.9% of the observable matter.

Plasma is a state where matter is fully or at least partially ionized, primarily in the form of ions and electrons. The difference between an ionized gas and plasma, is that plasma exhibits *collective* behavior. This means in practice that each charged particle making up the plasma affect and is affected by the rest of the particles that are far away from it. In an ionized gas, the dynamics of the particles are governed by collisions. However, in plasma, it is the electromagnetic force that is in control. Since the particles are charged, they are affected by the electromagnetic fields. In turn, fields are generated and modified by the motion of particles, making the plasma a state of constant ongoing interaction between a plethora of particles and fields which results in collective behavior. Plasma can be found almost everywhere in the Universe (see Figure 1.1). The Sun, like most stars, is essentially a hot ball of plasma. The matter originating from stars forming the interstellar medium is also in plasma state. As we approach the Earth, the aurora and even lightning are typical examples of plasmas. Here at Earth, we do not usually find plasma naturally, but in laboratories plasma can be formed. From lasers to accelerators and from gas discharges to fusion reactors, plasma is regularly used to conduct research and make brand new technological applications. In this work, however, we

will focus on a specific environment where plasma can be found, the solar system. Specifically, we will be talking about space plasma. This term typically includes the plasmas found close to the Earth, other planetary environments, the Sun, and the region in between. Another term typically used to enclose all these environments is the term *Heliophysics*, which is the area of physics studying the Sun and its connection with the solar system.

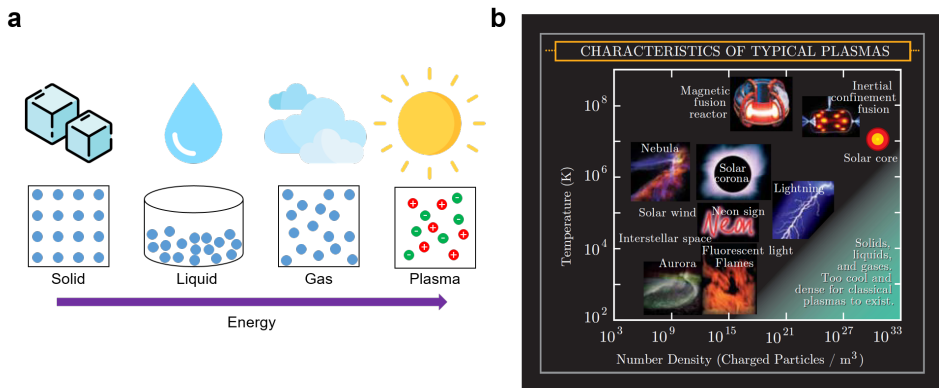

Figure 1.1: (**a**) The four states of matter, solid, liquid, gas, and plasma along with some typical examples. (**b**) The range of densities and temperatures of plasmas and of the rest of the ordinary matter. Notice that ordinary matter consists only of a very small corner on the temperature-density diagram. Image courtesy of Contemporary Physics Education Project (CPEP), `http://FusEdWeb.llnl.gov/CPEP`.

In the center of our solar system, the Sun apart from light, emits charged particles, due to the outward expansion of its corona, called the solar wind (SW). These particles travel through the solar system and interact with the rest of the celestial bodies. When the SW reaches Earth, it feels its magnetic field and forms a shock wave, which we call the bow shock. The region downstream of the shock is called the magnetosheath, the environment in which we observe the phenomenon that this thesis is all about, the magnetosheath jets.

Magnetosheath jets are high-speed plasma flows consisting of localized and transient dynamic pressure (velocity and/or density) enhancements downstream of Earth's bow shock. Their formation has been associated with several mechanisms, including solar transient phenomena and the dynamical evolution of the bow shock. After forming at the bow shock, jets can excite different waves and accelerate particles. As they reach Earth's magnetosphere, they can drive waves and modulate the geospace environment. Approaching the Earth, jets have been associated with substorms that can be the origin of the colorful phenomenon of the Aurora, directly observable from the Earth's surface via visible light.

Although in this thesis we attempt to provide a brief background on the overall magnetosheath jet research, our work is focused on tackling three questions:

1. How do jets form?
2. What are their typical properties, and how are these related to Earth's bow shock?
3. How do jets evolve, and how do they interact with the magnetosheath plasma?

The thesis consists of background information relevant to our work and of a summary of the six articles that are included. Apart from this introduction (Chapter 1), the work consists of 8 additional chapters. In Chapter 2, we introduce some basic space plasma physics concepts, focusing on different plasma descriptions and plasma quantities that we used in our work. In Chapter 3, we describe Earth's magnetospheric environment and focus more on the bow shock configuration and evolution. Chapter 4 describes the objectives and instrumentation of the spacecraft missions we used for *in-situ* measurements. In Chapter 5, we briefly introduce the notion of computer simulations in plasmas and describe the Vlasiator model that we used in parts of our work. Chapter 6 describes the different single and multi-spacecraft data analysis techniques that were used throughout our research. Chapter 7 is a short summary of the magnetosheath jet research done primarily before the start of this thesis (i.e., prior to 2019). Chapter 8 summarises the six papers. Finally, Chapter 9 consists of a discussion on the results and of an outlook regarding the future research of magnetosheath jets.

Chapter 2

Space plasma physics

In the sections below, we provide basic information regarding the space plasma environment while focusing on the different plasma descriptions and the quantities typically used in space plasma research. Most of the information shown here can be found in classic textbooks of general plasma (e.g., [Gurnett and Bhattacharjee, 2005, Chen, 2012, Fitzpatrick, 2014]) and space plasma (e.g., [Kivelson et al., 1995, Treumann and Baumjohann, 1997, Baumjohann and Treumann, 2012]) physics, where one can find substantially more details on the subject.

2.1 Plasma descriptions

The simplest way to describe a plasma is by investigating the motion of a single charged particle (typically an ion or electron) under the influence of electromagnetic fields. If we assume a charged (q) particle moving with a velocity ($\mathbf{v}$) in electric and magnetic fields, it will experience the Lorentz force:

$$\mathbf{F}_{\mathrm{L}} = m\frac{d\mathbf{v}}{dt} = q(\mathbf{E} + \mathbf{v} \times \mathbf{B}) \tag{2.1}$$

where m the mass, $\mathbf{E}$ the electric field, and $\mathbf{B}$ the magnetic field. As particles experience the different forces and variable fields, they will initiate a set of movements that can be obtained by solving the equation of motion. A typical result is a motion called drift, to which the general form for a force $\mathbf{F}$ can be written as:

$$\mathbf{v}_F = \frac{1}{q}\frac{\mathbf{F} \times \mathbf{B}}{B^2} \tag{2.2}$$

Before elaborating on the different drifts, the simplest motion occurs when a particle is under the influence of a constant magnetic field ($\mathbf{E} = 0$). Then, the particle will simply gyrate around a so-called *guiding center*. The frequency at which it gyrates is called the gyro/cyclotron frequency, and the radius of the gyration is called the gyro/cyclotron/Larmor radius. Following the derivation of a typical textbook (e.g., [Chen, 2012]) it is easy to show that ions gyrate clockwise (as viewed with a magnetic field pointing toward the observer) and have a larger radius than electrons that gyrate counterclockwise, resulting from their different mass and opposite charge. Imposing more realistic fields, such as non-uniform and time varying $\mathbf{E}$ and $\mathbf{B}$, a series of different drifts, resulting in a complex particle trajectory can be observed. A particularly interesting motion is occurring when we combine the motion of particles along the magnetic field lines with the different drifts they experience. If for example we assume a symmetric magnetic field geometry with maximum values on each side and a minimum field in the middle, we obtain a *magnetic bottle*. This configuration can effectively trap a particle between what we call *mirror points* and make it undergo a *bounce* motion between the maximum magnetic field locations. A summary of the most typically discussed motions is shown in Figure 2.1

The above description is relatively easy to comprehend, since it is based on classical physics (particles with a mass and a charge under the influence of a force that has a closed mathematical form). Therefore, one could in principle solve that set of equation for each particle and get a detailed description of the plasma behavior. However, for such description we assume that the fields can be analytically expressed which is not typically the case, and that the external field interaction is stronger compared to the effect that the particles have on each other. As a result, this description works fine in dilute plasmas (e.g., Earth's radiation belts) with strong external fields but is invalid when the fields are weak. Moreover, a typical plasma may include up to 10^{20} particles per cubic meter (m^3) and this means that there are many particles interacting both with each other and with the surrounding fields. As a result, to model their collective behavior, one needs to change the framework and describe the plasma with a rather coarse yet surprisingly effective way. This can be done by assuming that plasma evolves as a conductive fluid.

One of the most widely used ways to describe a plasma is the magnetohydrodynamics (MHD) description, in which plasma is treated as an electrically conductive fluid. This description is valid when we treat spatial scales typically much larger than the gyro-radius of ions and the Debye length, and time scales above the corresponding ion gyro-period and plasma frequency. These conditions are set to guarantee that, since we have a one-species description, the characteristic scales of the heaviest particles (in this case ions) are smaller than the variations observed in the phenomenon we study. Since a plasma is conductive, apart from a fluid description, one has to couple the evolution of electromagnetic fields through Maxwell's equations, which in differential form can be expressed as:

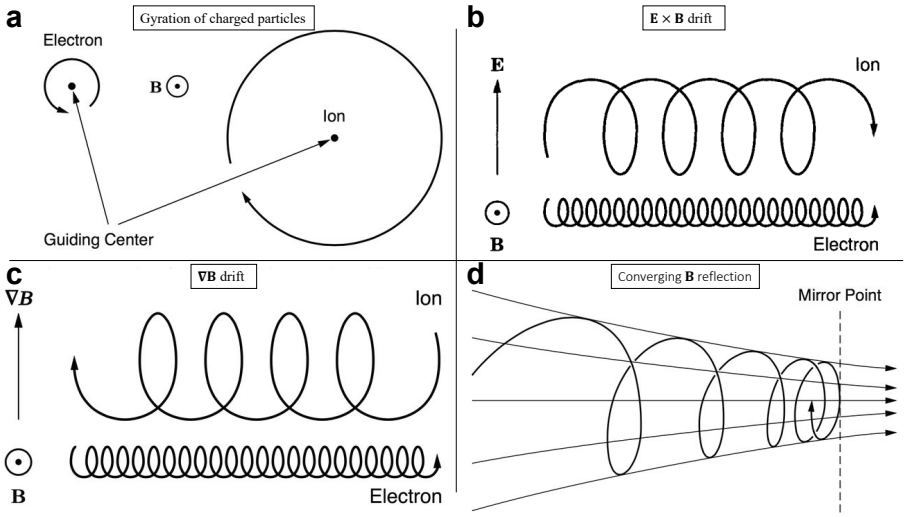

Figure 2.1: Particle motion under the influence of an electrostatic field. (**a**) Gyration of an electron and an ion around a guiding center under the influence of a uniform magnetostatic field. (**b**) Influence of $\mathbf{E} \times \mathbf{B}$ on an electron and an ion in the presence of electrostatic field. Both particle drift in the same direction, but due to their different mass, they have a different gyro-radius. (**c**) Influence of $\nabla \mathbf{B}$ on an electron and an ion in the presence of inhomogeneous magnetic field. Apart from the different radius, due to their charge, particles drift in different directions. (**d**) An ion getting reflected at a mirror point. The spiral motion is the result of the decreasing radius originating from the magnetic field increase. All figures were reproduced from [Baumjohann and Treumann, 2012].

$$\nabla \cdot \mathbf{E} = \frac{\rho}{\epsilon_0} \tag{2.3}$$

$$\nabla \cdot \mathbf{B} = 0 \tag{2.4}$$

$$\nabla \times \mathbf{E} = -\frac{\partial \mathbf{B}}{\partial t} \tag{2.5}$$

$$\nabla \times \mathbf{B} = \mu_0 \left(\mathbf{j} + \epsilon_0 \frac{\partial \mathbf{E}}{\partial t} \right) \tag{2.6}$$

where ρ is the charge density, ϵ_0 is the vacuum permittivity, $\mathbf{j}$ is the current density, and μ_0 is the vacuum magnetic permeability. Intuitively, one can think that Maxwell's equations show that, the change in the $\mathbf{E}$ is proportional to the charge (2.3), there are no magnetic monopoles (2.4), the magnetic field variations produce a rotational $\mathbf{E}$ and vice versa (2.5), and the rotation of $\mathbf{B}$ is produced by the time

variation of an electric field and/or by a current density (2.6).

Then, the resulting MHD equations basically consist of three conservation laws. The conservation of mass (continuity equation):

$$\frac{\partial n}{\partial t} + \nabla \cdot (n\mathbf{v}) = 0 \tag{2.7}$$

the conservation of momentum (equation of motion):

$$\frac{\partial (nm\mathbf{v})}{\partial t} + \nabla \cdot (nm\mathbf{v}\mathbf{v}) = -\nabla \cdot \mathbf{P} + \rho\mathbf{E} + \mathbf{j} \times \mathbf{B} \tag{2.8}$$

where the second term of the right-hand side ($\rho\mathbf{E}$) is neglected due to quasi-neutrality, and the conservation of energy:

$$\frac{\partial}{\partial t}\left[nm\left(\frac{\mathrm{v}^2}{2} + w\right) + \frac{B^2}{2\mu_0}\right] = -\nabla \cdot \mathbf{Q} \tag{2.9}$$

where w is the enthalpy density (sum of isotropic pressure and internal energy density), and $\mathbf{Q}$ is the heat flux density vector.

Finally, to close the set of equations, an equation of state is needed, such as the ideal gas law, and the Ohm's law, which in its simplest form can be written as:

$$\mathbf{E} + \mathbf{v} \times \mathbf{B} = 0. \tag{2.10}$$

When a plasma satisfies such an expression for Ohm's law, we say that it can be modelled by *ideal* MHD. This ideal one-fluid description misses several elements of plasma complexity (for example, a variety of waves and instabilities and scattering effects). After all, several assumptions have to be made to arrive to this description. As mentioned above, changes in the fields have to be smaller than the ion cyclotron frequency and the spatial scales therefore have to be larger than that of the ion gyro-radius. However, MHD can be very practical to get analytical expressions on plenty of phenomena that are of interest when studying large-scale dynamics. A direct consequence of MHD is the *frozen-in* condition, stating that the plasma and the magnetic field are frozen-in together. Any kind of plasma motion should therefore maintain the magnetic field line topology, and a breaking of that condition means that MHD is not applicable in this environment anymore.

Another direct application of MHD is to derive a set of equations aclled the *jump conditions*. These are particularly useful to describe transition layers across two different plasma regions, called *discontinuities*. From a macroscopic point of view, using MHD, one can derive a set of relations which describe how different plasma properties and fields change between a discontinuity. A series of additional assumptions have to be made at this point. Specifically, that the plasma can be treated as an 1D ideal state where the frozen-in condition is obeyed. Furthermore, as usually done, if the pressure tensor is isotropic, one can then derive the following Rankine-Hugoniot (RH) jump conditions:

$$\hat{\mathbf{n}} \cdot [n\mathbf{v}] = 0 \tag{2.11}$$

$$\hat{\mathbf{n}} \cdot [nm\mathbf{v}\mathbf{v}] + \hat{\mathbf{n}} \left[p + \frac{B^2}{2\mu_0} \right] - \frac{\hat{\mathbf{n}} \cdot [\mathbf{B}\mathbf{B}]}{\mu_0} = 0 \tag{2.12}$$

$$\hat{\mathbf{n}} \times [\mathbf{v} \times \mathbf{B}] = 0 \tag{2.13}$$

$$\left[nm\hat{\mathbf{n}} \cdot \mathbf{v} \left\{ \frac{u^2}{2} + w + \frac{1}{nm} \left(p + \frac{B^2}{\mu_0} \right) \right\} - \frac{1}{\mu_0} (\mathbf{v} \cdot \mathbf{B}) \hat{\mathbf{n}} \cdot \mathbf{B} \right] = 0 \tag{2.14}$$

$$\hat{\mathbf{n}} \cdot [\mathbf{B}] = 0 \tag{2.15}$$

where each quantity in brackets (i.e., $[X]$) denotes the jump of this quantity across the boundary layer, and $\hat{\mathbf{n}}$ is a vector pointing along the normal of the discontinuity. A particular family of discontinuities that we analyze in later chapters are the *collisionless shocks*. At this point, following [Baumjohann and Treumann, 2012], one can show that the RH relations along with the assumption of plasma behaving like an ideal gas (equation of state) produce the jump conditions for the so-called "fast" shocks, which describe how plasma gets compressed, thermalized and decelerated downstream of a fast-mode shock. A typical transition of a fast shock should contain a series of associated observations, as illustrated in Figure 2.2

So far, we have described the collective behavior of a plasma by treating it as a fluid. However, a more detailed description to model plasmas can be obtained through the kinetic theory, in which ones studies plasma through the evolution of distribution functions. These correspond to an ensemble-averaged phase space density (f). From statistical mechanics of ideal gasses, we know that the dynamical evolution of a distribution function can be modelled through the Boltzmann equation:

$$\frac{df}{dt} \equiv \frac{\partial f}{\partial t} + \mathbf{v} \cdot \nabla_x f + \frac{q}{m} (\mathbf{E} + \mathbf{v} \times \mathbf{B}) \cdot \nabla_v f = \left. \frac{\partial f}{\partial t} \right|_c \tag{2.16}$$

where ∇_x indicates differentiation with respect to the particle displacement and

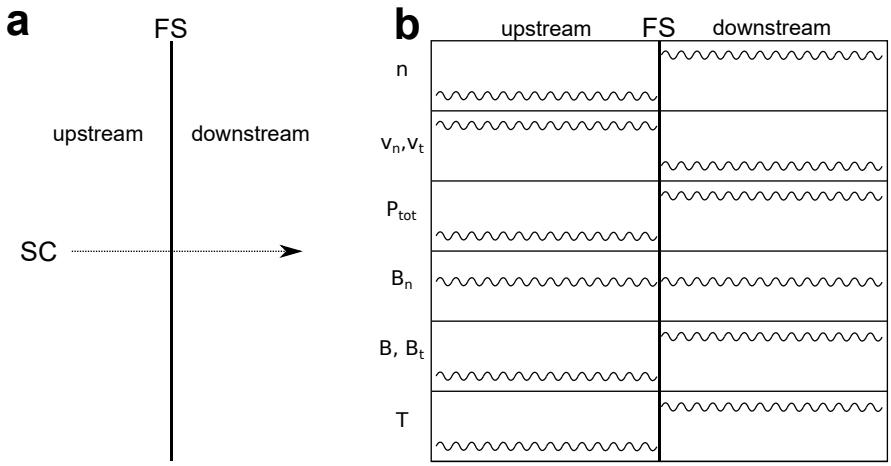

Figure 2.2: A fast shock transition. (**a**) A spacecraft crossing the fast shock from upstream to downstream. (**b**) Expected changes observed by the spacecraft. The subscript n refers to the vector normal to the shock, and t to the tangential component. (Top — bottom): number density, normal and tangential velocity, total pressure, normal to the shock magnetic field, total and tangential magnetic field, and temperature. Adapted from [Baumjohann and Treumann, 2012].

∇_v to the particle velocity. However, as we typically do not have collisions in space plasmas, the right-hand of (2.16) can be set to zero, which results in the Vlasov equation:

$$\frac{\partial f}{\partial t} + \mathbf{v} \cdot \nabla_x f + \frac{q}{m}(\mathbf{E} + \mathbf{v} \times \mathbf{B}) \cdot \nabla_v f = 0 \tag{2.17}$$

2.2 Velocity distribution functions

The velocity distribution function of a particle species (e.g., ions or electrons) of a plasma in thermodynamic equilibrium is known as a Maxwellian distribution, which in 1D can be expressed as:

$$f(u_x) = A_1 \cdot e^{-u_x^2/u_{\mathrm{th}}^2} \tag{2.18}$$

where $u_{\mathrm{th}} = (2k_B T/m)^{1/2}$, $A = n\left(\frac{m}{2\pi k_B T}\right)^{1/2}$, and k_B is Boltzmann's constant.

In 3D, it is easy to show that the Maxwell distribution is:

$$f(u_x, u_y, u_z) = A_3 \cdot e^{-(u_x^2+u_y^2+u_z^2)/u_{\rm th}^2} \tag{2.19}$$

where $A = n\left(\frac{m}{2\pi k_B T}\right)^{3/2}$.

Typically, however, the temperature is different parallel and perpendicular to the magnetic field direction. As a result, a more accurate distribution function for modeling space plasmas is a bi-Maxwellian (product of two Maxwellians) which can take the following form:

$$f(u_\perp, u_\parallel) = A_{\rm 2Bi} \cdot e^{-\frac{u_\perp^2}{\langle u_\perp\rangle^2} - -\frac{u_\parallel^2}{\langle u_\parallel\rangle^2}} \tag{2.20}$$

where $u_\parallel$ indicates the velocity parallel to the magnetic field, and $u_\perp$ perpendicular to it. The brackets indicate average velocities and $A_{\rm 2Bi} = \frac{n}{\pi^{3/2}\langle u_\perp\rangle^2\langle u_\parallel\rangle}$.

It should be noted that all these distributions are centered around 0. In reality, however, plasmas typically exhibit a drift. In the case of a bi-Maxwellian distribution, assuming that the plasma exhibits a perpendicular to the magnetic field drift velocity, the formula (2.20) can now be re-written as:

$$f(u_\perp, u_\parallel) = A_{\rm 2Bi} \cdot e^{-\frac{\left(u_\perp - u_{0,\perp}\right)^2}{\langle u_\perp\rangle^2} - -\frac{u_\parallel^2}{\langle u_\parallel\rangle^2}} \tag{2.21}$$

Examples of a Maxwellian and a drifting bi-Maxwellian distributions are shown in Figure 2.3.

All mentioned distributions (without the incorporation of a drift velocity) are derived from first principles of equilibrium statistical mechanics. However, in many cases the measured velocity distribution functions (VDFs) in collisionless space plasmas exhibit high-energy/velocity tails which make the deviation from Maxwellian quite significant. One common way to model the existence of a population with high-energy tails is to fit two different distributions, one Maxwellian and one power law distribution:

$$f(u) \propto \left(\frac{u}{u_0}\right)^{-\kappa} \tag{2.22}$$

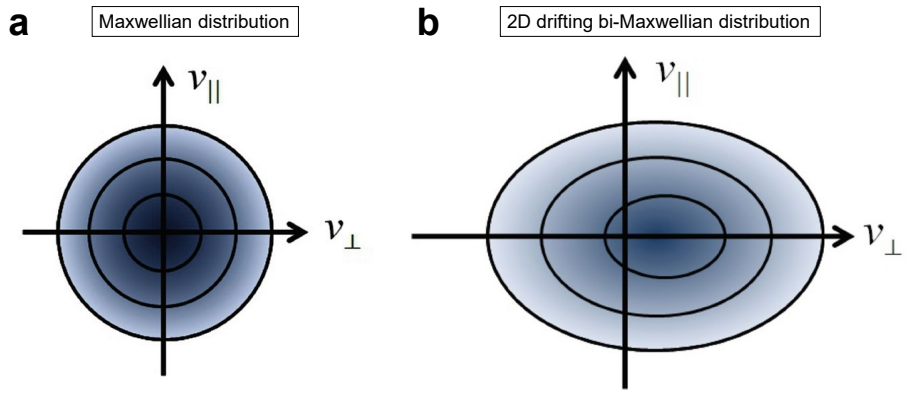

Figure 2.3: (**a**) Example of a 2D Maxwellian distribution in parallel and perpendicular to the magnetic field velocities. (**b**) Example of a 2D drifting bi-Maxwellian distribution with a perpendicular to the magnetic field velocity. Reproduced from [Koskinen and Kilpua, 2022].

with κ being a constant, indicating a fixed power decay.

A way to combine a Maxwellian core population along with a power law tail is described by the so-called *Kappa* (Lorentzian) distribution, which in 1D can be formulated as:

$$f_\kappa(u) = \frac{1}{(\pi w_\kappa^2)^{3/2}} \frac{\Gamma(\kappa+1)}{\Gamma(\kappa-\frac{1}{2})} \left(1 + \frac{u^2}{\kappa w_\kappa^2}\right)^{-(\kappa+1)} \tag{2.23}$$

$$w_k^2 = \left(1 - \frac{3}{2\kappa}\right)\left(\frac{2k_B T}{m}\right) \tag{2.24}$$

where w_κ is the effective velocity of the particles (corresponding to a thermal velocity), m is the mass, T is the effective temperature, n is the number density, and finally $\Gamma(x)$ is the Gamma function. It is trivial to show that for the limit of $k \to \infty$ (low energies), the kappa distribution degenerates to a Maxwellian and for large arguments it produces a power law [Lazar et al., 2012]. An illustration of how a Maxwellian distribution compares to Kappa in dimensionless units is shown in Figure 2.4.

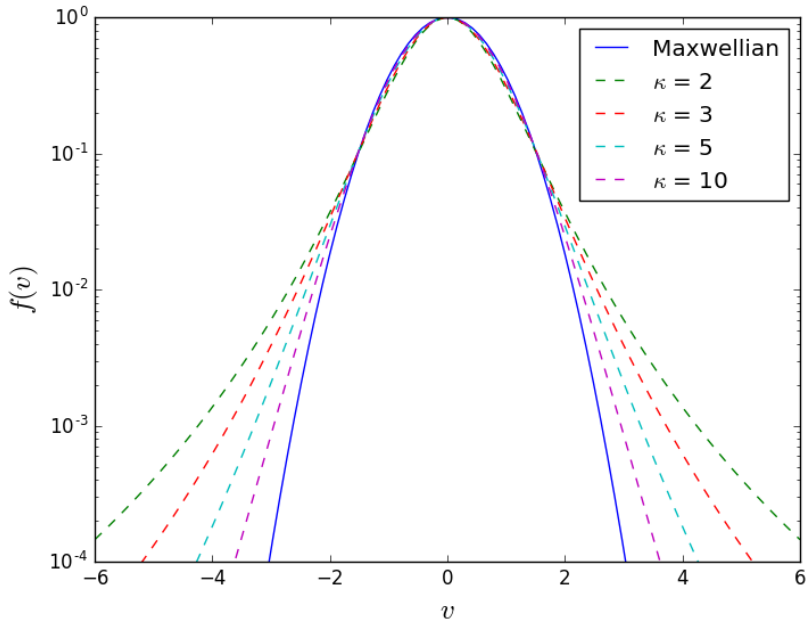

Figure 2.4: Comparison between an 1D dimensionless Kappa and an 1D dimensionless Maxwell distribution. For small speeds ($u \ll w_k$) the Kappa distribution becomes identical to a Maxwellian. At high energies ($u > w_k$), the suprathermal tails are more prominent, producing a different profile.

2.3 Useful quantities

In the above discussion, we missed a few vital quantities that we list below. Keep in mind that most are not motivated as typically done in textbooks, since we focus on highlighting their use rather than deriving them from first principles.

Typically, a plasma that has dimensions larger than the Debye length can be considered *quasi-neutral*, making it a fundamental length scale for every plasma description. It may also be described as the distance a thermal particle travels during a plasma oscillation. The Debye length can be formulated as:

$$\lambda_{D_e} = \sqrt{\frac{\epsilon_0 k_B T}{n e^2}} = \frac{u_{th}}{\sqrt{2}\omega_{pe}} \tag{2.25}$$

where u_{th} is the thermal speed of electrons, defined as the most probable speed of a

Maxwellian distribution (2.18). The plasma frequency is denoted as ω_{pe}, describing the reaction of electrons when a force is applied to a plasma. It is one of the most fundamental time scales of plasmas.

$$\omega_{pe} = \sqrt{\frac{ne^2}{m_e \epsilon_0}}. \tag{2.26}$$

Additionally, the ion plasma frequency (ω_{pi}) can be defined by using the above formula and the ion rather than the electron mass.

Another fundamental scale we use in space plasma physics is the electron and ion inertial length (or skin depth), defined respectively as:

$$d_{e,i} = \frac{c}{\omega_{pe,i}} \tag{2.27}$$

where, c is the speed of light in vacuum. Electron inertial length describes the depth to which radiation can penetrate the plasma. Ion inertial length can be viewed as the scale for which ions decouple from electrons, making the magnetic field frozen-in the bulk flow of the electron motion rather than that of the whole plasma flow.

The plasma beta (β) is another important parameter used to characterize several plasma environments, from solar wind to fusion experiments. It is defined as:

$$\beta = \frac{p_{\text{th}}}{p_{\text{mag}}} = \frac{nk_B T}{B^2/2\mu_0} \tag{2.28}$$

where p_{th} is the plasma (thermal) pressure, and p_{mag} is the magnetic pressure of the plasma.

Dynamic pressure is the kinetic energy per unit volume of a fluid. It is a key quantity for a magnetosheath jet, as most of the definitions typically used are based on it. For the ion population that we mainly study in this thesis, it can be formulated as:

$$p_{\text{dyn}} = \rho_i |\mathbf{v}_i|^2 = n_i m_p |\mathbf{v}_i|^2 \tag{2.29}$$

where i index refers to the ion population, and m_p is the proton mass.

Another useful quantity that is used to primarily characterize shock environments is the angle θ_{Bn}. At Earth's bow shock, it is defined as the angle between the interplanetary magnetic field (IMF) and the bow shock normal vector. This angle is identical to the cone angle ($\theta_{\rm cone}$) when examining the subsolar point of the shock (the point where the Sun – Earth line crosses the shock)

$$\theta_{\rm cone} = \arccos\left(\frac{|B_x|}{|\mathbf{B}|}\right) \tag{2.30}$$

Finally, when characterizing different plasmas and shocks in physics, we typically use a series of Mach numbers. Generally, Mach numbers are defined as the ratio of a velocity to a characteristic speed. One of the most widely used Mach numbers is the Alfvén Mach number, which can be mathematically expressed as:

$$M_{\rm A} = \frac{\rm v}{v_{\rm A}} = \frac{\rm v}{\sqrt{B^2/\mu_0\rho_i}} \tag{2.31}$$

where $v_{\rm A}$ is the Alfvén speed, μ_0 is the free space permeability and ρ_i is the ion mass density. When characterizing a medium, v typically refers to the velocity of the medium (e.g., $\rm v_{SW}$ for the solar wind), while for shocks it usually refers to the upstream normal flow speed typically along the shock normal direction ($\rm v_n$).

Another Mach number used is the magnetosonic Mach number, which is defined through the group speed of fast magnetosonic waves. For parallel to the magnetic field propagation, it is defined as:

$$v_{\rm MS} = \sqrt{v_s^2 + v_{\rm A}^2} \tag{2.32}$$

where the speed of sound is $v_s = \sqrt{\gamma \cdot \frac{p}{\rho}}$. In this expression, γ is the adiabatic index, p is the plasma pressure and ρ is the plasma mass density. Thus, the magnetosonic Mach number can be computed as:

$$M_{\rm MS} = \frac{\rm v}{v_{MS}} \tag{2.33}$$

It is worth noting that the expressions above are taken for a parallel to the magnetic field propagation. For an arbitrary propagation angle (θ), the expressions are different (see, e.g., [Swanson, 2012, Balogh and Treumann, 2013]).

Chapter 3

Earth's magnetospheric environment

The Sun, apart from radiation, constantly emits a stream of fast charged particles, called the solar wind (SW). As it propagates in the interplanetary environment, it causes a variety of different phenomena before eventually reaching Earth. Here, it interacts with Earth's magnetic field, causing the formation of a bow shock. The now shocked solar wind, continues towards the Earth causing a complex coupling with Earth's magnetic field which generates a magnetized environment called the *magnetosphere*. In this chapter, we briefly introduce some details of this environment.

3.1 Bow shock

Shock waves, like in gasses, also form in collisionless plasmas when a fast flow meets an obstacle. Typically, we say that a shock wave is formed when the speed of the flow is too high for waves to propagate and "inform" the medium of the obstacle's presence. In collisionless environments, the shocks are created by the long-range interactions of the electromagnetic fields rather than by collisions, which is the case at Earth's atmosphere (e.g., shock waves in front of supersonic airplanes).

Collisionless shocks can be found everywhere in the Universe, and they are well known for their ability to accelerate particles in different plasma environments (e.g., solar flares, [Ellison and Ramaty, 1985], cosmic rays [Bell, 2004] and supernovas [Koyama et al., 1995]). Studying Earth's bow shock via *in-situ* measurements provides a unique opportunity to determine its properties and generalize them to other laboratory, planetary, and astrophysical shock environments.

When the solar wind meets the Earth's magnetosphere, a bow shock is formed

at a stand-off distance of $\sim$ 15 $R_{\rm E}$ due to the long-range interaction caused by Earth's magnetic field on solar wind charged particles. The bow shock formed has a magnetosonic Mach number higher than a critical value, which makes it *supercritical* [Edmiston and Kennel, 1984], meaning that dissipation alone cannot slow down the particles. As a result, a part of the SW will get reflected at the shock. Below, we briefly discuss the two main categories of supercritical shocks, these being the quasi-parallel (Qpar) ($\theta_{Bn} \lessapprox 45°$) and Quasi-perpendicular (Qperp) ($\theta_{Bn} \gtrapprox 45°$) shocks. More details on this topic can be found in textbooks and review articles (e.g., [Treumann, 2009, Balogh and Treumann, 2013, Burgess and Scholer, 2015, Marcowith et al., 2016]).

Although we discuss some properties of the upstream and downstream regions of Qpar and Qperp shocks, it should be noted that in reality nature does not create a sharp boundary separating these environments. In practice, the dynamics of the particles and therefore the corresponding regions formed are highly variable and properties of both shock types may co-exist in some crossings. As a result, the transition from Qpar dominated dynamics to Qperp ones is not very distinct in *oblique* ($\sim 30 - 60°$) shocks.

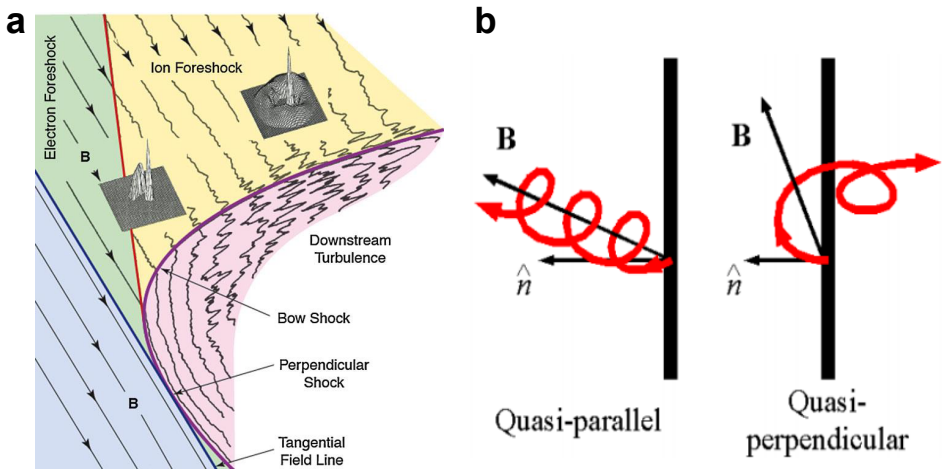

Figure 3.1: (**a**) View of the shock environment showing quasi-parallel, and quasi-perpendicular shock environments along with electron and ion foreshock regions. (**b**) Particle reflection in a Qpar and in a Qperp shock transition. Reproduced from [Balogh and Treumann, 2013].

The bow shock environment is shown in Figure 3.1(a) while in (b) we see the difference between the reflection of SW particles under a typical Qpar and Qperp case. Examples of a Qpar and a Qperp shock crossing using MMS fast data (see Chapter 4) are shown in Figure 3.2.

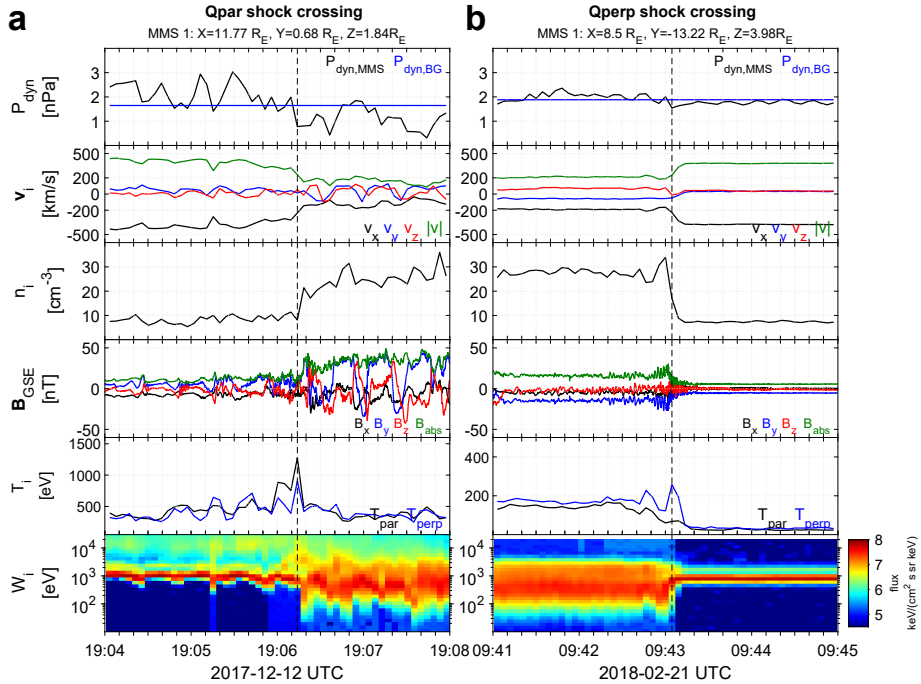

Figure 3.2: (**a**) Example of an inbound Qpar bow shock crossing. (**b**) Example of an outbound Qperp bow shock crossing. (Top — bottom): ion dynamic pressure, ion velocity in GSE coordinates, ion number density, magnetic field vector, ion temperature, and ion differential energy spectrum. Measurements are taken from MMS1.

Quasi-perpendicular shock

The distinction between Qpar and Qperp shocks is made under the assumption of specular reflection of charged particles at a shock. In other words, particles get reflected and initially meet the "weaker" magnetic field of the SW on their way back upstream. This increases their gyro-radius, allowing them to move back at the shock in the case where the magnetic field is "close" to perpendicular with respect to the shock's normal. So, in Earth's environment, when the IMF direction is almost perpendicular to the bow shock, the particles can gyrate briefly and get convected back to the shock region, crossing into the magnetosheath without having strong interaction with the approaching solar wind. This makes both the transitions of Qperp shocks and their downstream regions less turbulent than the Qpar ones. The shock *ramp* of a Qperp shock is the location where the ion reflection and heating occurs, while the area where the particles are gyrating upstream after they get reflected is called *foot*. The transition regions before the plasma enters the magnetosheath contains a diffuse hot ion population that has been effectively

heated and accelerated at the shock. Qperp shocks and their surrounding regions have been associated with several phenomena, such as the generation of upstream whistler waves [Lalti et al., 2022b], an increase in electron kinetic entropy [Lindberg et al., 2022], the existence of field-aligned beams [Kucharek et al., 2004], particle acceleration [Trotta and Burgess, 2019, Amano et al., 2020], and suprathermal protons inducing a downstream proton enthalpy flux increase [Schwartz et al., 2022].

Quasi-parallel shock

When the IMF direction is almost parallel to the shock normal, a large portion of the solar wind is reflected and travels upstream along the field lines, interacting with the incoming solar wind. This interaction forms an extended shocked region, the *foreshock* [Eastwood et al., 2005]. In this dynamic environment, several different phenomena are generated, with the most noticeable being the characteristic ultra-low frequency (ULF) waves [Greenstadt et al., 1995, Wilson III, 2016].

As these waves are convected back to the shock by the solar wind, they non-linearly evolve and get steepened, forming shocklets [Wilson III et al., 2013, Liu et al., 2022b], and Short Large Amplitude Magnetic Structures (SLAMS) [Schwartz et al., 1992]. There are many more phenomena that form at the foreshock, including hot flow anomalies (HFAs), spontaneous hot flow anomalies (SHFAs), foreshock bubbles, foreshock cavities, etc. [Zhang et al., 2022]. The Qpar shock (including the foreshock) appears to be an even more efficient particle accelerator than the Qperp shock [Turner et al., 2018, Liu et al., 2019a, Johlander et al., 2021].

The foreshock and its associated structures create an environment where the upstream and downstream regions are much harder to distinguish compared to Qperp shocks. While most researchers would agree on the position of a Qperp shock crossing, Qpar shocks tend to have a much larger ambiguity as to where the upstream and downstream regions start and end. However, there are cases where the transition, while more turbulent, can still be identified, as shown in Figure 3.2. Comparing the Qperp shock crossing (Figure 3.2b) where the heating occurs rapidly and results in a thermalized plasma, we see that in the Qpar case (Figure 3.2a), it is mainly the compression and the deceleration which indicates the transition to the magnetosheath region.

In practice, all shocks locally at ion (and smaller) scales, can be treated as "more" Qperp due to the presence of upstream waves. These waves cause an out of plane component, increasing the θ_{Bn} to marginally Qperp domain [Baumjohann and Treumann, 2012, Balogh and Treumann, 2013].

Shock non-stationarity

Non-stationarity of the shock means that the shock is an extended and time-variable structure. The non-stationarity of the Earth's bow shock has been theoretically predicted for a long time and was initially observed in laboratory collisionless shocks [Morse et al., 1972]. The variation it exhibits can originate from several effects. These include an observational difficulty to determine the shock front, and a series of physical mechanisms that change the location of the shock front in time. At Earth's bow shock, it has been observed to be a very prominent feature of the quasi-parallel shock, but also of the quasi-perpendicular one. In either shock transition, the effects that have been mainly associated to the non-stationarity are the *reformation* and the *ripples* of the shock. We briefly introduce both phenomena in Qpar and Qperp shock transitions.

Qperp (self-)reformation, describes the downstream plasma as being essentially the collection of the old shock ramps left from the shock-foot reformation cycles. This shock front reformation has been associated with upstream whistler waves, evolving in a nonlinear way and interacting with the front, forming a new shock front upstream of the old one. This has been shown in simulations for over 20 years [Lembège and Savoini, 2002, Hellinger et al., 2002] and more recently in *in-situ* measurements [Mazelle et al., 2010, Sulaiman et al., 2015, Dimmock et al., 2019].

The ripples observed in the Qperp shock can be described as ion-kinetic waves along the shock. These have been observed in quasi-perpendicular shocks in simulations [Lowe and Burgess, 2003] and in *in-situ* measurements [Johlander et al., 2016, Johlander et al., 2018]. Their scales are around 4 and their amplitude around 0.5 ion inertial lengths. Observations of Qperp shocks have also provided signatures of both non-stationarity phenomena taking place at the same time (e.g., [Madanian et al., 2021]).

For Qpar shocks, similar terminology is used, but it corresponds to a different picture (both however are associated with particle reflection). Shock reformation in Qpar shocks has been shown in simulations multiple times [Burgess, 1989, Hao et al., 2017, Battarbee et al., 2020b], and was recently shown in observations as well (e.g., [Liu et al., 2021, Johlander et al., 2022, Raptis et al., 2022]). However, reformation here corresponds to a different mechanism. Specifically, it corresponds to the notion of a patchwork formation of the Quasi-parallel shock, where the shock is effectively formed by several non-linearly evolved ULF waves, like the short large-amplitude magnetic structures (SLAMS) [Schwartz and Burgess, 1991, Schwartz et al., 1992]. All these ULF waves are essentially compressive magnetic structures that form the bow shock. Then the SW particles get reflected from this pile-up patchwork bow shock, travel far upstream, interact with the incoming solar wind, allowing the formation of new ULF waves. These in turn evolve, get steepened

and increase in amplitude forming the new shock front further upstream of the old one, in a cyclic manner. This process occurs at larger scales than the reformation process described for the Qperp shocks. Moreover, as SLAMS and other foreshock structures can be locally treated as Qperp shocks, the (self-)reformation described for Qperp shocks can apply for each individual structure forming the Qpar shock (e.g., [Turner et al., 2021, Chen et al., 2021, Raptis et al., 2022]). This makes the Qpar shock a highly variable environment where phenomena of different scale occur at the same time. An example where both phenomena took place was shown in Paper V. To avoid any confusion, we used the word "evolution" to describe the (self-)reformation cycle of a SLAMS and the word "reformation" to describe the global process of the non-stationarity of the Qpar shock. Finally, we should mention that recently, evidence of current sheets and reconnection events at the transition region of shocks has been reported, additionally modifying the reformation process [Wang et al., 2019, Gingell et al., 2020, Ng et al., 2022].

The shock ripples have also been associated with Qpar shocks [Hietala et al., 2009]. The phenomenon as shown in simulations (e.g., [Hao et al., 2016]) can change the shock's normal ($\hat{\mathbf{n}}$) drastically, causing large variations θ_{Bn}. The ripples in Qpar shock essentially refer to the foreshock presence, which effectively allows the location of the shock to be extended in some places far more upstream than in others. This causes the shock to become "rippled" to spatial scales of tens of ion inertial lengths [Karimabadi et al., 2014, Hao et al., 2017]. This, however, is not the same ripple we discuss in Qperp shocks, or at least it is not certain if the phenomena are of similar nature. It could be that ripples in this scenario, lacking the periodic nature of Qperp shock ripples, are the result of a reformation process that exhibits different cyclic behavior along the spatial extent of the shock. If this is true, the rippling of Qpar shock is a manifestation of the reformation cycle described above, being locally driven and essentially spatially and temporally independent.

We should note that some observations of ripples of similar size to the Qperp ones were reported to be found in marginally Qpar shocks. However, these remain similar in nature phenomena to Qperp shock ripples, with the exception that they appear to be a transient rather than a stable property of the shock and are modulated by the reformation process [Gingell et al., 2017].

Finally, some studies mentioned above referring to the Qpar shock, are technically under oblique θ_{Bn} (e.g., [Liu et al., 2021]). However, in these cases the foreshock related dynamics, and the presence of foreshock compressive structures (FCS) is still prominent, making a distinction redundant.

3.2 Magnetosheath

Crossing the bow shock, the downstream plasma environment forms a region called the *magnetosheath* [Lucek et al., 2005]. The shocked solar wind, now compressed, heated, and decelerated to sub-magnetosonic velocities, forms this highly turbulent region. Similarly to the shock classification between Qpar and Qperp, the magnetosheath region downstream of a Qpar shock is very different from that of a Qperp one. As it has been shown in the last couple of years in great detail, several compressive magnetic structures observed upstream of the shock can be transmitted downstream (e.g., [Suni et al., 2021, Kajdič et al., 2021a, Trotta et al., 2022]). This makes the Qpar magnetosheath a highly turbulent environment, where all the foreshock phenomena we mentioned above influence and modulate the surrounding plasma. HFAs [Eastwood et al., 2008], and foreshock bubbles [Archer et al., 2015] for example, can have strong effects on the magnetosheath environment. Apart from the foreshock's direct influence, new phenomena manifest downstream of the Qpar shock.

Examples of such phenomena are the strong reconnecting current sheets, that are more common close to the bow shock [Yordanova et al., 2016, Yordanova et al., 2020, Gingell et al., 2021]. The spectral profiles also indicate that the Qpar magnetosheath is more turbulent than the quasi-perpendicular one [Vörös et al., 2017, Gurchumelia et al., 2022]. The Qperp magnetosheath, as expected, is more influenced by the Qperp shock dynamics. As a result, several of the phenomena connected to foreshock dynamics are absent in this case. One of the most characteristic differences is the presence of mirror mode waves, which is significantly more prominent downstream of the Qperp shock [Dimmock et al., 2015]. Current sheets may also (less frequently) be observed [Alexandrova et al., 2004, Kajdič et al., 2021b]. Similarly, magnetosheath jets may appear less frequently in the Qperp magnetosheath and as we discuss in later chapters are associated with different phenomena [Plaschke et al., 2018, Kajdič et al., 2021b].

Regarding the statistically expected plasma properties, the magnetosheath downstream of the quasi-parallel shocks tends to have lower ion temperature anisotropy [Fuselier et al., 1994], increased flux of high-energy ions [Fuselier, 1994] and high magnetic field variability [Luhmann et al., 1986]. These properties appear to be associated with the foreshock presence and may also be used to determine whether the observed downstream plasma originated from a Qpar or a Qperp shock crossing [Raptis et al., 2020b, Karlsson et al., 2021].

3.3 Magnetopause and magnetosphere

The next obstacle that the now "shocked" magnetosheath plasma encounters is the magnetopause, which separates the outer geospace plasma environment from the

magnetosphere of the Earth. Physically, as the magnetosheath plasma approaches Earth, it reaches a point where there is a pressure balance between its pressure (primarily thermal) and the magnetic pressure from Earth's magnetic field. This generates a current system known as the Chapman-Ferraro current, which effectively defines the large-scale flow and the magnetopause environment. As the flow continues to be diverted, it moves towards the flanks of the magnetosheath, getting accelerated and reaching the night side of Earth's magnetosphere. As these regions are not relevant to our work, we will not go into more details. An illustration of the magnetospheric environment of Earth is shown in Figure 3.3.

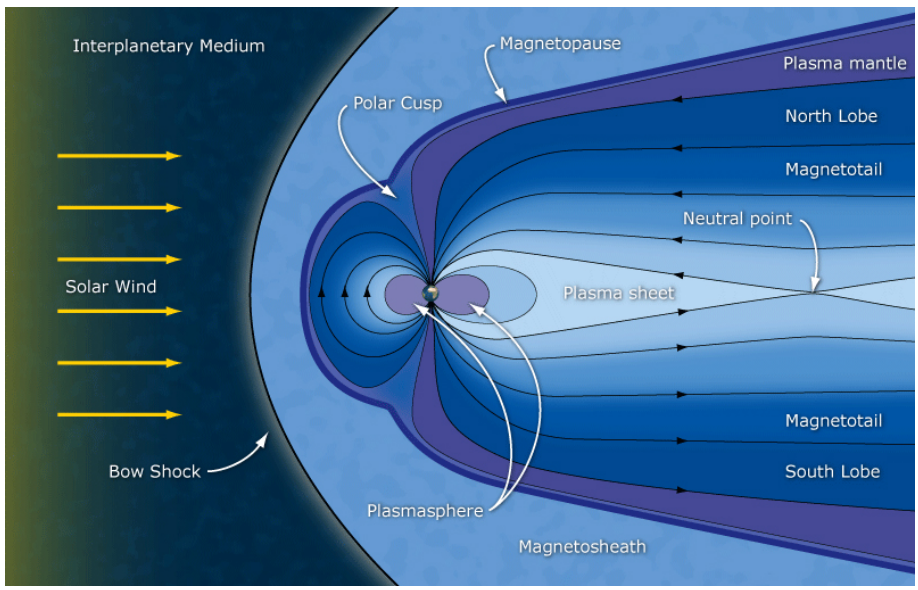

Figure 3.3: Illustration of Earth's magnetosphere, indicating some of the most important regions of interest for magnetospheric physics. Credit: ESA/C. T. Russel.

Chapter 4

Spacecraft missions and data products

The focus of this thesis has been observational research, using *in-situ* measurements. Most of the work is centered on the usage and analysis of magnetic field and plasma measurements using the Magnetospheric Multiscale (MMS) mission [Burch et al., 2016]. However, Time History of Events and Macroscale Interactions during Substorms (THEMIS) mission [Angelopoulos, 2009], and the OMNIweb dataset [King and Papitashvili, 2005] have also been used. In the sections below, we introduce and summarize the instrumentation and data products used in our research.

4.1 Magnetospheric Multiscale (MMS)

The Magnetosphere Multiscale (MMS) is a NASA mission launched in March 2015. It consists of four identical satellites that are typically in a tetrahedron formation orbiting the Earth. The main objective of the mission has been to study magnetic reconnection [Burch et al., 2016]. However, due to the advanced instruments on-board, several ground-breaking results on space and plasma physics have been obtained, including plasma processes at the Earth's foreshock, bow shock and magnetosheath regions. For our work, there have also been campaign formations (*string-of-pearl*) that, due to the larger separation between the satellites, produced measurements ideal for investigating processes in the scale of magnetosheath jets (see Figure 4.1). MMS has a burst system that allows high-resolution measurements to be obtained when a region of interest is observed. The selections are made by a *scientist-in-the-loop* (SITL) operation. During this process, a researcher from the MMS community selects certain periods through a ranking system by looking at low-resolution (survey/fast) data. Then, based on that manual evaluation, high-resolution (burst) measurements are down-linked for the specific regions along with a short description and justification of the reasoning behind each selection.

While the main objective of MMS prioritizes selections of magnetopause crossings, there are plenty of bow shock crossings, foreshock structures and turbulent magnetosheath selections made over the years. This makes the MMS mission ideal to study a variety of space physics related phenomena in small scales that take place in different plasma environments. MMS measurements[1] were used in Papers I – III, and V – VI.

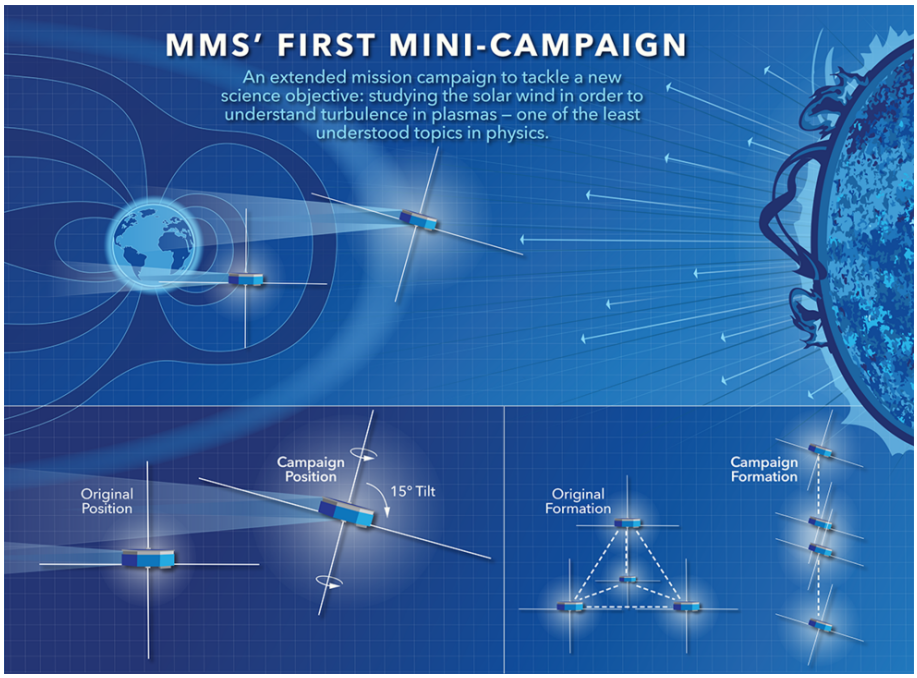

Figure 4.1: Illustration and infographic of the typical (tetrahedron) and the campaign (string-of-pearls) formation of Magnetosphere Multiscale (MMS) mission. Credits: NASA's Goddard Space Flight Center/Mary Pat Hrybyk-Keith.

Fast Plasma Investigation (FPI)

Every MMS spacecraft has four dual spectrometers for ions (DIS) and electrons (DES). The resolution is 11.25° in azimuthal angle and 15° in polar, while energies ∼10 eV – 30 keV can be resolved. One of the key features of FPI is that the sensors can sample the entire 360° view without relying on the spacecraft spin (like for example in Cluster mission), resulting in a much higher time resolution. For ions, distribution functions during burst measurements are provided every 150 ms and for electrons every 30 ms. During low-resolution (fast) mode, the measurements are available every 4.5 s for ions and electrons [Pollock et al., 2016].

[1] Accessible via `https://lasp.colorado.edu/mms/sdc/public/about/browse-wrapper`.

Fluxgate Magnetometer (FGM)

FGM [Russell et al., 2016] is part of the FIELDS instrumentation site [Torbert et al., 2016] of MMS. The goal of this instrument is to measure magnetic fields from DC up to 64 Hz. It consists of two magnetometers, one analog (AFG) and one digital (DFG) that are mounted on 5-m long deployable booms. On the low-resolution (survey) mode, data are available every 0.1250 s, and during high-resolution (burst) every 0.0078 s.

4.2 Time History of Events and Macroscale Interactions during Substorms (THEMIS)

THEMIS is a NASA mission launched in February 2007 consisting of 5 identical probes (Figure 4.2). Its main objective has been to study substorms and other geomagnetic disturbances. In 2010, three of the probes continued to orbit the Earth, while two of them changed their orbit to investigate new scientific objectives around the Moon. This new mission was named ARTEMIS (Acceleration, Reconnection, Turbulence and Electrodynamics of the Moon's Interaction with the Sun) [Angelopoulos, 2010].

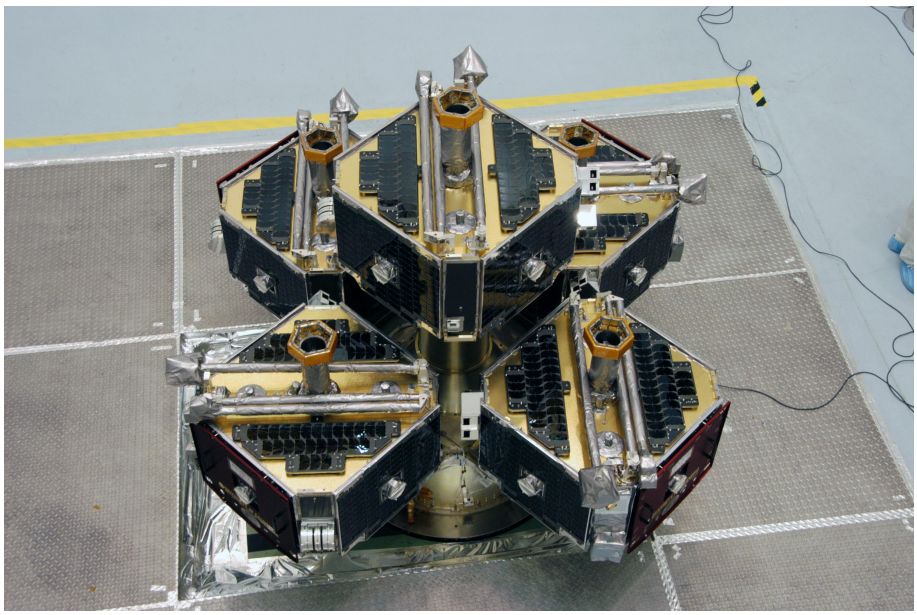

Figure 4.2: The five identical satellites of THEMIS-ARTEMIS mission seen from above. Credits: NASA/George Shelton.

Instruments relevant to our work include the FGM (fluxgate magnetometer) [Auster

et al., 2008] and the ESA (Electrostatic Analyzer) [McFadden et al., 2008] on board of each probe. Similar to MMS, FGM provides measurements of the magnetic field vector with 3 s resolution. The Electrostatic Analyzer provides plasma distributions and moments for ions and electrons with the same resolution. THEMIS measurements[2] were used in Paper IV.

4.3 High-resolution OMNI dataset

For parts of our work, we needed a solar wind monitor to obtain information on the upstream conditions. One of the most widely used products describing the upstream environment at the subsolar bow shock is the 1-min resolution OMNI database [King and Papitashvili, 2005]. This set is created using several spacecraft measurements, primarily from missions residing at the Lagrangian 1 (L1) point, such as Wind [Harten and Clark, 1995] and ACE [Stone et al., 1998]. The measurements are then time shifted to the subsolar nose of the Earth's bow shock. More information, along with the freely available dataset, can be found in the OMNIWeb repository[3]. The OMNI database was used for all the papers of this thesis.

[2] Accessible via `http://themis.ssl.berkeley.edu/data_products/index.php`.
[3] Accessible via `https://omniweb.gsfc.nasa.gov/ow.html`.

Chapter 5

Computer simulations

Traditionally, in scientific research, a theory would make a prediction and observations would either satisfy or falsify the theory. However, after the growth of computing power during the 20^{th} century, the field of mathematical modeling via computer simulations has been established in the scientific community. Today, simulations can act as the bridge between theory and experiment, providing insight and determining new research objectives. In plasmas, one can use a variety of different simulation setups depending on the accuracy level they want to achieve and the scales of the phenomena investigated. Even looking at the different plasma descriptions mentioned in Chapter 2 one can imagine that there are several ways to simulate a plasma environment.

One way to model plasmas is through a fluid or MHD (conductive fluid) approach. In this case, the plasma is treated as a single-species or two-species fluid. As these descriptions tend to be less computational heavy than the ones described below, they have often been used in the early magnetospheric simulation research. They are still used to describe systems of very large scales such as the solar system, the solar wind evolution and astrophysical environments (e.g., [Porth et al., 2014])

Another approach is to use a Hybrid-Vlasov description, which uses the Vlasov equation (2.17). Also, rather than having an ideal Ohm's law (2.10), a generalised form is used, such as:

$$\mathbf{E} + \mathbf{v} \times \mathbf{B} = \frac{\mathbf{j}}{\sigma} + \frac{\mathbf{j} \times \mathbf{B}}{n_e e} - \frac{\nabla \cdot P_e}{n_e e} + \frac{m_e}{n_e e^2} \frac{\partial \mathbf{j}}{\partial t} \tag{5.1}$$

where σ is the conductivity, and e is the elementary charge. The terms of the right-hand side from left to right are describing, the resistivity, the Hall, the elec-

tron pressure gradient and the electron inertia term. So, going back to the ideal Ohm's law, if the right-hand side is zero, the description is very limiting since we effectively model a plasma with, infinite conductivity (1st term), no cross field currents (2nd term), no electron pressure divergence (3rd term) and no inertial effects from electrons (4th term).

It should be noted that while the above Ohm's law allows many of the observed phenomena to emerge, it does not include terms that describe the correlation between fluid velocity and current or MHD turbulence. Furthermore, it lacks a term that describes time variation of low frequency waves. These are typically not included in simulations, but could play a role in small-scale dynamics [Baumjohann and Treumann, 2012]. Generally, hybrid descriptions tend to be very accurate while allowing simulations to run on realistic spatial and time scales. The goal is to combine the benefits of kinetic description for ions with the reduced computational aspects and complexity of electrons that are typically treated as fluids. These types of simulations have several applications in planetary environments and in astrophysics [Palmroth et al., 2018a]. It should be noted that whether that description is sufficient to model certain planetary environments or not is still under debate (e.g., Mercury [Lapenta et al., 2022]).

Another way to model plasmas is through the PIC (Particle-in-cell) or PM (Particle-mesh) methods. These refer to techniques that solve a specific set of differential equations. In these methods, particles are tracked in a continuous phase space, whereas every moment of the distribution is computed in stationary points. PIC includes interactions of particles only through the average fields [Hatzky and Bottino, 2010,Markidis et al., 2010]. In practice, PIC is very useful to study small-scale effects where electron particle distributions are vital, like the electron diffusion region (EDR) in magnetic reconnection (e.g., [Lu et al., 2020]). However, such methods can be computationally expensive, and it is very hard to perform simulation on large/global scales or with realistic number of particles and mass ratios. As a result, apart from a few exceptions (e.g., [Lin et al., 2021]) with the current computational power, global simulations are typically done using MHD or Hybrid-Vlasov simulations rather than PIC. A schematic illustrating the different plasma descriptions typically used in simulations, along with their basic scaling range, is shown in Figure 5.1.

5.1 Hybrid-Vlasov simulations - Vlasiator

For Paper III, we used the Vlasiator model [Palmroth et al., 2013, Von Alfthan et al., 2014, Palmroth et al., 2018a]. Vlasiator is a hybrid-Vlasov model simulating the Earth's magnetosphere. It treats protons as distribution functions $f(r, v, t)$, while electrons are treated as a massless charge-neutralizing fluid. This results, in an accurate description of the ion kinetic effects while electron effects are ignored.

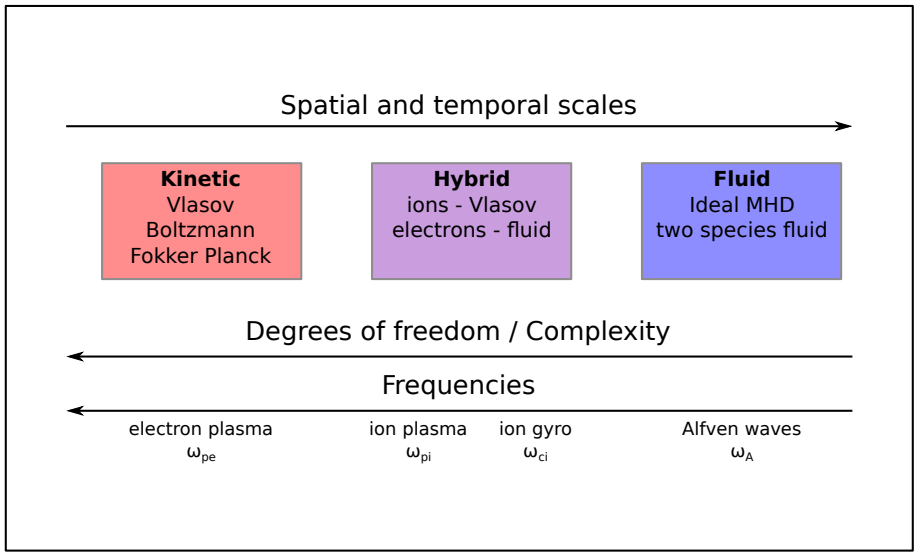

Figure 5.1: Schematic of the basic plasma descriptions typically used in simulation studies, and how the complexity and different scale sizes change for each description.

However, large-scale effects and in particular ion scale phenomena and distributions that we study in this work, should in principle be accurately described. The Vlasiator model has been used to model and evaluate a variety of different phenomena, such as foreshock particle composition and waves (e.g., [Von Alfthan et al., 2014, Palmroth et al., 2015, Turc et al., 2018, Battarbee et al., 2020a]), magnetosheath jets (e.g., [Palmroth et al., 2018b, Palmroth et al., 2021, Suni et al., 2021]), and magnetic reconnection (e.g., [Pfau-Kempf et al., 2020, Runov et al., 2021]).

The specific Vlasiator runs used in our work are 2D runs, and as discussed above do not treat electrons kinetically. Recently, however, Vlasiator has been upgraded and can provide results that treat electron distributions more accurately [Alho et al., 2022], while 3D global modeling of Earth's magnetosphere has also been developed [Palmroth, 2022].

An illustration from a Vlasiator simulation, modeling the dayside magnetosphere and the shock environment, is shown in Figure 5.2.

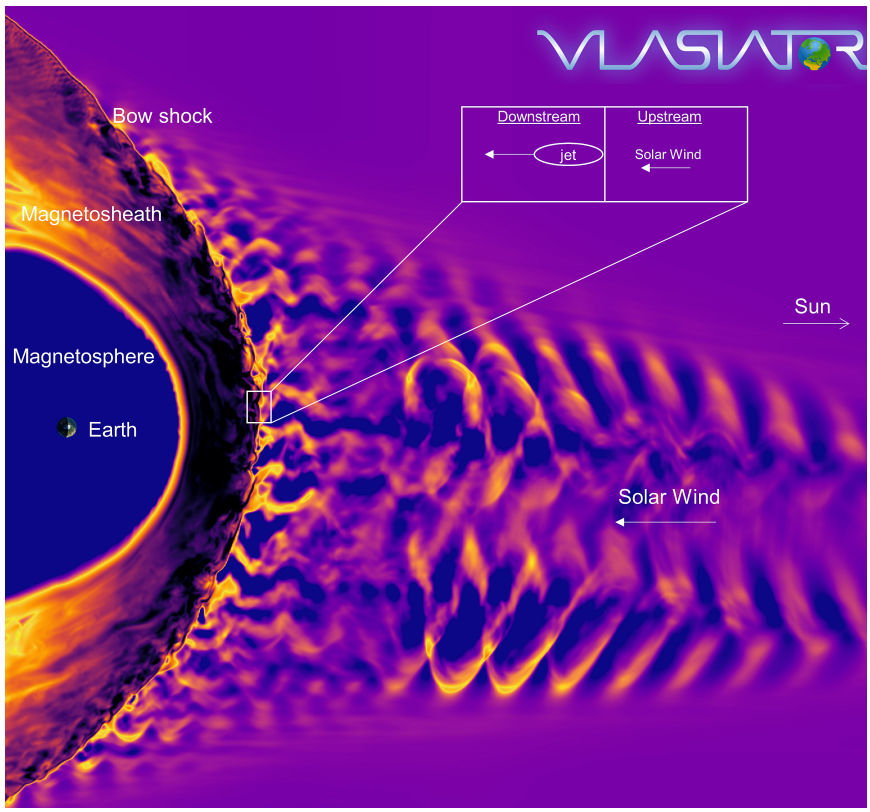

Figure 5.2: Earth's geospace environment as modeled by the Vlasiator model. Special indications are made to show the different regions and the close to the bow shock environments where magnetosheath jets are typically formed. Reproduced from the online Nature community post "How the solar wind slips through Earth's bow shock". Credits: M. Palmroth, U Helsinki.

Chapter 6

Data analysis methods

For our work, we used a variety of data analysis techniques. Some methods are based on single spacecraft observations, while others on multi-spacecraft ones. Furthermore, we briefly introduce neural networks and plasma moment derivation methods that we used in our work. Many of the techniques we discuss were developed for the Cluster mission [Escoubet et al., 2001]. However, both Cluster and MMS typically use tetrahedron formation and while corresponding to different spatial scales, the application of most of the techniques is useful for both missions. Below, we discuss the methods used, although a much more detailed description can be found in the classic book of "analysis methods for multi-spacecraft data" [Paschmann and Daly, 1998, Paschmann and Schwartz, 2000] and its complementary update [Paschmann and Daly, 2008]. Another relevant read for multi-spacecraft analysis focusing on ionospheric application was also recently published [Dunlop and Lühr, 2020].

6.1 Single-spacecraft techniques

Wavelet transforms

One way to perform spectral analysis (transforming and analyzing signals to the frequency domain) is to make a Wavelet transform, which is similar to Fourier transform. In our work we use Continuous Wavelet Transform (CWT) (see more information in [Torrence and Compo, 1998]) which uses the Morlet Wavelets [Morlet et al., 1982].

Since wavelet transform is a widely used technique in many fields, more information can be found in standard signal processing textbooks (e.g., [Strang and Nguyen, 1996]). In our case, Morlet wavelets can be treated as modulated sinusoidal oscillations that allow us to expand a signal in basis functions that are not only localized

in frequency (like Fourier transform) but also in time. Following the derivation of [Eriksson, 1998] one can derive the Morlet wavelet transformation (MWT) of a signal as:

$$C(\tau, f) = \int u(t) h^*_{f\tau}(t) dt \tag{6.1}$$

where $u(t)$ is the signal and $h^*_{f\tau}$ indicate the wavelet kernels. Then, a continuous wavelet transformation consists of evaluating (6.1) on a set of chosen f and t.

Minimum variance analysis (MVA)

Minimum variance analysis (MVA) is a useful technique to estimate the direction normal to an 1D plasma transition layer (i.e., a discontinuity). The technique is based on an idealised situation where only one dimension is used for expressing the divergence of the magnetic field ($\mathbf{B}$):

$$\nabla \cdot \mathbf{B} = \frac{\partial B_z}{\partial z} = 0 \tag{6.2}$$

where z is taken to be part of a local coordinate system, along the normal vector $\hat{\mathbf{n}}$. Then, by assuming that $\mathbf{B} \cdot \hat{\mathbf{n}} = 0$, and by measuring the magnetic field before, during and after the layer transition, one can estimate the normal vector $\hat{\mathbf{n}}$. In practice, the estimation is being done by minimizing the variance of the magnetic field projected over the normal vector, $\mathbf{B}_m \cdot \hat{\mathbf{n}}$, where $m = 1, 2, 3, ...M$ and M is the total number of magnetic field measurements used. The variance is then calculated as:

$$\sigma^2 = \frac{1}{M} \sum_{m=1}^{M} |\mathbf{B}_m - \langle \mathbf{B} \rangle) \cdot \hat{\mathbf{n}}|^2 \tag{6.3}$$

Then one can compute three components representing the minimum, intermediate, and maximum variance direction (see steps on, e.g., [Sonnerup and Scheible, 1998]). A direct application of MVA is to generate the so-called *hodograms*. After generating the eigenvectors that correspond to the maximum, intermediate, and minimum variance of a vector (in this example the magnetic field), one can visualise them by plotting different combinations in a plane (e.g., $\mathbf{B}_{\min}$ versus $\mathbf{B}_{\text{inter}}$). By doing so, the polarization of the structure can be inferred. For example, as shown in Figure 6.1, we have a typical case of circularly left-hand polarized magnetic field waves, which in this case is attributed to a time interval of whistler waves upstream of Earth's bow shock [Raptis et al., 2022]. See chapter 8 of [Paschmann and Daly,

1998] for more information on the usage and possible caveats of this method, along with how to derive error estimates.

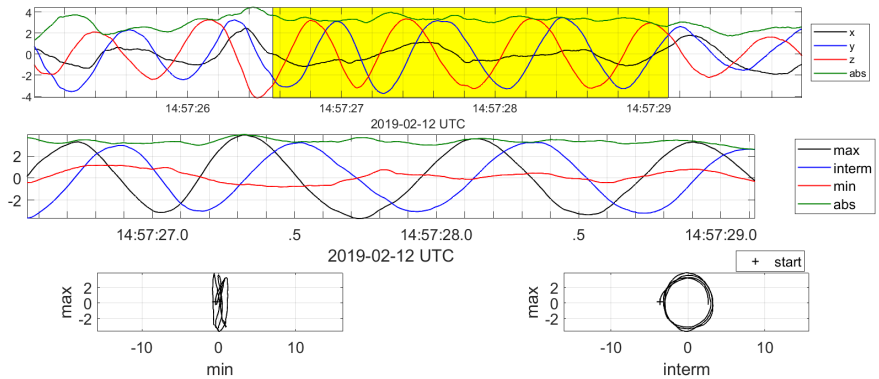

Figure 6.1: An example of minimum variance analysis (MVA) applied to a time series of whistler waves. A clear left-handed circular polarization is illustrated by the hodogram of the maximum and intermediate component of the magnetic field (bottom right).

Coplanarity methods

From the Rankine-Hugoniot relations (2.11 - 2.15) one can derive the coplanarity relation to obtain the normal vector of the bow shock:

$$\hat{\mathbf{n}} = \pm \frac{(\mathbf{B}_\mathrm{d} \times \mathbf{B}_\mathrm{u}) \times \Delta\mathbf{B}}{|\mathbf{B}_\mathrm{d} \times \mathbf{B}_\mathrm{u} \times \Delta\mathbf{B}|} \tag{6.4}$$

where u denotes the upstream and d the downstream environment of the shock. This method, however, breaks down when we have $\theta_{Bn} \to 0$. In these cases, there are alternative ways to estimate $\hat{\mathbf{n}}$, for example through the use of upstream and downstream velocity vector [Paschmann and Daly, 1998].

6.2 Multi-spacecraft techniques

Timing

To reliably determine the velocity of a discontinuity or a shock, one typically needs more than one spacecraft. While one can estimate the normal vector ($\hat{\mathbf{n}}$) and speed via the single spacecraft techniques we discussed above, all of them have a series of strong assumptions. Typically, a better estimation can be done if there are four spacecraft in tetrahedron formation (like the typical formation MMS and Cluster).

When such measurements are available, one can mark the different time that the disturbances are observed on each spacecraft, for example by cross correlating the different signals. Then, based on the position of the different satellites (and the precision of its determination), one can estimate the orientation and speed of the disturbance. While timing of the signals can be performed in other formations (e.g., string-of-pearl), conclusions regarding the normal vector are highly susceptible to errors. Therefore, an estimation of the normal vector via single-spacecraft techniques or by combining both is typically preferred (see more information on Chapter 10 of [Paschmann and Daly, 1998]).

Cross-wavelet analysis

In Paper IV, we used cross-spectral analysis, which means to compare two time series and investigate the relation between their respective spectra. In our case, this is done to investigate if two observed signals originating from different locations are in-phase or not. Using the relationships obtained above on single-spacecraft wavelets, the relationship of the cross-wavelet transform is defined as:

$$W_n^{AB} = W_n^A \cdot W_n^{B*} \tag{6.5}$$

where * denotes the complex conjugate, W_n^{AB} is the average global wavelet spectrum made from the wavelet transformation for a specific frequency (f) of two timeseries, A and B. From the argument of the cross wavelet transform, one can obtain the relative phase difference between the signal observed in the timeseries. The phase spectrum is obtained by examining:

$$\phi = \arctan\left(\frac{\mathrm{Im}\left(|W_n^{AB}|\right)}{\mathrm{Re}\left(|W_n^{AB}|\right)}\right) \tag{6.6}$$

More information about this methodology can be found in several articles and textbooks (e.g., [Eriksson, 1998, Grinsted et al., 2004, Katsavrias et al., 2022]). Finally, an estimate for the level of the statistical significance can be obtained by evaluating the wavelet coherence[1]. What is effectively obtained through that method is a correlation coefficient for every point in time and frequency space [Torrence and Compo, 1998].

[1]See, for example, implementation in MATLAB `https://se.mathworks.com/help/wavelet/ref/wcoherence.html`.

6.3 Bow shock and magnetosphere models

Modeling the bow shock position and shape can be done through a variety of different approaches. One way is to run a model using an MHD or kinetic description and determine the position of the bow shock by modeling the interaction of the planet's magnetic field with the solar wind. These models are computationally expensive and since simulations are run for a prefixed set of solar wind parameters, they cannot be used in occasions that the actual parameters are significantly different. Still, under a specific set of parameters they can be quite accurate [Merka et al., 2003, Ledvina et al., 2008].

Another way, typically used when there are available *in-situ* measurements over a crossing, is the generation of an empirical model. Using this approach, the bow shock is described as a conical surface which varies based on upstream solar wind parameters (primarily dynamic pressure and magnetic field direction). The exact description is usually statistically derived from many measurements that have been gathered from several bow shock crossings over the years (see e.g., [Slavin and Holzer, 1981, Chao et al., 2002, Jelínek et al., 2012]). Such models can be quite useful and are in good agreement with "average" properties, since they have been empirically derived, but may be inaccurate under rare upstream conditions. Some recent studies, try to combine simulations with empirical modeling, creating the so-called semi-empirical models (e.g., [Kotova et al., 2015, Kotova et al., 2021]).

If there are available measurements, one can force a model to fit at the location of the spacecraft that observed the shock transition. If, however, there are no measurements available, one can use upstream solar wind data from values propagated to the shock (e.g., OMNIweb database). These models can then be used either to derive the normal vector of the shock at the position of the spacecraft, or to get an estimate of the bow shock location to study the evolution of phenomena observed in other locations (e.g., magnetosheath or magnetosphere).

Similarly, for the magnetopause, a similar approach is being considered. As a result, most of the studies discussed above address the location and shape of both surfaces (e.g., [Chao et al., 2002, Jelínek et al., 2012]). In Papers, I, II and IV we used the model of [Chao et al., 2002] for the modeling of Earth's bow shock and magnetopause.

6.4 Artificial neural networks

One of the most popular machine learning approaches consists of using artificial neural networks (ANNs). ANNs have been heavily inspired by the research of biological neurons, hence the name. In a simple model of how the human brain works, different neurons are activated based on what signals they receive. Throughout our

life, our brain learns which neurons to activate by changing the activation threshold and the weights of each synapse. Through this process, new connections are generated, allowing us to learn new information and adapt our reaction to them. The field of ANNs has developed drastically in the last few decades due to pioneering research and the increase in computing resources. The main principles, however, are relatively simple to comprehend if one limits the discussion to the framework of a simple input/output problem. Let's take a simple problem description within this framework to explain the main concepts.

The Modified National Institute of Standards and Technology (MNIST) database consists of 70.000, 28×28 pixel images (input), corresponding to handwritten digits (1-9) that have been already labeled by humans. This database is used in ML benchmarking, by imposing a *supervised learning* problem[2], in which the input is the grayscale images, and the output is a label from 1 to 9. This problem, is an example of supervised multi-class classification.

ANNs have an input layer, a series of hidden layers and an output layer, each with a number of neurons. Both the number of layers and neurons are what we typically call *hyper-parameters* and can vary significantly from one application to another. Assuming we have an *architecture* consisting of several neurons and layers ready, the next step is to split the dataset to training, validation and test set. The training set is used to adapt the parameters of the neural network, the validation set to optimize its hyper-parameters, and the test set to evaluate its performance. In practice, the goal of this data splitting is to train the neural network with a set of data and then test it with unknown information to see if it can accurately find the expected result. Sometimes, validation and test set can be combined if hyper-parameter optimization is trivial or the data sample is relatively small.

Before the training, the neural network can be thought of as a series of connections (basically how each neuron reacts to each input) with randomized parameters, indicating the degree of activation. By providing an input which we know the answer of (i.e., an image of number 5) we can see "how far" is the initially random result from the correct answer, and establish an error function depending on the problem. For a typical regression task it can be the mean-squared error (MSE) and for a classification like the one we describe here, is usually the cross-entropy error. Then, by using a method called *back-propagation*, the neural network adapts the parameters of its hidden layers and sequentially continues the training process by accepting new input. By changing the parameters proportionally to the error, its parameters get adapted accordingly. A detailed analysis of the process that we describe above can be found in any machine learning textbook or review article (e.g., [Bishop and Nasrabadi, 2006, James et al., 2013, Mohri et al., 2018]).

[2]Problems with pre-labeled output such as this one are named supervised. Alternatively, if the output is not known *a priori*, they are called unsupervised.

From a purely mathematical perspective, ANNs are essentially flexible non-linear function approximators that can be tuned (trained) to mimic any kind of function consisting of multidimensional input and output. This makes them particularly useful in solving generalized optimization problems [Goodfellow et al., 2016].

Modern adaptations of neural networks include the use of convolution layers, allowing to more easily analyze visual imagery, and the average/max pooling data reduction layers forming the convolutional neural network (CNN) (see e.g., [Raptis et al., 2018]). Other adaptations use recurrent layers, corresponding to a recurrent neural network (RNN) to allow easier modeling of temporal sequences like voice recognition and auto-complete text (see e.g., [Yeakel et al., 2022]). Finally, in the last few decades, the addition of physical information by introducing physical laws in the form of differential equations in the loss function has inspired the development of physics-informed neural networks (PINNS) [Raissi et al., 2019, Karniadakis et al., 2021, Markidis, 2021]. These architectures have multiple applications already in many scientific fields, and very recently also in magnetospheric research (e.g., [Camporeale et al., 2022]).

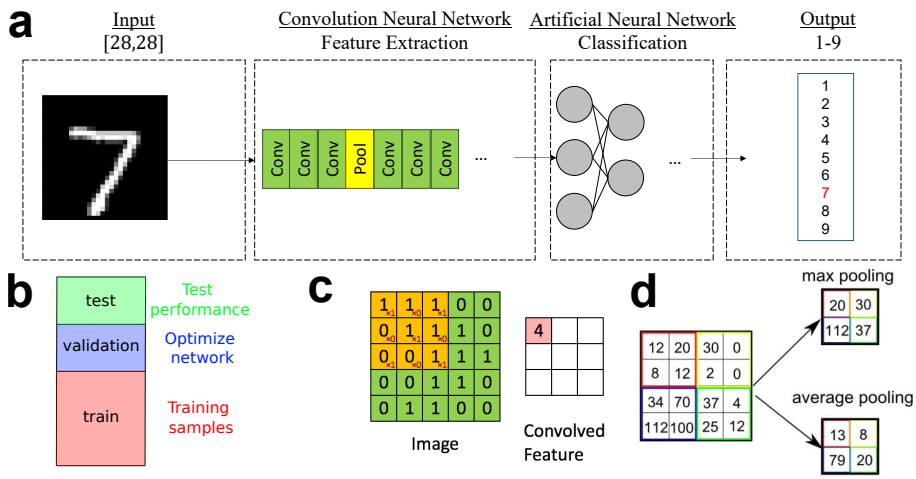

Figure 6.2: (**a**) Visualisation of a convolutional neural network (CNN) classifying the number 7 of the MNIST database. (**b**) A typical split of the dataset with $\sim 25\%$ of data corresponds to validation and testing sets and the remaining $\sim 50\%$ form the test set. (**c**) Example of the convolution process used during feature extraction. (**d**) Examples of maximum and average max pooling layers used for dimensionality reduction. Sub-figures **c** and **d** are credited to Sumit Saha.

For Paper II, we used Google's library TensorFlow [Abadi et al., 2015] and its high-level API Keras [Chollet, 2015] to model a neural network. Examples of how to use Keras to solve supervised learning problems such as the one using the MNIST

database described above can be easily found online[3]. An illustration of how a CNN is used to classify the MNIST database, along with some additional information of the modeling process, is shown in Figure 6.2.

6.5 Plasma moment derivation

Velocity moments derived from distributions can be used to quantify and evaluate bulk properties of plasmas, used for single and multi-point data analysis. In principle, one can derive single-species fluid moments through the measured VDFs of ions and electrons. These moments correspond to number density (0^{th} moment), bulk velocity(1^{st} moment), pressure tensor (2^{nd} moment) and heat flux tensor (3^{rd} moment), while the charge density and current density may also be computed. In our work (Paper VI), we derived the ion density, velocity and temperature (from the trace of the pressure tensor).

$$n = \int f(\mathbf{v}) d^3v \tag{6.7}$$

$$\mathbf{v}_b = \frac{1}{n} \int \mathbf{v} f(\mathbf{v}) d^3v \tag{6.8}$$

$$T = \frac{m}{3k_B n} \int (\mathbf{v} - \mathbf{v}_b) \cdot (\mathbf{v} - \mathbf{v}_b) f(\mathbf{v}) d^3v \tag{6.9}$$

It should be noted that T in this case can be calculated for any type of distribution. However, it is not the same temperature as described under a thermodynamic framework. Only under the assumption that plasma is in a thermal equilibrium and can be effectively modeled by a Maxwellian velocity distribution (2.19), a temperature derived from plasma moments is in agreement with thermodynamics $\left(T = \frac{m\langle v \rangle^2}{2k_B}\right)$.

Calculating moments is not a trivial task, since there can be several errors involved. These can include errors originating from the energy binning of the instrument, directional resolution, time variations, photo-electrons, spacecraft charging, calibration errors and even different ion composition [Paschmann et al., 1998, Gershman et al., 2015].

Furthermore, the computation of moments may sometimes provide information that is not very useful. For example, when there are simultaneous measurements of two different populations, the moments computed over the whole distribution do not properly characterize either of the populations. A typical and well-known

[3] e.g., `https://github.com/SavvasRaptis/machine-learning-examples`

example of this can be found upstream of the quasi-parallel shock at the foreshock region. If one computes the full moments, then a lower velocity compared to the pristine solar wind can be found. However, that result is heavily influenced by the reflected particles from the shock presence. As a result, in these environments, *partial moments* can be useful, where part of the distribution is used for the computation of the moments rather than the whole VDF (e.g., [Liu et al., 2017, Liu et al., 2022a].

An alternative way to estimate macroscopic quantities that describe plasmas such as bulk velocity, density, and temperature is by fitting a distribution function to the model and estimating the parameters via essentially solving an optimization problem. In the simplest case of a Maxwellian distribution in 1D (2.18), one can fit this expression to reduced (integrated) 1D VDFs and get meaningful estimates of quantities for the measured plasma. This technique can be particularly useful if more than one plasma population are measured, since multiple distribution can be fitted to consider the different populations. A typical example of this situation is the measurements of electron VDFs in the pristine solar wind. The SW can be modelled via assuming three distinct populations corresponding to a bi-Maxwellian distribution each (core, halo and strahl electrons). The resulted fitted quantities can provide information about the evolution of the different populations (e.g., [Abraham et al., 2022]).

Chapter 7

Magnetosheath jets

Magnetosheath jets are transient and localized dynamic pressure enhancements corresponding to a velocity and/or density increase relative to the background ambient magnetosheath. Most of the jet related research has been summarized in a relatively recent review article and aspects that we do not cover, such as the typical properties of jets or their morphology, can be found there [Plaschke et al., 2018]. However, since then, several studies that directly or indirectly contributed to the body of knowledge regarding magnetosheath jets have been published. In the sections below, we provide a brief introduction to the jet phenomenon. Some of the latest results are further discussed in the final chapter of this thesis.

7.1 Definition and nomenclature

As stated above, jets are dynamic pressure enhancements. Therefore, a typical definition can be formulated as:

$$P_{\mathrm{dyn}} \geq 2 \cdot P_{\mathrm{dyn,MSH}} \tag{7.1}$$

where $P_{\mathrm{dyn,MSH}}$ is typically defined through a moving mean or median value of a 10-20 minutes window (see e.g., [Archer and Horbury, 2013, Karlsson et al., 2015]. This is also the definition used in all the papers of this thesis.

However, the definition used in literature varies considerably (see discussion in [Plaschke et al., 2018]). Other works have used slightly different thresholds for the increase (e.g., 3 rather than 2 [Koller et al., 2022]) while others have used the upstream solar wind measurements to define a jet (see e.g., [Plaschke et al., 2013]). A good rule of thumb is to question what type of dataset is needed for the specific analysis that is conducted. If the goal for example is to analyze jets

close to the subsolar region, then a criterion based on the upstream solar wind measurements works well. However, at the flanks, the bulk flow of magnetosheath plasma accelerates, and its dynamic pressure exceeds the one upstream. Therefore, such a criterion would not be useful, since it would classify the whole flow as a "jet". It should be noted, that comparing different criteria can provide a very different dataset (see figure 6 of [Plaschke et al., 2018]). This should be taken under consideration when comparing statistical results.

Finally, apart from the definitions, there is a large variety of different terms used for magnetosheath jets. The first jets were reported in 1998, and were named "transient flux enhancements" [Němeček et al., 1998]. Since then, several names have been used, such as high kinetic energy jets [Amata et al., 2011], super-magnetosonic jets [Hietala et al., 2009] and embedded (density driven), or fast (velocity driven) plasmoids [Karlsson et al., 2012]. It should be noted that these terms (especially jet and plasmoid) are also typically used in other adjacent fields, for example in magnetic reconnection (e.g., [Samtaney et al., 2009, Khotyaintsev et al., 2019, Cozzani et al., 2021]) and in night-side bursty bulk flows (BBFs) (e.g., [Birn et al., 2011]) studies. Again, similarly to the definition, the context, and the plasma environment are vital when comparing "plasma jets" or "plasmoids".

7.2 Occurrence and origin

Jets are found downstream of the Qpar shock roughly 10 times more frequently than downstream of the Qperp shock [Vuorinen et al., 2019, Raptis et al., 2020b]. This is also shown in the SW conditions where a smaller θ_{Bn} is correlated to an increase number of jet observations as shown by numerous studies in the past (e.g., [Plaschke et al., 2013, Archer and Horbury, 2013, LaMoury et al., 2021]). Another upstream condition that seem to increase the jet occurrence, in particularly close to the magnetopause, is a high Alfvén Mach number (e.g., [Hao et al., 2016, LaMoury et al., 2021]). Although occurrence varies significantly, typically it is expected to obtain from 1 to 10 jets per hour of magnetosheath measurements[1]. Jets appear more frequently close to the shock than close to the magnetopause [Archer and Horbury, 2013, Palmroth et al., 2021] but upstream conditions influence how far they may reach. Specifically, for high solar wind speed and low θ_{Bn} many more will reach the magnetopause than usual [LaMoury et al., 2021]. Finally, the occurrence of jets also seems to vary with transient solar phenomena, namely solar flares, stream interaction regions (SIRs), and high-speed streams (HSSs). When magnetic ejecta of flares arrive at Earth, the number of jets seems to decrease, while during SIRs and HSSs an increased frequency has been observed [Koller et al., 2022].

Many models can describe how jets can be formed downstream of Earth's shock.

[1] [Archer and Horbury, 2013] reported 2% of their magnetosheath dataset being classified jets using THEMIS. A similar survey on the MMS dataset of Paper I showed matching results of $\sim 3\%$.

After all, a jet is effectively an observation of enhanced density and/or velocity, and this can be done through a series of different phenomena and associated effects. Therefore, there may not be a single, unique way to generate jets downstream of a shock, and depending on the observations and scales some mechanisms are more likely to be the origin than others. To discuss some ways jets form downstream of the shock, we separate the jets to those found downstream of Qpar shocks and those found downstream of Qperp.

At the Qperp MSH, the relatively rare jets are associated with a variety of different processes. Some of them may be linked to magnetic flux tubes which are connected to quasi-parallel transitions, while others include current sheets, reconnection exhausts, and mirror-mode waves [Blanco-Cano et al., 2020, Kajdič et al., 2021b]. Small-scale jets may also be connected to Qperp shock ripples like the ones we discuss in the previous chapter [Raptis et al., 2020b]. This, however, has not been established or observed for now.

At the Qpar MSH, jets are typically more common, more energetic, and have a longer duration [Raptis et al., 2020b]. Their origin has been connected to upstream rotational discontinuities [Dmitriev and Suvorova, 2012, Archer et al., 2012] that can change the foreshock location and therefore the local shock parameters such as θ_{Bn}, and Alfvén Mach number. Furthermore, jets could be associated with ripples of the Quasi-parallel shock [Hietala et al., 2009, Hietala and Plaschke, 2013]. Other suggestions include the association of jets to reconnection close to the shock [Preisser et al., 2020], or to foreshock phenomena such as HFA [Savin et al., 2012] and foreshock cavities [Sibeck et al., 2021].

More recently, the focus has been shifted to the connection of jet formation to the ion foreshock [Karlsson et al., 2015, Sibeck et al., 2021, Suni et al., 2021, Raptis et al., 2022] and to the global reformation process of the quasi-parallel shock [Preisser et al., 2020, Omelchenko et al., 2021, Raptis et al., 2022]. While a clear answer to which mechanism is most prominent is yet to be determined, it appears that the foreshock dynamics and the upstream waves modulating the shock properties are directly connected to the formation of dynamic pressure enhancements in the magnetosheath region. An example of a hybrid simulation showing a magnetosheath jet reaching the magnetopause is shown in Figure 7.1a. On the same figure, panel b illustrates a secondary bow shock/wave upstream of the Earth's bow shock due to a foreshock transient and downstream due to the increased velocity of a jet. Finally, Figure 7.1c shows a typical jet measured by MMS1 at the turbulent quasi-parallel magnetosheath.

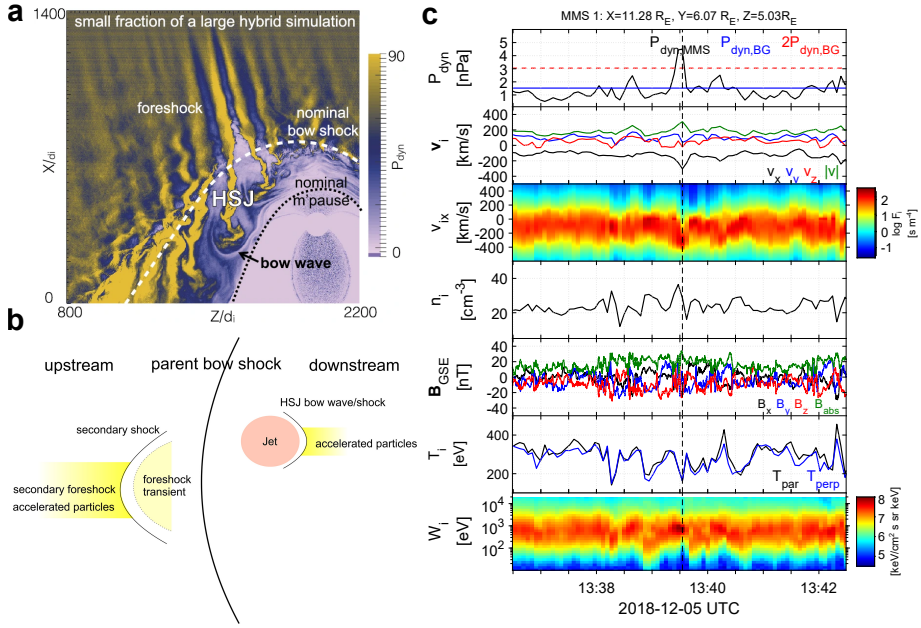

Figure 7.1: (**a**) Example of a hybrid simulation illustrating the presence of a magnetosheath jet, abbreviated as high-speed jet (HSJ). Taken from the simulation run by [Karimabadi et al., 2014]. (**b**) Schematic of secondary bow shocks/waves caused by the upstream foreshock transient and the downstream jets. Reproduced from [Liu et al., 2020a]. (**c**) Typical example of a Qpar magnetosheath jet observed by MMS1. (Top — bottom): ion dynamic pressure, ion velocity vector, reduced VDF in the x GSE direction, ion number density, magnetic field vector, ion temperature, and ion differential energy spectrum. Reproduced from Paper VI

7.3 Importance to shock and magnetospheric physics

The study of magnetosheath jets has been motivated by several factors. First, they provide a fascinating environment where mixing of plasma can occur, allowing fast SW-like plasma to reach the magnetosphere without being decelerated like the rest of the MSH plasma. Furthermore, as we discussed above, collisionless shocks are the origin of jets, and in a sense jets can be viewed as solar wind packets slipping through the bow shock and directly reaching the magnetosphere. Thus, jet research is directly connected to collisionless shock research and therefore to problems that are relevant to other fields, such as the acceleration of cosmic rays [Morlino and Caprioli, 2012, Ginzburg and Syrovatskii, 2013].

As jets form and propagate towards the magnetopause, they may drive bow waves in front of them, accelerating electrons [Liu et al., 2019b, Liu et al., 2020b, Liu

et al., 2020a,Vuorinen et al., 2022] and interacting with the ambient magnetosheath, changing the direction of the background flow and magnetic field [Plaschke et al., 2017, Plaschke et al., 2020, Katsavrias et al., 2021]. Some of them manage to reach the magnetopause, where they interact with it and possibly initiate magnetopause reconnection [Hietala et al., 2018, Escoubet et al., 2020, Vuorinen et al., 2021, Ng et al., 2021]. Furthermore, they may even contribute to direct plasma penetration, allowing magnetosheath plasma to enter the magnetospheric region [Gunell et al., 2012, Dmitriev and Suvorova, 2015, Karlsson et al., 2015]. Jets have also been associated with effects in the inner magnetosphere and ionosphere, causing localized flow enhancements [Hietala et al., 2012], magnetospheric compression, and aurora brightening [Wang et al., 2018]. A magnetosheath jet has also been connected to the generation of a substorm [Nykyri et al., 2019], while an association between jets and ground magnetometers observations was also recently reported [Norenius et al., 2021]. Finally, we should also mention that jets have been associated with the excitation of wave modes both in the magnetosheath and in the outer magnetosphere environment [Gunell et al., 2014, Archer et al., 2019, Katsavrias et al., 2021, Archer et al., 2021]. We speculate on this more in the discussion chapter.

Chapter 8

Summary of the included papers

Below, a summary of the appended papers is presented.

Paper I – Classifying Magnetosheath Jets Using MMS: Statistical Properties

In Paper I, we studied the different classes of magnetosheath jets and how their properties vary between each category. The classification was based on whether the jet was found downstream of the quasi-parallel or the quasi-perpendicular shock. Since the MMS separation does not typically allow simultaneous measurements of upstream solar wind and downstream magnetosheath, it was not possible to estimate the angle between the bow shock's normal vector and the IMF (θ_{Bn}) with certainty. As a result, we developed a methodology of classifying local magnetosheath measurements based on in-situ measurements. The algorithm used a combination of different quantities to classify the magnetosheath regions. These included the high-energy ion differential energy flux, the magnetic field variance and the ion temperature anisotropy. In this manner, we generated a classified dataset of magnetosheath jets[1] with which we statistically analyzed the different classes of jets using fast/survey measurements.

Based on our statistical observations, we concluded that jets downstream of the *Quasi-parallel* shock are the most common and energetic. They typically have a velocity (earthward) and density increase and could be connected to both ripples and foreshock structures (e.g., SLAMS). *Quasi-perpendicular* jets, on the other hand, appear to be mainly velocity-driven, with smaller duration and occur far less frequently. Their formation may be associated with magnetic reconnection or mirror mode wave activity. Jets found between Qpar and Qperp magnetosheath

[1] `https://zenodo.org/record/3739553`.

transitions were named *boundary* jets. They had similar properties to the Qpar jets, indicating a possibly common origin. Similarly to Qpar jets, their long duration and high dynamic pressure make them excellent candidates for the magnetospheric effects found in previous studies. The last category was named *encapsulated* jets. These high dynamic pressure structures were found in a Qpar-like plasma, while the surrounding magnetosheath had Qperp-like properties. They are the least common type, and are primarily velocity-driven, with $\sim 50\%$ of them exhibiting a density decrease. Their origin could be connected to either the outer magnetosphere vertices, dayside magnetopause reconnection or rapid changes of the IMF that cause a swift foreshock buildup in different upstream locations.

We concluded that previously hypothesized generation mechanisms such as the connection to bow shock ripples and foreshock structures are statistically supported. However, there were properties that could not be explained, indicating that other phenomena such as waves and instabilities along with acceleration mechanisms might play an important role in jets' formation and evolution.

Contribution: I organized the study, performed the data analysis and wrote the article with the help of edits and comments by the co-authors.

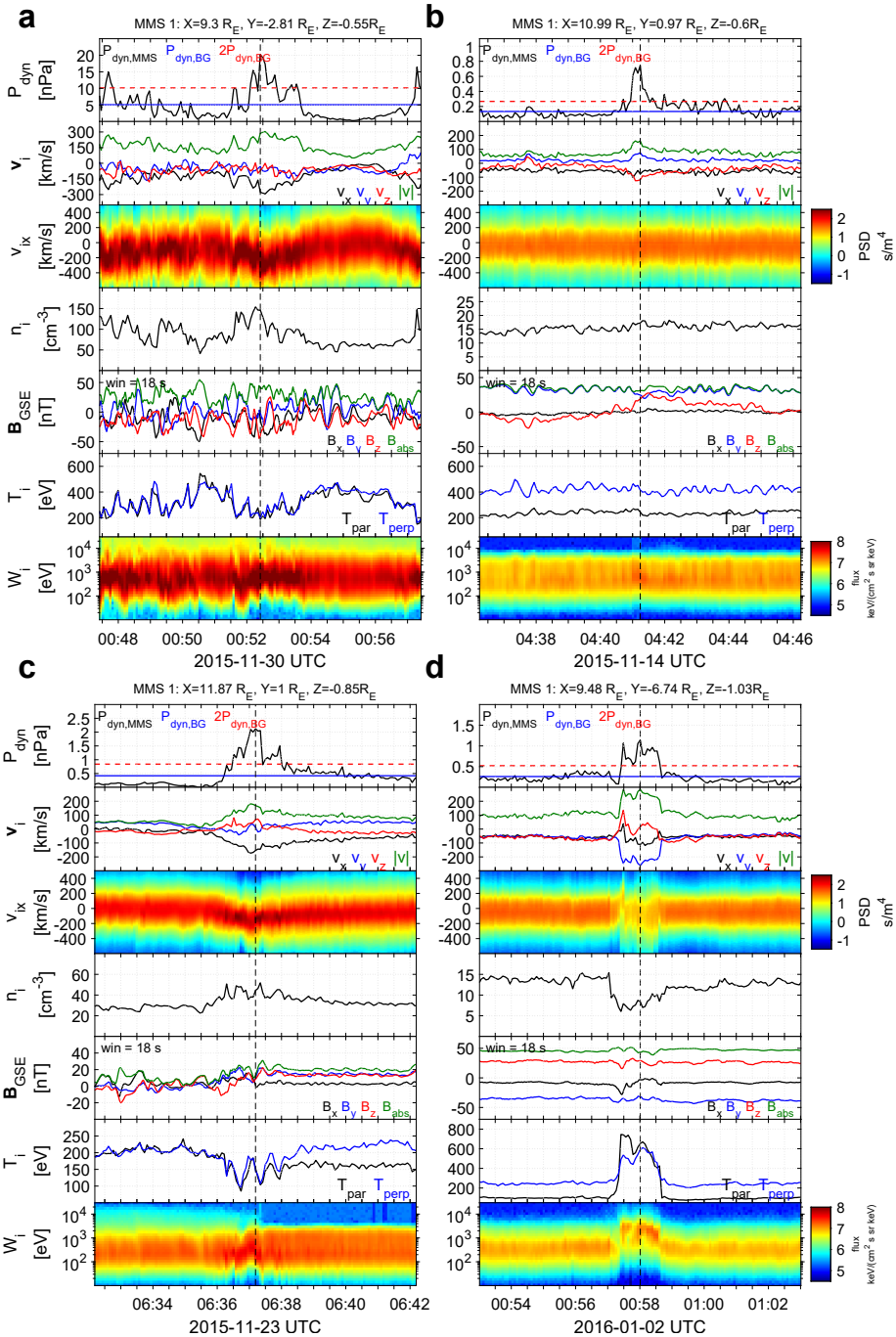

Figure 8.1: Examples of a quasi-parallel (**a**), quasi-perpendicular (**b**), boundary (**c**) and encapsulated (**d**) jet. (Top — bottom): ion dynamic pressure and background ambient level, ion velocity in GSE coordinates, reduced 1D VDFs in the x GSE direction, ion number density, magnetic field measurements, ion temperature, and ion differential energy spectrum. Adapted from figure 2 of [Raptis et al., 2020b].

Paper II – Classification of Magnetosheath Jets Using Neural Networks and High Resolution OMNI (HRO) Data

In Paper II, we used a machine learning technique (neural networks) to classify the jets obtained from the methodology of Paper I. In particular, we focused on differentiating between quasi-parallel (class 1) and quasi-perpendicular (class 2) jets. Methodologically, the work corresponds to a supervised binary classification problem, which is addressed by modeling an artificial neural network. The input used was OMNIweb upstream measurements, and the output was the class of the jet observed by MMS (see Paper I). To compare the accuracy of the neural networks, we also implemented 3 different standard techniques for the determination of the downstream characterization, namely approximating θ_{Bn} via the cone angle, making a bow shock model, and using the coplanarity method (see Chapter 6)

Our results showed that neural networks (Figure 8.2a) outperformed all the other methods, as shown in Figure 8.2b. It was found that the number of misclassifications was much lower when using a neural network compared to the other methods. Furthermore, we discovered that an accurate prediction of the jet class can be obtained even in the absence of upstream magnetic field measurements (IMF) from the input space. This was at first glimpse surprising since at least theoretically the determination of whether a shock crossing will be quasi-parallel or quasi-perpendicular is fully determined by the IMF vector and the bow shock normal vector. However, as we discuss in the article, three explanations could justify this result. The most probable is that the jets are occurring under specific solar wind conditions, and the neural network is capable of recognizing the pattern corresponding to the combination of upstream parameters associated with each class. Another reason would be that Qpar and Qperp jets are fundamentally easier to be observed under specific conditions, simply because their definition is threshold-based. Since their criterion relies on a percentage increase, a very low velocity and density environment would require a smaller absolute increase. Such biases could exist in our dataset, and in that case, the neural network would exploit them. Finally, one of the most intriguing suggestions is that different solar wind classes exist, corresponding to plasma properties that favor the generation of a particular IMF. This in turn can adapt the foreshock formation and produce different Qpar and Qperp shock transitions taking place upstream of the MSH jet observations.

Contribution: I organized the study, performed the data analysis and wrote the article with the help of edits and comments by the co-authors.

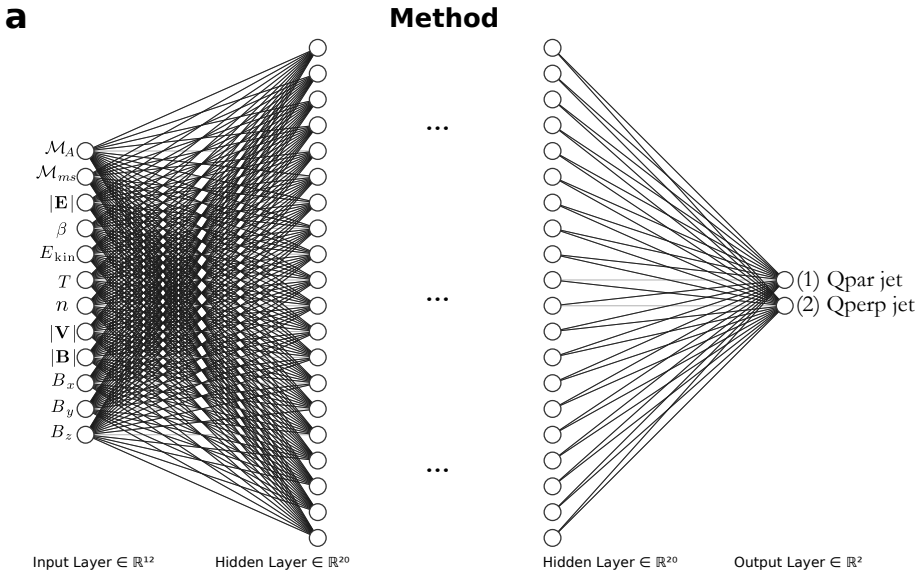

b **Results**

Class	Neural network (B) (%)	Neural network (No -B) (%)	θ_{cone} (%)	Coplanarity (%)	Modeling (%)
Qpar	98	95	61	81	74
Qperp	88	87	94	79	86

Figure 8.2: (**a**) Schematic of the neural network architecture, input, and output that was used. (**b**) Results of the classification made by the neural network with and without IMF as input, along with the results by the $\theta_{\rm cone}$, coplanarity method, and bow shock modeling methods. Adapted from figure 3 and tables 4 and 5 of [Raptis et al., 2020a].

Paper III – Magnetosheath Jet Evolution as a Function of Lifetime: Global Hybrid-Vlasov Simulations Compared to MMS Observations

In Paper III, we compared the statistical properties of magnetosheath jets observed by MMS with the ones simulated by the Vlasiator global-Vlasov model. Compared to the dataset introduced in Paper I, we had to post-process the dataset to better resemble the initial (upstream) condition set by Vlasiator simulations. Doing so, we used 6142 jets from MMS and 924 jets from Vlasiator and compared them statistically. An example of how jets are observed in measurements and in simulations is shown in Figure 8.3.

Our results showed that Vlasiator is in quantitative agreement with MMS observations. After confirming that the physical picture of the jet phenomenon is well captured by Vlasiator, we used the simulated measurements to see how jets evolve while propagating in the magnetosheath region. We showed how the jet density, dynamic pressure and magnetic field magnitude decrease as they travel towards the magnetopause. Furthermore, the shape of jets gets more flattened while they maintain their speed and direction. Moreover, we showed that for low upstream Alfvén Mach numbers, jets in Vlasiator are shorter and have a lower dynamic pressure and absolute magnetic field compared to the ones simulated with high Alfvén Mach numbers. Finally, the overall statistics of the Vlasiator jets showed that jet flows are typically colder than the surrounding plasma, similar to what has been previously reported in other observational works (e.g., Paper I).

Contribution: I performed the data analysis of the MMS measurements. I also wrote parts of the article concerning the determination and analysis of the observations. Finally, I contributed to the discussion and conclusions of the paper.

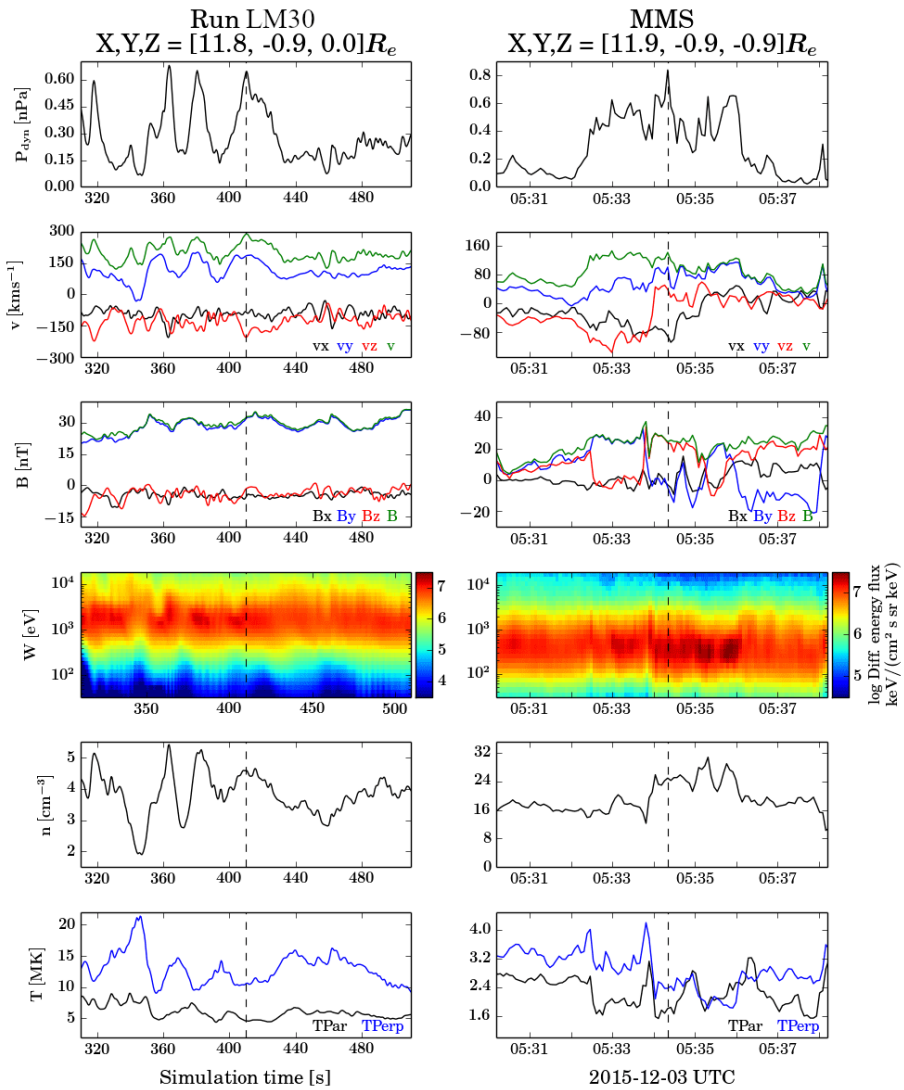

Figure 8.3: Examples of a quasi-parallel jet as shown by Vlasiator (left), and MMS (right). (Top — bottom): ion dynamic pressure, ion velocity in GSE coordinates, ion number density, magnetic field measurements, ion differential energy spectrum, ion number density and ion temperature. Reproduced from Figure 2 of [Palmroth et al., 2021].

Paper IV – On The Generation of Pi2 Pulsations due to Plasma Flow Patterns Around Magnetosheath Jets

In Paper IV, we focused on a case-study event, using THEMIS measurements, showing a magnetosheath jet associated with Pi2 pulsations that first appear in the magnetosheath region and later in the magnetosphere. THEMIS-A resides in the turbulent magnetosheath, observing pulsations in two frequency ranges (7.6 -9.2 and 12-17 mHz). These pulsations were found to be associated with the after flow (AF) of the jet, corresponding to a stagnated flow occurring immediately after the jet observation downstream of a quasi-parallel shock crossing (Figure 8.4). While the observations of the jet correspond to a typical quasi-parallel magnetosheath plasma, the upstream IMF has a clear rotation which indicates that THEMIS-A resides downstream, in proximity to the boundary of the ion foreshock.

After performing cross-wavelet analysis with THEMIS-D which was located inside the magnetosphere, it was found that the pulsations were coherently observed inside the magnetosphere with a 140-second time lag. The propagation time corresponds to a disturbance travelling approximately at the same speed as the computed Alfvénic speed. These results suggest that high-speed jets and their interaction with the background magnetosheath are associated with the excitation of irregular pulsations in the Pi2 frequency range. While the origin of these pulsations could not be determined due to the lack of upstream measurements, we argue that the frequency range is such that it makes a foreshock origin unlikely. As a result, the interaction of the jet with the background flow is a more probable cause, allowing the waves to be generated locally in the magnetosheath.

Contribution: I did part of the data analysis regarding the characterization of the magnetosheath jet and its surrounding plasma environment. I generated and motivated Figure 1 of the manuscript. Finally, I contributed to the writing of the discussion and conclusions of the article.

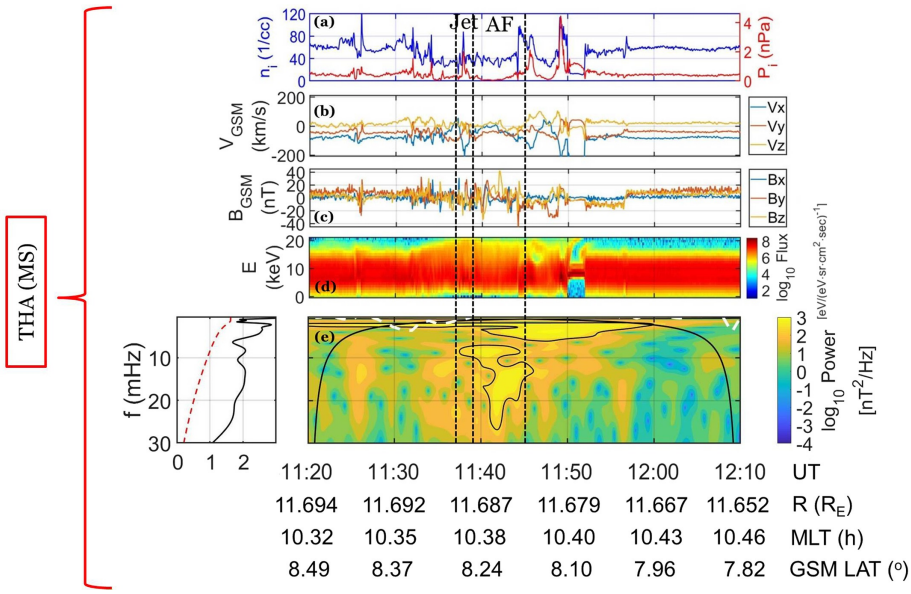

Figure 8.4: Observations of THEMIS-A residing in the magnetosheath. (Top — bottom): (a) ion density and dynamic pressure, (b) ion velocity, (c) magnetic field vector, (d) ion energy spectrum, (e) wavelet spectrum of $\mathbf{B}^2$. Confidence intervals (CI) are provided as black solid lines for the wavelet spectrum of panel (e) and as red dotted line for the left panel. The horizontal dotted lines indicate the jet observations and the after flow (AF) region. Adapted from Figure 2 of [Katsavrias et al., 2021].

Paper V – Downstream High-speed Plasma Jet Generation as a Direct Consequence of Shock Reformation

In Paper V, using MMS, we showed how the bow shock's cyclic behavior along with the evolution of its upstream waves can generate high-speed jets in Earth's magnetosheath. To do so, we used all MMS spacecraft during a string-of-pearl campaign in order to accurately observe the formation of a magnetosheath jet close to the bow shock. Due to the larger than usual separation, we were able to capture a fortunate case in which MMS2 resides upstream of the shock while MMS3 observed the equivalent downstream (shocked) plasma.

As shown in Figure 8.5a the shaded red area (1) corresponds to a compressive magnetic structure (i.e. a SLAMS) forming the local bow shock front. The same structure is observed from all the MMS satellites, starting from furthest from the Earth (MMS2) all the way to MMS3. By cross-correlating the magnetic field signals, we showed how structure (1) is moving towards the Earth. While structure (1) moves downstream, a new shock front emerges, initially observed by MMS4, by the shaded area number (2). This new structure encloses the solar wind and completes a reformation cycle. The solar wind along with its initially upstream foreshock waves are now effectively downstream of the new shock front, giving rise to a magnetosheath jet (Figure 8.5b).

The jet has typical properties when viewed by the FPI measurements, with an increase in both density and velocity corresponding to an increase of $\sim 200\%$ in dynamic pressure. Furthermore, a partial moment derivation showed that the velocity of the jet remains supermagnetosonic with respect to the Earth, indicating the origin of the jet to be the undisturbed upstream solar wind. The presented generation mechanism showed that downstream jet observations are a result of the evolution of the upstream waves found in the solar wind, along with its entrapment by the cyclic reformation of the quasi-parallel bow shock.

Contribution: I organized the study, performed the data analysis and wrote the article with the help of edits and comments by the co-authors.

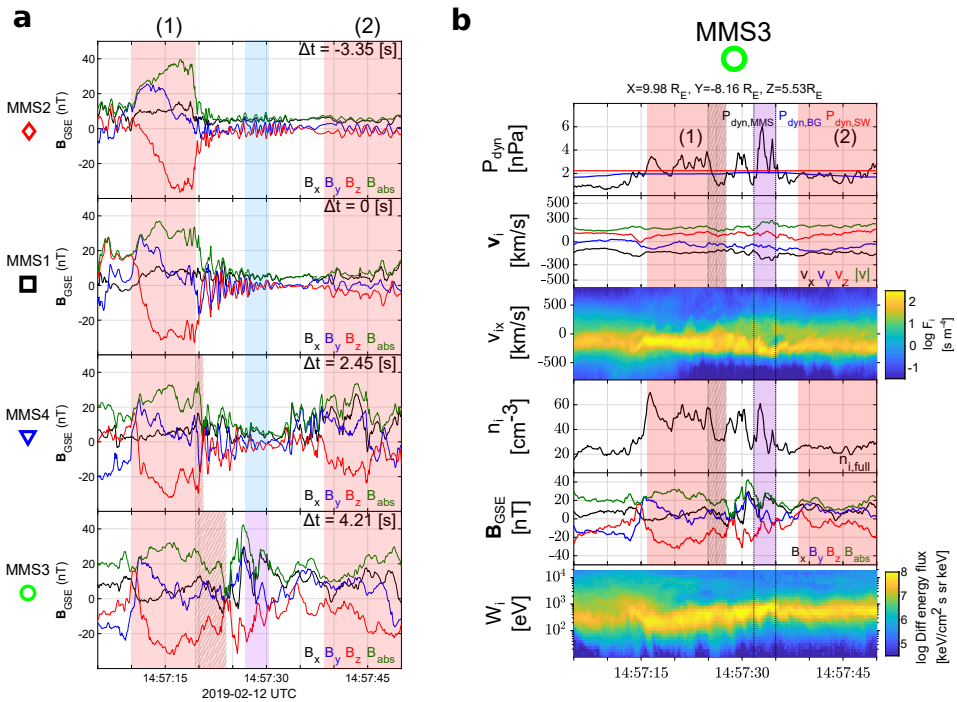

Figure 8.5: (**a**) (Top — bottom): magnetic field measurements for MMS2, MMS1, MMS4, and MMS3. All measurements are time-shifted with respect to MMS1 (black square) and each panel indicates the time lag used for each spacecraft. (**b**) (Top — bottom): ion dynamic pressure along with solar wind and magnetosheath background level, ion velocity, reduced 1D Velocity Distribution Function (VDF) in the x GSE direction, ion number density, magnetic field measurements, and differential energy spectrum. The red-shaded regions correspond to the compressive structures acting as the local shock fronts, while the patterned red-shaded region show how the first structure evolved. The shaded blue region corresponds to the upstream waves observed by MMS1, 2 and 4 while the magnetosheath jet observation (purple) is observed by MMS3. Adapted from figures 6 and 7 of [Raptis et al., 2022].

Paper VI – On Magnetosheath Jet Kinetic Structure and Plasma Properties

In Paper VI, using MMS, we examined a typical jet downstream of the turbulent quasi-parallel magnetosheath and showed jets are inherently kinetic structures. In particular, we focus on the characterization and evolution of the jet velocity distribution function (VDF) and on the derivation of partial plasma moments. Our analysis showed that jets can have a highly variable VDF throughout their life. The measured VDFs exhibit both a cold/fast jet beam and a hotter/slower background magnetosheath population. As a result, the jet is shown to co-exist and interact with the background plasma, highlighting the limitations of the single fluid treatment used in previous studies.

To derive the partial moments in order to isolate the jet population from the background plasma, we used two different methods. The first approach was to cut parts of the VDF based on the measured thermal spread ("cut") and the other was to fit two Maxwellian distributions to characterize the two existing populations, the jet, and the background MSH independently ("fit"). The methods along with the derived partial moments are illustrated in Figure 8.6. The study of the partial moments and the corresponding VDFs showed that jets have properties more similar to the non-shocked upstream solar wind and its associated foreshock structures than previously thought, providing insight to their origin. Finally, we suggest that jets can drive waves by interacting with the magnetosheath and may also remain super-magnetosonic as they propagate towards the magnetopause, which could possibly allow them to drive shock waves close to the magnetosphere.

Contribution: I organized the study, performed the data analysis and wrote the article with the help of edits and comments by the co-authors.

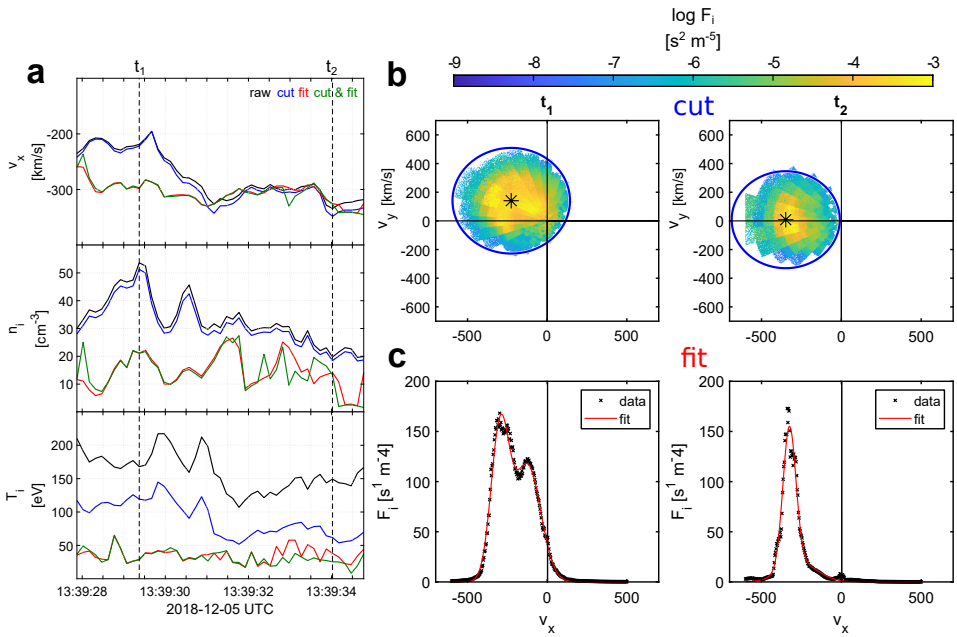

Figure 8.6: (**a**) (Top — bottom): ion velocity in the x GSE direction, ion number density and ion temperature from the original MMS full moments and for the three different approaches (fit, cut, cut & fit) discussed in Paper VI methodology section. The 1D reduced VDFs that are fitted are smoothed by averaging over $\pm$ 1 measurement points. The dotted lines show t_1 which is the time of maximum dynamic pressure and t_2 which is the time of maximum absolute velocity. (**b**) 2D reduced VDFs in xy GSE coordinates for t_1 and t_2 with removed data corresponding to measurements with higher velocity than a sphere with a radius of a thermal velocity (V_{th}). (**c**) 1D reduced VDFs in x GSE coordinate for t_1 and t_2 fitted with the sum of two Maxwellian distributions. The "cut & fit" method produced results that were virtually identical to the ones shown in panel (**c**). Reproduced from Figure 3 of Paper VI.

Chapter 9

Discussion and outlook

At the introduction, we stated that in this thesis we will be trying to answer three questions:

1. How do jets form?

2. What are their typical properties, and how are these related to Earth's bow shock?

3. How do jets evolve, and how do they interact with the magnetosheath plasma?

The questions have been addressed throughout the papers included in the thesis, but we will summarize the main points. Starting with the first question, we already mentioned that there can be more than one mechanism involved in the generation of jets. Our work provided observational evidence of a new mechanism for the generation of high-speed jets. As shown in Paper V, jets can form through the shock reformation and the evolution of upstream waves. This, however, does not rule out other mechanisms such as the association to ripples and even more to the connection with FCS that Papers I, III, and VI provided support for. FCS are essentially the building blocks of the reforming Qpar shock, making both mechanisms compatible.

In Papers I and II, we focused on the statistical properties of jets. In contrast to previous work, our analysis consisted of first classifying jets with respect to the geometry of the shock they originated from, before proceeding to analyze them. This new approach allowed us to see how Qpar jets have properties reassembling upstream foreshock structures (e.g., SLAMS) and undisturbed solar wind. Different statistical trends were obtained for other classes of jets, while the overall properties appear to vary considerably between each class. In Paper III, we continued the statistical investigation by comparing simulated data with observations.

Regarding the jet evolution, in Paper III, we also focused on how properties of simulated jets vary from their formation at the shock to the end of their journey at the magnetopause. The obtained variability, highlighted that the interaction with the background magnetosheath can have a clear effect on the jet development and on its properties. In Paper IV, we showed that it is not only the jet that gets affected, but also the background magnetosheath. It appears that magnetosheath jets can be connected to the excitation of Pi2 pulsations that are later observed inside the magnetosphere region. Finally, in Paper VI we showed in detail how jets are kinetic structures, affecting the magnetosheath and getting affected by their interaction with the ambient population. The measured VDFs can exhibit more than one plasma population (jet and background), highlighting the limitation of single fluid modeling. This result also showed that jets may drive waves and indicated the complexity of their anatomy.

In the process of addressing these questions, more objectives were obtained. While the statistical datasets used for Papers I, II, and III are available, an updated list with further description is provided. The current MMS jet dataset contains both fast/survey and burst measurements, and is described in the table 9.1, while it can be accessed by its associated Zenodo link[1] [Raptis, 2022]. This version of the dataset has not been peer-reviewed, and suggestions or questions are welcome. Below we discuss a few ways to use this list along with other available material to continue the investigation of magnetosheath jets and answer some of their unsolved long-lasting questions.

It should be noted that Papers V and VI are case studies taken from this list for cases that contained burst measurements. As a result, this dataset can be used not only for statistical research, but also to investigate particular cases of jets. Many of the results we showed in this thesis originated from the clear separation of jets in different classes. Such separation can reveal important properties. When dealing with a phenomenon that can originate from several different underlying processes, a classification is a vital pre-process step to conduct proper statistical analysis. As shown in Paper I, analyzing Qpar jets showed an anti-correlation between the temperature and velocity change of jets, indicating that jets can be viewed as "less heated" solar wind. Furthermore, a correlation between density and magnetic field increase was found, pointing towards a relation with foreshock structures that exhibit similar trends. An updated and clearer version of this result is shown with a subset of jets from the "border" category, shown in Table 9.1. In Figure 9.1 we used a small part of the dataset that we determined as being close, yet downstream of a quasi-parallel bow shock crossing. Such correlations would appear different, if not fully absent, if one takes all observed jets under consideration. For example, in the case of Qperp jets, an anti-correlation between maximum magnetic field and density difference was obtained. Combining such diverse datasets that most likely

[1] Accessible via `https://zenodo.org/record/7085778`.

Table 9.1: Classified dataset of magnetosheath jets observed by MMS1 during the period 05/2015 – 06/2020 (N=9196). Final cases correspond to the manually verified jets, used in the papers of this thesis. The number in a parenthesis correspond to the number of jets having full burst data available.

Subset	Number	Percentage (%)
Quasi-parallel	2928 (428)	31.8
Final cases	**901 (84)**	9.8
Quasi-perpendicular	1229 (34)	13.6
Final cases	**213 (3)**	2.3
Boundary	1505 (204)	16.4
Final cases	**191 (35)**	2.1
Encapsulated	67 (32)	0.73
Final cases	**60 (31)**	0.65
Other	3467 (753)	37.7
Unclassified	1921 (255)	20.9
Border	1500 (495)	16.3
Data Gap	46 (3)	0.5

originate from totally different mechanisms can provide misleading results.

Many questions on jet research still remain open, and most can be found in a recent review paper [Plaschke et al., 2018]. However, below, we briefly discuss the ones we find particularly interesting and relevant to the latest results of this thesis.

How are jets connected to the excitation of waves in the magnetosheath and magnetosphere region?

As shown in many studies (e.g., [Gunell et al., 2014,Archer et al., 2019,Archer et al., 2021], including Paper IV of this thesis, jets can excite waves both while propagating in the magnetosheath but also when they hit the magnetopause. Recently, it has been shown that in the turbulent Qpar magnetosheath whistler waves can be generated (e.g., [Svenningsson et al., 2022]). This result may be affected by the presence of jets that contain distributions similar to the ones shown in Paper VI (see, e.g., Figure. 8.6). Such non-Maxwellian VDFs can be found in Earth's MSH (e.g., [Graham et al., 2021]) and in other plasma environment have been shown to excite waves (e.g., comets [Odelstad et al., 2022]). However, it is very hard to determine whether waves associated with jets are directly caused by the jet or due to embedded magnetic structures from the foreshock region that may also be transmitted together. The exact relationship between fast plasma flows and wave excitation is important in magnetospheric physics, as fundamental phenomena such as magnetic reconnection appear to be affected by the presence of waves (e.g., [Graham et al., 2022]). A proper statistical analysis of different plasma environments

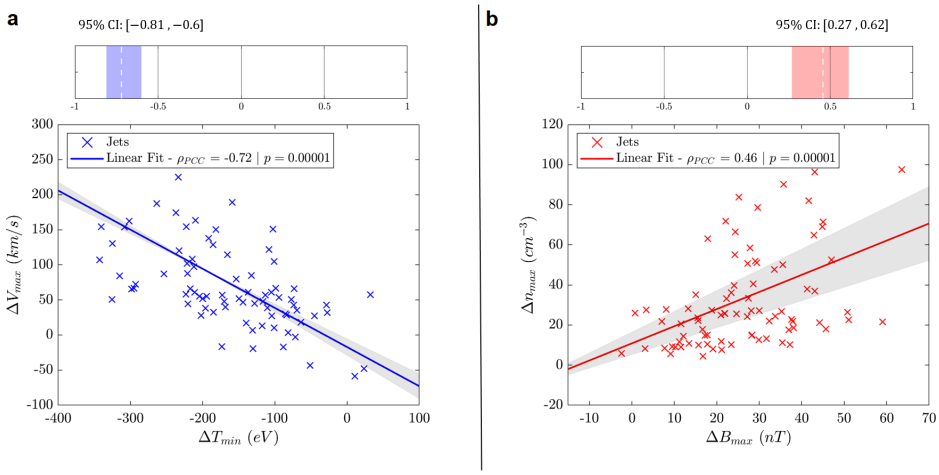

Figure 9.1: (**a**) Difference between the maximum observed ion velocity and the background one plotted against the difference between the minimum observed ion temperature and the background one. (**b**) Difference between the maximum observed ion density and the background one plotted against the difference between the maximum observed magnetic field magnitude and the background one. Linear regression lines are shown for visual guidance, while Pearson correlation coefficients, p-values and confidence intervals (CIs) are also included. The subset used for this plot contains Qpar jets found very close to a Qpar bow shock transition. *Unpublished results.*

with and without the presence of plasma jets could determine whether jets are a statistically significant factor for the excitation of waves locally or not. For the connection to magnetospheric effects, such statistical work is difficult due to the necessity of simultaneous measurements. As a result, global computer simulations may be a preferable approach.

How do jets properties evolve as they propagate in the magnetosheath?

Several studies have tried to address how properties and occurrence of jets change from the bow shock to the Earth (e.g., [Archer and Horbury, 2013, Palmroth et al., 2021, LaMoury et al., 2021]). For our part, in Paper VI we showed how the VDFs of a jet display an interaction with the background magnetosheath, indicating that its properties will most likely change as it propagates towards the magnetopause (Figure. 9.2). In Paper I, we also discussed how certain classes of jets are more prominent at different distances from the bow shock and magnetopause, possibly contributing to the difference in their statistical properties. However, there are still open questions to be addressed. The next step in determining the evolution of jets

in the magnetosheath could consist of the evaluation of the kinetic properties of jets as simulated by hybrid simulations or through the usage of conjunctions of different satellite missions. Such conjunctions can offer complementary measurements to see how a jet observed in different stages of its life changes as it interacts with the background magnetosheath.

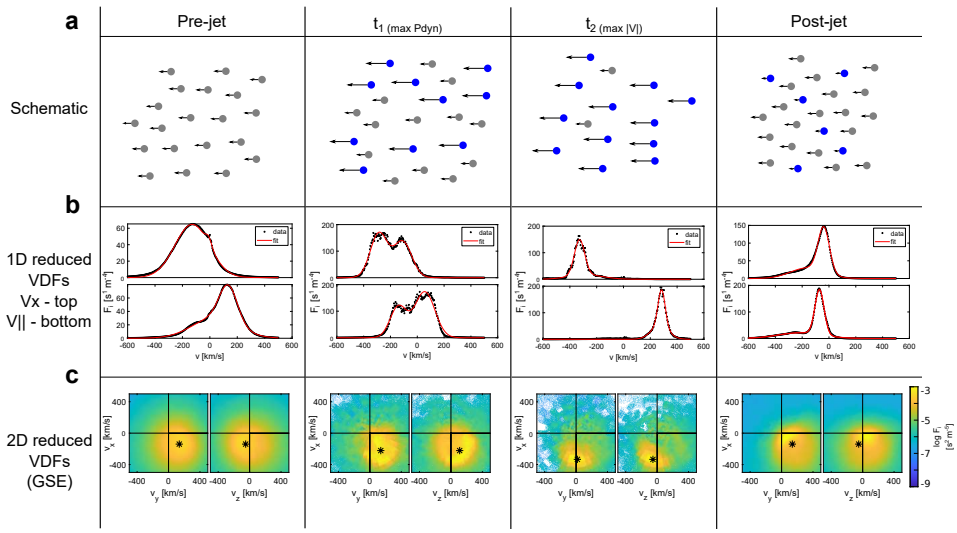

Figure 9.2: Illustration of the evolution of a jet compared to the background magnetosheath. Jet observations from MMS are shown for four different occasions. (Left — right): Pre-jet magnetosheath corresponding to average distribution of 50 measurements during 13:39:14 – 13:39:21 of 2018-12-5, t_1 corresponding to the peak of ion dynamic pressure, t_2 corresponding to the peak of absolute ion velocity, post-jet magnetosheath corresponding to an average distribution of 40 measurements during 13:39:41 – 13:39:47 of 2018-12-5. (**a**) Schematic of the interaction and the corresponding density/velocity profiles of the jet and background magnetosheath population. Blue circles represent the jet population and gray the background magnetosheath. (**b**) 1D reduced VDFs in x GSE coordinates and parallel to the magnetic field. (**c**) 2D reduced VDFs in GSE coordinates. Reproduced from Figure 4 of Paper VI.

What is the connection between foreshock structures and magnetosheath jets?

Recently, it was argued that up to 75% of jets can be connected to foreshock compressive structures (i.e., shocklets, SLAMS etc.) [Suni et al., 2021]. In Paper V we essentially provided observational evidence that reformation of the shock can generate downstream jets. Simultaneously, we showed an example of a SLAMS also being potentially classified as a jet due to its enhanced density. According

to these results, the components of the shock (FCS) or its non-stationary nature (reformation) are causing jets to form. However, there are still observations of jets that have a considerable duration (and therefore size) that make them unlikely to be originating from these mechanisms (see e.g., MMS observations of [Escoubet et al., 2020]). A jet with a duration of more than 30 seconds and a velocity of higher than 300 km/s corresponds to scales that are significantly higher than those for example reported for SLAMS. These could perhaps result from a large-scale reformation process and FCS pileup combined effect. However, there are cases where the jet duration and associated magnetic field do not have such signatures (see e.g., Figure 8.1(d)). Can these large-scale jets be the ones associated with large scale Qpar ripples or with rotational discontinuities? While significant efforts have been made in the last few years, there is still no clear answer. Determining how prominent each mechanism is requires a more detailed approach. Specific predictions of scales and properties need to be made for each mechanism. Then, these predictions can be tested with observations to provide a confidence level for the likelihood of each mechanism. Another approach would require 3D simulations to be made in order to capture events such as ripples and reformation in their full extent and compare the different properties observed. This could be done similarly to previous works (e.g., [Hao et al., 2017,Preisser et al., 2020]) but with a global view and a statistical approach.

Are jets a universal collisionless shock phenomenon?

Apart from Earth's bow shock, collisionless shocks can occur in laser-driven experiments (e.g., [Boella et al., 2021, Yamazaki et al., 2022]) and reformation has been observed even in laboratories (e.g., [Yao et al., 2021]). One could then hypothesize that if jets are fundamentally connected somehow to the foreshock or the reformation process (e.g., [Raptis et al., 2022]), maybe small-scale high-speed jets are also a universal property of collisionless shocks. Also, in principle similar phenomena can appear in some other planetary (e.g., Mercury: [Karlsson et al., 2016]), astrophysical, and even laboratory shocks (see discussion in [Plaschke et al., 2018]). However, with the very few studies available, and the very different shock environments, it is hard to directly answer this question. Simulations that cover a wide range of shock parameters could provide insight on this issue. Furthermore, with future missions and with collaborations of fields that work with different shock environments, proper investigations can take place to provide a definitive answer.

What are the magnetospheric effects of jets?

Very recently, several articles have focused on the effects of dayside transient phenomena on the inner magnetosphere. These include review papers (e.g., [Zhang et al., 2022]) and research articles (e.g., [Wang et al., 2022]). However, most of these studies fail to address the connection these phenomena have to magnetosheath high-speed jets. Similarly, high-speed jets research focusing on magnetospheric effects,

fail to address the connection with foreshock and solar wind transients (e.g., [Norenius et al., 2021]). This is expected since the main expertise of each research group is typically focused on a specific phenomenon/environment. The same issue essentially applies to the work presented in this thesis. As a result, we still do not have a clear answer whether it is jets or other phenomena (e.g., associated foreshock transients) that are the underlying cause of the observable magnetospheric effects. Similar to the wave excitation discussion above, to unravel the situation, a careful statistical study needs to be done where the presence of either or both phenomena take place. As this is difficult due to the data availability, simulations would be a better candidate to provide initial indications.

9.1 Outlook and final words

In this thesis, we have investigated the origin and properties of magnetosheath jets. The MMS mission and its state-of-the-art instrument provided us with opportunities to investigate these issues in a novel way. The next step of jet research but also of the general space, shock and magnetospheric observational field greatly relies on the availability of well-organized datasets. There are considerable efforts made to provide such datasets, like the SHARP project[2], where one can obtain a shock database with MMS, Cluster, and THEMIS data (see also [Lalti et al., 2022a]). Similar efforts have been made to provide classified plasma regions (e.g., for MMS [Breuillard et al., 2020, Olshevsky et al., 2021]). Such openly available datasets are vital to conduct conjunction studies and to combine the data products of several missions. These datasets can also be combined with inner magnetospheric missions such as the Van Allen probe (VAP) or the Arase[3]. Then researchers can do even more advanced conjunction studies and perform multi-mission investigations of phenomena that appear in vastly different environments. As we discussed briefly above, this is an intriguing approach to solve many of the open questions regarding jets. However, similar open questions exist for many transient events of foreshock and SW origin. Some of these, like shocklets, SLAMS, or magnetic Holes (MHs), may have similar effects as jets. As a result, similar conjunction-based studies could be applicable to these phenomena and may provide insight on their possible effects as well. An illustration of dayside transient phenomena and their relevance to the Earth's magnetospheric environment is shown in Figure 9.3.

In combination with the data sets described above, the usage of large-scale simulation projects, such as Vlasiator [Palmroth et al., 2018a] will certainly be useful in the efforts to tackle the current open questions. More projects have recently started working on the combination of different modeling techniques to address multi-scale issues (see discussion of Chapter 5) such as the MAGE model from the Center for

[2]Accessible via : `https://sharp.fmi.fi/`.

[3]Formerly known as Exploration of energization and Radiation in Geospace (ERG).

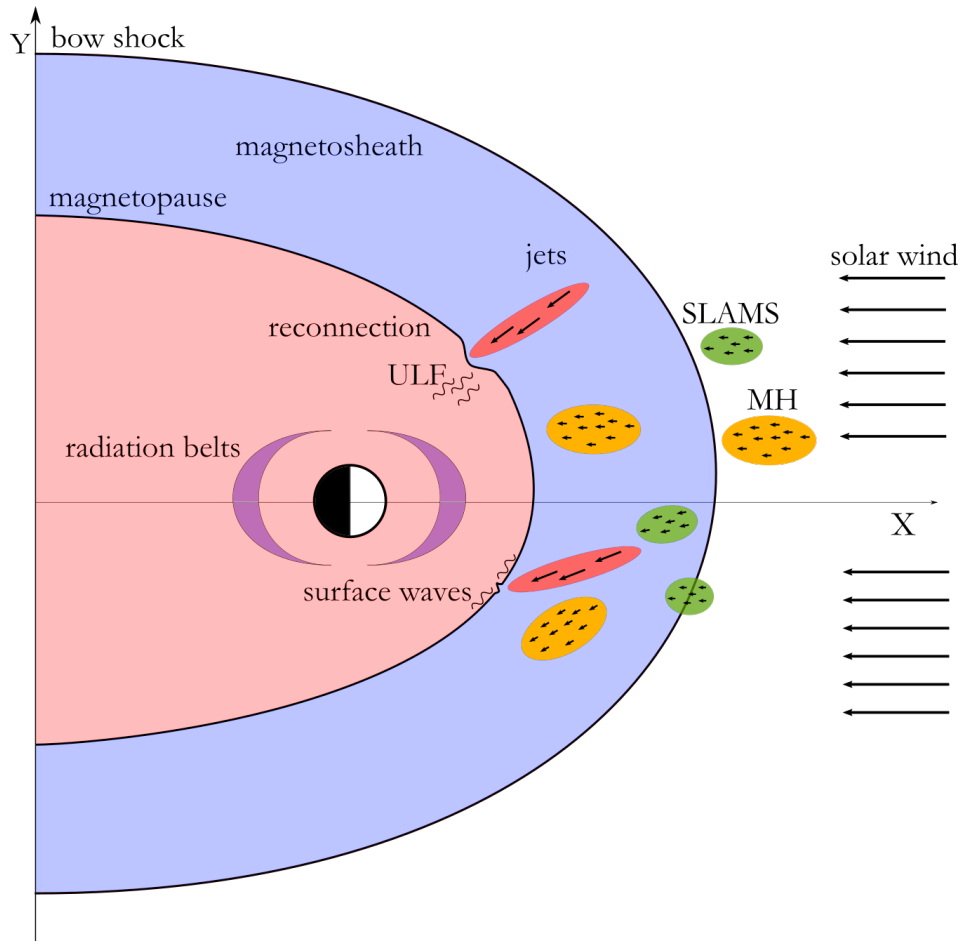

Figure 9.3: Illustration of the Earth's magnetospheric environment. The transient events appearing in the solar wind and magnetosheath region such as magnetosheath jets, SLAMS and MHs may be the cause of several effects observed throughout the geospace environment.

Geospace Storms[4]. Furthermore, the usage of observational data for the enhancement of computer modeling is also a very promising approach. This can be done through data mining (e.g., [Sitnov et al., 2021a, Sitnov et al., 2021b]) or through data assimilation techniques (e.g., [Kalnay, 2003, Millas et al., 2020, Zhelavskaya et al., 2021]).

The use of simulations can be motivated and amplified by the usage of datasets

[4]More information can be found via `https://cgs.jhuapl.edu/Models/mage.php`.

obtained though recent missions that explore different environments. For example, NASA's Parker Solar Probe launched in 2018 [Fox et al., 2016], and ESA's Solar Orbiter in 2020 [Müller et al., 2020], are two missions that will help to address various solar physics questions. On planetary environments, ESA's/JAXA's Bepi-Colombo launched in 2018 to study Mercury [Benkhoff et al., 2010] and NASA's MAVEN launched in 2013 to study Mars [Jakosky et al., 2015], are two notable missions that can be used to study the universality of the phenomena observed at Earth. Furthermore, future missions are also expected to contribute significantly. Examples are, ESA's Solar wind Magnetosphere Ionosphere Link Explorer (SMILE) that concentrates on measuring the solar wind and its interaction with the magnetosphere [Raab et al., 2016], or NASA's Sun Radio Interferometer Space Experiment (SunRISE) that focuses more on radio emission from the Sun [Kasper et al., 2021]. Directly relevant to collisionless shocks, there are ongoing proposed missions focusing on objectives that could also be extremely useful to tackle questions relevant to transient phenomena occurring close to shock environments. For example, the Multi-point Assessment of the Kinematics Of Shocks (MAKOS) mission has been suggested with a goal to understand the partition and conversion of energy at collisionless shocks.

Finally, regardless of the origin of a dataset, whether it is observational or computer simulated, the use of statistical applications in an automated way based on the utilization of supercomputers has been expanding in many fields. We very briefly touched the relevant topic of a particular machine learning algorithm (neural networks) in this thesis. However, there are many even more advanced techniques that are already used in physical research, such as physics-informed neural networks (e.g., [Camporeale et al., 2022]), generative adversarial networks (e.g., [Paganini et al., 2018]) and unsupervised learning approaches like self-organizing maps (e.g., [Innocenti et al., 2021]). These techniques should be carefully considered in future investigations, since they have already provided intriguing results and are widely used in many adjacent fields. The wide usage of these techniques is also accompanied by a rapid development, originating from different scientific fields, of both new applications (e.g., [Callaham et al., 2021]) but also of new evaluation metrics (e.g., [Chicco and Jurman, 2020]). Understanding the applicability of these advances is crucial for modernizing and developing any scientific field, including space physics. These new approaches along with proper physical understanding of the underlying phenomena can enable future research to answer not only jet related questions, but also to address fundamental collisionless plasma challenges.

References

[Abadi et al., 2015] Abadi, M., Agarwal, A., Barham, P., Brevdo, E., Chen, Z., Citro, C., Corrado, G. S., Davis, A., Dean, J., Devin, M., Ghemawat, S., Goodfellow, I., Harp, A., Irving, G., Isard, M., Jia, Y., Jozefowicz, R., Kaiser, L., Kudlur, M., Levenberg, J., Mané, D., Monga, R., Moore, S., Murray, D., Olah, C., Schuster, M., Shlens, J., Steiner, B., Sutskever, I., Talwar, K., Tucker, P., Vanhoucke, V., Vasudevan, V., Viégas, F., Vinyals, O., Warden, P., Wattenberg, M., Wicke, M., Yu, Y., and Zheng, X. (2015). TensorFlow: Large-scale machine learning on heterogeneous systems. Software available from tensorflow.org.

[Abdullah et al., 2020] Abdullah, M. H., Klypin, A., and Wilson, G. (2020). Cosmological constraints on ωm and σ8 from cluster abundances using the galwcat19 optical-spectroscopic sdss catalog. *The Astrophysical Journal*, 901(2):90.

[Abraham et al., 2022] Abraham, J. B., Owen, C. J., Verscharen, D., Bakrania, M., Stansby, D., Wicks, R. T., Nicolaou, G., Whittlesey, P. L., Rueda, J. A. A., Jeong, S.-Y., et al. (2022). Radial evolution of thermal and suprathermal electron populations in the slow solar wind from 0.13 to 0.5 au: Parker solar probe observations. *The Astrophysical Journal*, 931(2):118.

[Alexandrova et al., 2004] Alexandrova, O., Mangeney, A., Maksimovic, M., Lacombe, C., Cornilleau-Wehrlin, N., Lucek, E., Décréau, P., Bosqued, J.-M., Travnicek, P., and Fazakerley, A. (2004). Cluster observations of finite amplitude alfvén waves and small-scale magnetic filaments downstream of a quasi-perpendicular shock. *Journal of Geophysical Research: Space Physics*, 109(A5).

[Alho et al., 2022] Alho, M., Battarbee, M., Pfau-Kempf, Y., Khotyaintsev, Y. V., Nakamura, R., Cozzani, G., Ganse, U., Turc, L., Johlander, A., Horaites, K., et al. (2022). Electron signatures of reconnection in a global evlasiator simulation. *Geophysical Research Letters*, 49(14):e2022GL098329.

[Amano et al., 2020] Amano, T., Katou, T., Kitamura, N., Oka, M., Matsumoto, Y., Hoshino, M., Saito, Y., Yokota, S., Giles, B., Paterson, W., et al. (2020). Observational evidence for stochastic shock drift acceleration of electrons at the earth's bow shock. *Physical Review Letters*, 124(6):065101.

[Amata et al., 2011] Amata, E., Savin, S., Ambrosino, D., Bogdanova, Y., Marcucci, M., Romanov, S., and Skalsky, A. (2011). High kinetic energy density jets in the earth's magnetosheath: A case study. *Planetary and Space Science*, 59(7):482–494.

[Angelopoulos, 2009] Angelopoulos, V. (2009). The themis mission. In *The THEMIS mission*, pages 5–34. Springer.

[Angelopoulos, 2010] Angelopoulos, V. (2010). The artemis mission. In *The ARTEMIS mission*, pages 3–25. Springer.

[Archer et al., 2021] Archer, M., Hartinger, M., Plaschke, F., Southwood, D., and Rastaetter, L. (2021). Magnetopause ripples going against the flow form azimuthally stationary surface waves. *Nature communications*, 12(1):1–14.

[Archer et al., 2019] Archer, M., Hietala, H., Hartinger, M. D., Plaschke, F., and Angelopoulos, V. (2019). Direct observations of a surface eigenmode of the dayside magnetopause. *Nature communications*, 10(1):1–11.

[Archer and Horbury, 2013] Archer, M. and Horbury, T. (2013). Magnetosheath dynamic pressure enhancements: occurrence and typical properties. In *Annales Geophysicae*, volume 31, pages 319–331. Copernicus GmbH.

[Archer et al., 2012] Archer, M., Horbury, T., and Eastwood, J. (2012). Magnetosheath pressure pulses: Generation downstream of the bow shock from solar wind discontinuities. *Journal of Geophysical Research: Space Physics*, 117(A5).

[Archer et al., 2015] Archer, M., Turner, D., Eastwood, J., Schwartz, S., and Horbury, T. (2015). Global impacts of a foreshock bubble: Magnetosheath, magnetopause and ground-based observations. *Planetary and Space Science*, 106:56–66.

[Auster et al., 2008] Auster, H., Glassmeier, K., Magnes, W., Aydogar, O., Baumjohann, W., Constantinescu, D., Fischer, D., Fornacon, K., Georgescu, E., Harvey, P., et al. (2008). The themis fluxgate magnetometer. *Space science reviews*, 141(1):235–264.

[Balogh and Treumann, 2013] Balogh, A. and Treumann, R. A. (2013). *Physics of collisionless shocks: space plasma shock waves*. Springer Science & Business Media.

[Battarbee et al., 2020a] Battarbee, M., Blanco-Cano, X., Turc, L., Kajdič, P., Johlander, A., Tarvus, V., Fuselier, S., Trattner, K., Alho, M., Brito, T., et al. (2020a). Helium in the earth's foreshock: a global vlasiator survey. In *Annales Geophysicae*, volume 38, pages 1081–1099. Copernicus GmbH.

[Battarbee et al., 2020b] Battarbee, M., Ganse, U., Pfau-Kempf, Y., Turc, L., Brito, T., Grandin, M., Koskela, T., and Palmroth, M. (2020b). Non-locality

of earth's quasi-parallel bow shock: injection of thermal protons in a hybrid-vlasov simulation. In *Annales Geophysicae*, volume 38, pages 625–643. Copernicus GmbH.

[Baumjohann and Treumann, 2012] Baumjohann, W. and Treumann, R. A. (2012). *Basic space plasma physics*. World Scientific.

[Bell, 2004] Bell, A. (2004). Turbulent amplification of magnetic field and diffusive shock acceleration of cosmic rays. *Monthly Notices of the Royal Astronomical Society*, 353(2):550–558.

[Benkhoff et al., 2010] Benkhoff, J., Van Casteren, J., Hayakawa, H., Fujimoto, M., Laakso, H., Novara, M., Ferri, P., Middleton, H. R., and Ziethe, R. (2010). Bepicolombo—comprehensive exploration of mercury: Mission overview and science goals. *Planetary and Space Science*, 58(1-2):2–20.

[Birn et al., 2011] Birn, J., Nakamura, R., Panov, E., and Hesse, M. (2011). Bursty bulk flows and dipolarization in mhd simulations of magnetotail reconnection. *Journal of Geophysical Research: Space Physics*, 116(A1).

[Bishop and Nasrabadi, 2006] Bishop, C. M. and Nasrabadi, N. M. (2006). *Pattern recognition and machine learning*, volume 4. Springer.

[Blanco-Cano et al., 2020] Blanco-Cano, X., Preisser, L., Kajdič, P., and Rojas-Castillo, D. (2020). Magnetosheath microstructure: Mirror mode waves and jets during southward ip magnetic field. *Journal of Geophysical Research: Space Physics*, 125(9):e2020JA027940.

[Boella et al., 2021] Boella, E., Bingham, R., Cairns, R., Norreys, P., Trines, R., Scott, R., Vranic, M., Shukla, N., and Silva, L. (2021). Collisionless shock acceleration in the corona of an inertial confinement fusion pellet with possible application to ion fast ignition. *Philosophical Transactions of the Royal Society A*, 379(2189):20200039.

[Breuillard et al., 2020] Breuillard, H., Dupuis, R., Retino, A., Le Contel, O., Amaya, J., and Lapenta, G. (2020). Automatic classification of plasma regions in near-earth space with supervised machine learning: Application to magnetospheric multi scale 2016–2019 observations. *Frontiers in Astronomy and Space Sciences*, 7:55.

[Burch et al., 2016] Burch, J., Moore, T., Torbert, R., and Giles, B. (2016). Magnetospheric multiscale overview and science objectives. *Space Science Reviews*, 199(1):5–21.

[Burgess, 1989] Burgess, D. (1989). Cyclic behavior at quasi-parallel collisionless shocks. *Geophysical research letters*, 16(5):345–348.

[Burgess and Scholer, 2015] Burgess, D. and Scholer, M. (2015). *Collisionless Shocks in Space Plasmas: Structure and Accelerated Particles*. Cambridge Atmospheric and Space Science Series. Cambridge University Press.

[Callaham et al., 2021] Callaham, J. L., Koch, J. V., Brunton, B. W., Kutz, J. N., and Brunton, S. L. (2021). Learning dominant physical processes with data-driven balance models. *Nature communications*, 12(1):1–10.

[Camporeale et al., 2022] Camporeale, E., Wilkie, G. J., Drozdov, A. Y., and Bortnik, J. (2022). Data-driven discovery of fokker-planck equation for the earth's radiation belts electrons using physics-informed neural networks. *Journal of Geophysical Research: Space Physics*, 127(7):e2022JA030377. e2022JA030377 2022JA030377.

[Chao et al., 2002] Chao, J., Wu, D., Lin, C.-H., Yang, Y.-H., Wang, X., Kessel, M., Chen, S., and Lepping, R. (2002). Models for the size and shape of the earth's magnetopause and bow shock. In *Cospar Colloquia series*, volume 12, pages 127–135. Elsevier.

[Chen, 2012] Chen, F. F. (2012). *Introduction to plasma physics*. Springer Science & Business Media.

[Chen et al., 2021] Chen, L.-J., Wang, S., Ng, J., Bessho, N., Tang, J.-M., Fung, S. F., Le, G., Gershman, D., Giles, B., Russell, C. T., et al. (2021). Solitary magnetic structures at quasi-parallel collisionless shocks: Formation. *Geophysical Research Letters*, 48(1):e2020GL090800.

[Chicco and Jurman, 2020] Chicco, D. and Jurman, G. (2020). The advantages of the matthews correlation coefficient (mcc) over f1 score and accuracy in binary classification evaluation. *BMC genomics*, 21(1):1–13.

[Chollet, 2015] Chollet, F. (2015). keras. `https://github.com/fchollet/keras`.

[Cozzani et al., 2021] Cozzani, G., Khotyaintsev, Y. V., Graham, D. B., Egedal, J., André, M., Vaivads, A., Alexandrova, A., Le Contel, O., Nakamura, R., Fuselier, S., et al. (2021). Structure of a perturbed magnetic reconnection electron diffusion region in the earth's magnetotail. *Physical Review Letters*, 127(21):215101.

[Dimmock et al., 2015] Dimmock, A., Osmane, A., Pulkkinen, T., and Nykyri, K. (2015). A statistical study of the dawn-dusk asymmetry of ion temperature anisotropy and mirror mode occurrence in the terrestrial dayside magnetosheath using themis data. *Journal of Geophysical Research: Space Physics*, 120(7):5489–5503.

[Dimmock et al., 2019] Dimmock, A. P., Russell, C. T., Sagdeev, R. Z., Krasnoselskikh, V., Walker, S. N., Carr, C., Dandouras, I., Escoubet, C. P., Ganushkina, N., Gedalin, M., et al. (2019). Direct evidence of nonstationary collisionless shocks in space plasmas. *Science advances*, 5(2):eaau9926.

[Dmitriev and Suvorova, 2012] Dmitriev, A. and Suvorova, A. (2012). Traveling magnetopause distortion related to a large-scale magnetosheath plasma jet: Themis and ground-based observations. *Journal of Geophysical Research: Space Physics*, 117(A8).

[Dmitriev and Suvorova, 2015] Dmitriev, A. and Suvorova, A. (2015). Large-scale jets in the magnetosheath and plasma penetration across the magnetopause: Themis observations. *Journal of Geophysical Research: Space Physics*, 120(6):4423–4437.

[Dunlop and Lühr, 2020] Dunlop, M. W. and Lühr, H. (2020). *Ionospheric Multi-Spacecraft Analysis Tools: Approaches for Deriving Ionospheric Parameters*. Springer Nature.

[Eastwood et al., 2005] Eastwood, J., Lucek, E., Mazelle, C., Meziane, K., Narita, Y., Pickett, J., and Treumann, R. (2005). The foreshock. *Space Science Reviews*, 118(1):41–94.

[Eastwood et al., 2008] Eastwood, J., Sibeck, D., Angelopoulos, V., Phan, T., Bale, S., McFadden, J., Cully, C., Mende, S., Larson, D., Frey, S., et al. (2008). Themis observations of a hot flow anomaly: Solar wind, magnetosheath, and ground-based measurements. *Geophysical Research Letters*, 35(17).

[Edmiston and Kennel, 1984] Edmiston, J. and Kennel, C. (1984). A parametric survey of the first critical mach number for a fast mhd shock. *Journal of plasma physics*, 32(3):429–441.

[Ellison and Ramaty, 1985] Ellison, D. C. and Ramaty, R. (1985). Shock acceleration of electrons and ions in solar flares. *The Astrophysical Journal*, 298:400–408.

[Eriksson, 1998] Eriksson, A. I. (1998). Spectral analysis. *Analysis methods for multi-spacecraft data*, 1:5–42.

[Escoubet et al., 2001] Escoubet, C., Fehringer, M., and Goldstein, M. (2001). Introduction the cluster mission. In *Annales Geophysicae*, volume 19, pages 1197–1200. Copernicus GmbH.

[Escoubet et al., 2020] Escoubet, C. P., Hwang, K.-J., Toledo-Redondo, S., Turc, L., Haaland, S., Aunai, N., Dargent, J., Eastwood, J. P., Fear, R. C., Fu, H., et al. (2020). Cluster and mms simultaneous observations of magnetosheath high speed jets and their impact on the magnetopause. *Frontiers in Astronomy and Space Sciences*, page 78.

[Fitzpatrick, 2014] Fitzpatrick, R. (2014). *Plasma physics: an introduction*. Crc Press.

[Fox et al., 2016] Fox, N., Velli, M., Bale, S., Decker, R., Driesman, A., Howard, R., Kasper, J. C., Kinnison, J., Kusterer, M., Lario, D., et al. (2016). The solar probe plus mission: humanity's first visit to our star. *Space Science Reviews*, 204(1):7–48.

[Fuselier, 1994] Fuselier, S. A. (1994). Suprathermal ions upstream and downstream from the earth's bow shock. *Washington DC American Geophysical Union Geophysical Monograph Series*, 81:107–119.

[Fuselier et al., 1994] Fuselier, S. A., Anderson, B. J., Gary, S. P., and Denton, R. E. (1994). Inverse correlations between the ion temperature anisotropy and plasma beta in the earth's quasi-parallel magnetosheath. *Journal of Geophysical Research: Space Physics*, 99(A8):14931–14936.

[Gershman et al., 2015] Gershman, D. J., Dorelli, J. C., F.-Viñas, A., and Pollock, C. J. (2015). The calculation of moment uncertainties from velocity distribution functions with random errors. *Journal of Geophysical Research: Space Physics*, 120(8):6633–6645.

[Gingell et al., 2020] Gingell, I., Schwartz, S., Eastwood, J., Stawarz, J., Burch, J., Ergun, R., Fuselier, S., Gershman, D., Giles, B., Khotyaintsev, Y. V., et al. (2020). Statistics of reconnecting current sheets in the transition region of earth's bow shock. *Journal of Geophysical Research: Space Physics*, 125(1):e2019JA027119.

[Gingell et al., 2021] Gingell, I., Schwartz, S., Kucharek, H., Farrugia, C., and Trattner, K. (2021). Observing the prevalence of thin current sheets downstream of earth's bow shock. *Physics of Plasmas*, 28(10):102902.

[Gingell et al., 2017] Gingell, I., Schwartz, S. J., Burgess, D., Johlander, A., Russell, C. T., Burch, J. L., Ergun, R. E., Fuselier, S., Gershman, D. J., Giles, B. L., et al. (2017). Mms observations and hybrid simulations of surface ripples at a marginally quasi-parallel shock. *Journal of Geophysical Research: Space Physics*, 122(11):11–003.

[Ginzburg and Syrovatskii, 2013] Ginzburg, V. L. and Syrovatskii, S. I. (2013). *The origin of cosmic rays*. Elsevier.

[Goodfellow et al., 2016] Goodfellow, I., Bengio, Y., and Courville, A. (2016). *Deep learning*. MIT press.

[Graham et al., 2022] Graham, D., Khotyaintsev, Y. V., André, M., Vaivads, A., Divin, A., Drake, J., Norgren, C., Le Contel, O., Lindqvist, P.-A., Rager, A., et al. (2022). Direct observations of anomalous resistivity and diffusion in collisionless plasma. *Nature Communications*, 13(1):1–9.

[Graham et al., 2021] Graham, D. B., Khotyaintsev, Y. V., André, M., Vaivads, A., Chasapis, A., Matthaeus, W. H., Retino, A., Valentini, F., and Gershman, D. J. (2021). Non-maxwellianity of electron distributions near earth's magnetopause. *Journal of Geophysical Research: Space Physics*, 126(10):e2021JA029260.

[Greenstadt et al., 1995] Greenstadt, E., Le, G., and Strangeway, R. (1995). Ulf waves in the foreshock. *Advances in Space Research*, 15(8-9):71–84.

[Grinsted et al., 2004] Grinsted, A., Moore, J. C., and Jevrejeva, S. (2004). Application of the cross wavelet transform and wavelet coherence to geophysical time series. *Nonlinear processes in geophysics*, 11(5/6):561–566.

[Gunell et al., 2012] Gunell, H., Nilsson, H., Stenberg, G., Hamrin, M., Karlsson, T., Maggiolo, R., André, M., Lundin, R., and Dandouras, I. (2012). Plasma penetration of the dayside magnetopause. *Physics of Plasmas*, 19(7):072906.

[Gunell et al., 2014] Gunell, H., Stenberg Wieser, G., Mella, M., Maggiolo, R., Nilsson, H., Darrouzet, F., Hamrin, M., Karlsson, T., Brenning, N., De Keyser, J., et al. (2014). Waves in high-speed plasmoids in the magnetosheath and at the magnetopause. In *Annales Geophysicae*, volume 32, pages 991–1009. Copernicus GmbH.

[Gurchumelia et al., 2022] Gurchumelia, A., Sorriso-Valvo, L., Burgess, D., Yordanova, E., Elbakidze, K., Kharshiladze, O., and Kvaratskhelia, D. (2022). Comparing quasi-parallel and quasi-perpendicular configuration in the terrestrial magnetosheath: Multifractal analysis. *Frontiers in Physics*, page 506.

[Gurnett and Bhattacharjee, 2005] Gurnett, D. A. and Bhattacharjee, A. (2005). *Introduction to plasma physics: with space and laboratory applications*. Cambridge university press.

[Hao et al., 2017] Hao, Y., Gao, X., Lu, Q., Huang, C., Wang, R., and Wang, S. (2017). Reformation of rippled quasi-parallel shocks: 2-d hybrid simulations. *Journal of Geophysical Research: Space Physics*, 122(6):6385–6396.

[Hao et al., 2016] Hao, Y., Lu, Q., Gao, X., and Wang, S. (2016). Ion dynamics at a rippled quasi-parallel shock: 2d hybrid simulations. *The Astrophysical Journal*, 823(1):7.

[Harten and Clark, 1995] Harten, R. and Clark, K. (1995). The design features of the ggs wind and polar spacecraft. *Space Science Reviews*, 71(1):23–40.

[Hatzky and Bottino, 2010] Hatzky, R. and Bottino, A. (2010). Particle-in-cell methods in plasma physics. *Summer School on P3C challenges in Computational Sciences*, pages 4–7.

[Hellinger et al., 2002] Hellinger, P., Travnicek, P., and Matsumoto, H. (2002). Reformation of perpendicular shocks: Hybrid simulations. *Geophysical research letters*, 29(24):87–1.

[Hietala et al., 2009] Hietala, H., Laitinen, T. V., Andréeová, K., Vainio, R., Vaivads, A., Palmroth, M., Pulkkinen, T., Koskinen, H. E., Lucek, E., and Rème, H. (2009). Supermagnetosonic jets behind a collisionless quasiparallel shock. *Physical Review Letters*, 103(24):245001.

[Hietala et al., 2012] Hietala, H., Partamies, N., Laitinen, T., Clausen, L. B., Facskó, G., Vaivads, A., Koskinen, H., Dandouras, I., Rème, H., and Lucek, E. (2012). Supermagnetosonic subsolar magnetosheath jets and their effects: From the solar wind to the ionospheric convection. In *Annales Geophysicae*, volume 30, pages 33–48. Copernicus GmbH.

[Hietala et al., 2018] Hietala, H., Phan, T., Angelopoulos, V., Oieroset, M., Archer, M. O., Karlsson, T., and Plaschke, F. (2018). In situ observations of a magnetosheath high-speed jet triggering magnetopause reconnection. *Geophysical Research Letters*, 45(4):1732–1740.

[Hietala and Plaschke, 2013] Hietala, H. and Plaschke, F. (2013). On the generation of magnetosheath high–speed jets by bow shock ripples. *Journal of Geophysical Research: Space Physics*, 118(11):7237–7245.

[Innocenti et al., 2021] Innocenti, M. E., Amaya, J., Raeder, J., Dupuis, R., Ferdousi, B., and Lapenta, G. (2021). Unsupervised classification of simulated magnetospheric regions. In *Annales Geophysicae*, volume 39, pages 861–881. Copernicus GmbH.

[Jakosky et al., 2015] Jakosky, B. M., Lin, R. P., Grebowsky, J. M., Luhmann, J. G., Mitchell, D., Beutelschies, G., Priser, T., Acuna, M., Andersson, L., Baird, D., et al. (2015). The mars atmosphere and volatile evolution (maven) mission. *Space Science Reviews*, 195(1):3–48.

[James et al., 2013] James, G., Witten, D., Hastie, T., and Tibshirani, R. (2013). *An introduction to statistical learning*, volume 112. Springer.

[Jelínek et al., 2012] Jelínek, K., Němeček, Z., and Šafránková, J. (2012). A new approach to magnetopause and bow shock modeling based on automated region identification. *Journal of Geophysical Research: Space Physics*, 117(A5).

[Johlander et al., 2022] Johlander, A., Battarbee, M., Turc, L., Ganse, U., Pfau-Kempf, Y., Grandin, M., Suni, J., Tarvus, V., Bussov, M., Zhou, H., et al. (2022). Quasi-parallel shock reformation seen by magnetospheric multiscale and ion-kinetic simulations. *Geophysical Research Letters*, 49(2):e2021GL096335.

[Johlander et al., 2021] Johlander, A., Battarbee, M., Vaivads, A., Turc, L., Pfau-Kempf, Y., Ganse, U., Grandin, M., Dubart, M., Khotyaintsev, Y. V., Caprioli, D., et al. (2021). Ion acceleration efficiency at the earth's bow shock: Observations and simulation results. *The Astrophysical Journal*, 914(2):82.

[Johlander et al., 2016] Johlander, A., Schwartz, S., Vaivads, A., Khotyaintsev, Y. V., Gingell, I., Peng, I., Markidis, S., Lindqvist, P.-A., Ergun, R., Marklund, G., et al. (2016). Rippled quasiperpendicular shock observed by the magnetospheric multiscale spacecraft. *Physical Review Letters*, 117(16):165101.

[Johlander et al., 2018] Johlander, A., Vaivads, A., Khotyaintsev, Y. V., Gingell, I., Schwartz, S. J., Giles, B. L., Torbert, R. B., and Russell, C. T. (2018). Shock ripples observed by the mms spacecraft: ion reflection and dispersive properties. *Plasma Physics and Controlled Fusion*, 60(12):125006.

[Kajdič et al., 2021a] Kajdič, P., Pfau-Kempf, Y., Turc, L., Dimmock, A. P., Palmroth, M., Takahashi, K., Kilpua, E., Soucek, J., Takahashi, N., Preisser, L., et al. (2021a). Ulf wave transmission across collisionless shocks: 2.5 d local hybrid simulations. *Journal of Geophysical Research: Space Physics*, 126(11):e2021JA029283.

[Kajdič et al., 2021b] Kajdič, P., Raptis, S., Blanco-Cano, X., and Karlsson, T. (2021b). Causes of jets in the quasi-perpendicular magnetosheath. *Geophysical Research Letters*, 48(13):e2021GL093173.

[Kalnay, 2003] Kalnay, E. (2003). *Atmospheric modeling, data assimilation and predictability*. Cambridge university press.

[Karimabadi et al., 2014] Karimabadi, H., Roytershteyn, V., Vu, H., Omelchenko, Y., Scudder, J., Daughton, W., Dimmock, A., Nykyri, K., Wan, M., Sibeck, D., et al. (2014). The link between shocks, turbulence, and magnetic reconnection in collisionless plasmas. *Physics of Plasmas*, 21(6):062308.

[Karlsson et al., 2012] Karlsson, T., Brenning, N., Nilsson, H., Trotignon, J.-G., Vallières, X., and Facsko, G. (2012). Localized density enhancements in the magnetosheath: Three-dimensional morphology and possible importance for impulsive penetration. *Journal of Geophysical Research: Space Physics*, 117(A3).

[Karlsson et al., 2015] Karlsson, T., Kullen, A., Liljeblad, E., Brenning, N., Nilsson, H., Gunell, H., and Hamrin, M. (2015). On the origin of magnetosheath plasmoids and their relation to magnetosheath jets. *Journal of Geophysical Research: Space Physics*, 120(9):7390–7403.

[Karlsson et al., 2016] Karlsson, T., Liljeblad, E., Kullen, A., Raines, J. M., Slavin, J. A., and Sundberg, T. (2016). Isolated magnetic field structures in mercury's magnetosheath as possible analogues for terrestrial magnetosheath plasmoids and jets. *Planetary and Space Science*, 129:61–73.

[Karlsson et al., 2021] Karlsson, T., Raptis, S., Trollvik, H., and Nilsson, H. (2021). Classifying the magnetosheath behind the quasi-parallel and quasi-perpendicular bow shock by local measurements. *Journal of Geophysical Research: Space Physics*, 126(9):e2021JA029269.

[Karniadakis et al., 2021] Karniadakis, G. E., Kevrekidis, I. G., Lu, L., Perdikaris, P., Wang, S., and Yang, L. (2021). Physics-informed machine learning. *Nature Reviews Physics*, 3(6):422–440.

[Kasper et al., 2021] Kasper, J., Lazio, J., Romero-Wolf, A., Lux, J., and Neilsen, T. (2021). The sun radio interferometer space experiment (sunrise) mission. In *2021 IEEE Aerospace Conference (50100)*, pages 1–11. IEEE.

[Katsavrias et al., 2022] Katsavrias, C., Papadimitriou, C., Hillaris, A., and Balasis, G. (2022). Application of wavelet methods in the investigation of geospace disturbances: A review and an evaluation of the approach for quantifying wavelet power. *Atmosphere*, 13(3):499.

[Katsavrias et al., 2021] Katsavrias, C., Raptis, S., Daglis, I. A., Karlsson, T., Georgiou, M., and Balasis, G. (2021). On the generation of pi2 pulsations due to plasma flow patterns around magnetosheath jets. *Geophysical Research Letters*, 48(15):e2021GL093611.

[Khotyaintsev et al., 2019] Khotyaintsev, Y. V., Graham, D. B., Norgren, C., and Vaivads, A. (2019). Collisionless magnetic reconnection and waves: Progress review. *Frontiers in Astronomy and Space Sciences*, 6:70.

[King and Papitashvili, 2005] King, J. and Papitashvili, N. (2005). Solar wind spatial scales in and comparisons of hourly wind and ace plasma and magnetic field data. *Journal of Geophysical Research: Space Physics*, 110(A2).

[Kivelson et al., 1995] Kivelson, M. G., Kivelson, M. G., and Russell, C. T. (1995). *Introduction to space physics*. Cambridge university press.

[Koller et al., 2022] Koller, F., Temmer, M., Preisser, L., Plaschke, F., Geyer, P., Jian, L. K., Roberts, O. W., Hietala, H., and LaMoury, A. T. (2022). Magnetosheath jet occurrence rate in relation to cmes and sirs. *Journal of Geophysical Research: Space Physics*, 127(4):e2021JA030124. e2021JA030124 2021JA030124.

[Koskinen and Kilpua, 2022] Koskinen, H. E. J. and Kilpua, E. K. J. (2022). *From Charged Particles to Plasma Physics*, pages 63–83. Springer International Publishing, Cham.

[Kotova et al., 2015] Kotova, G., Verigin, M., and Bezrukikh, V. (2015). Physics-based reconstruction of the 3-d density distribution in the entire quiet time plasmasphere from measurements along a single pass of an orbiter. *Journal of Geophysical Research: Space Physics*, 120(9):7512–7521.

[Kotova et al., 2021] Kotova, G., Verigin, M., Gombosi, T., Kabin, K., Slavin, J., and Bezrukikh, V. (2021). Physics-based analytical model of the planetary bow shock position and shape. *Journal of Geophysical Research: Space Physics*, 126(6):e2021JA029104.

[Koyama et al., 1995] Koyama, K., Petre, R., Gotthelf, E., Hwang, U., Matsuura, M., Ozaki, M., and Holt, S. (1995). Evidence for shock acceleration of high-energy electrons in the supernova remnant sn1006. *Nature*, 378(6554):255–258.

[Kucharek et al., 2004] Kucharek, H., Möbius, E., Scholer, M., Mouikis, C., Kistler, L., Horbury, T., Balogh, A., Réme, H., and Bosqued, J. (2004). On the origin of field-aligned beams at the quasi-perpendicular bow shock: multi-spacecraft observations by cluster. In *Annales Geophysicae*, volume 22, pages 2301–2308. Copernicus GmbH.

[Lalti et al., 2022a] Lalti, A., Khotyaintsev, Y. V., Dimmock, A., Johlander, A., Graham, D., and Olshevsky, V. (2022a). A database of mms bow shock crossings compiled using machine learning. *arXiv preprint arXiv:2203.04680*.

[Lalti et al., 2022b] Lalti, A., Khotyaintsev, Y. V., Graham, D. B., Vaivads, A., Steinvall, K., and Russell, C. T. (2022b). Whistler waves in the foot of quasi-perpendicular supercritical shocks. *Journal of Geophysical Research: Space Physics*, 127(5):e2021JA029969.

[LaMoury et al., 2021] LaMoury, A. T., Hietala, H., Plaschke, F., Vuorinen, L., and Eastwood, J. P. (2021). Solar wind control of magnetosheath jet formation and propagation to the magnetopause. *Journal of Geophysical Research: Space Physics*, 126(9):e2021JA029592.

[Lapenta et al., 2022] Lapenta, G., Schriver, D., Walker, R. J., Berchem, J., Echterling, N. F., El Alaoui, M., and Travnicek, P. (2022). Do we need to consider electrons' kinetic effects to properly model a planetary magnetosphere: The case of mercury. *Journal of Geophysical Research: Space Physics*, 127(4):e2021JA030241. e2021JA030241 2021JA030241.

[Lazar et al., 2012] Lazar, M., Schlickeiser, R., and Poedts, S. (2012). Suprathermal particle populations in the solar wind and corona. *Exploring the Solar Wind*, page 241.

[Ledvina et al., 2008] Ledvina, S., Ma, Y.-J., and Kallio, E. (2008). Modeling and simulating flowing plasmas and related phenomena. In *Comparative aeronomy*, pages 143–189. Springer.

[Lembège and Savoini, 2002] Lembège, B. and Savoini, P. (2002). Formation of reflected electron bursts by the nonstationarity and nonuniformity of a collisionless shock front. *Journal of Geophysical Research: Space Physics*, 107(A3):SMP–X.

[Lin et al., 2021] Lin, Y., Wang, X. Y., Fok, M.-C., Buzulukova, N., Perez, J. D., Cheng, L., and Chen, L.-J. (2021). Magnetotail-inner magnetosphere transport associated with fast flows based on combined global-hybrid and cimi simulation. *Journal of Geophysical Research: Space Physics*, 126(3):e2020JA028405. e2020JA028405 2020JA028405.

[Lindberg et al., 2022] Lindberg, M., Vaivads, A., Raptis, S., Lindqvist, P.-A., Giles, B. L., and Gershman, D. J. (2022). Electron kinetic entropy across quasi-perpendicular shocks. *Entropy*, 24(6):745.

[Liu et al., 2017] Liu, T. Z., Angelopoulos, V., Hietala, H., and Wilson III, L. B. (2017). Statistical study of particle acceleration in the core of foreshock transients. *Journal of Geophysical Research: Space Physics*, 122(7):7197–7208.

[Liu et al., 2019a] Liu, T. Z., Angelopoulos, V., and Lu, S. (2019a). Relativistic electrons generated at earth's quasi-parallel bow shock. *Science advances*, 5(7):eaaw1368.

[Liu et al., 2021] Liu, T. Z., Hao, Y., Wilson III, L. B., Turner, D. L., and Zhang, H. (2021). Magnetospheric multiscale observations of earth's oblique bow shock reformation by foreshock ultralow-frequency waves. *Geophysical Research Letters*, 48(2):e2020GL091184.

[Liu et al., 2019b] Liu, T. Z., Hietala, H., Angelopoulos, V., Omelchenko, Y., Roytershteyn, V., and Vainio, R. (2019b). Themis observations of particle acceleration by a magnetosheath jet-driven bow wave. *Geophysical Research Letters*, 46(14):7929–7936.

[Liu et al., 2020a] Liu, T. Z., Hietala, H., Angelopoulos, V., Omelchenko, Y., Vainio, R., and Plaschke, F. (2020a). Statistical study of magnetosheath jet-driven bow waves. *Journal of Geophysical Research: Space Physics*, 125(7):e2019JA027710.

[Liu et al., 2020b] Liu, T. Z., Hietala, H., Angelopoulos, V., Vainio, R., and Omelchenko, Y. (2020b). Electron acceleration by magnetosheath jet-driven bow waves. *Journal of Geophysical Research: Space Physics*, 125(7):e2019JA027709.

[Liu et al., 2022a] Liu, T. Z., Zhang, H., Turner, D., Vu, A., and Angelopoulos, V. (2022a). Statistical study of favorable foreshock ion properties for the formation of hot flow anomalies and foreshock bubbles. *Journal of Geophysical Research: Space Physics*, page e2022JA030273.

[Liu et al., 2022b] Liu, Z.-Y., Zong, Q.-G., Zhang, H., Zhao, J.-T., Rankin, R., Pollock, C. J., and Le, G. (2022b). Ion behavior at shocklets: A case study of mms observations. *Geophysical Research Letters*, 49(17):e2022GL100449. e2022GL100449 2022GL100449.

[Lowe and Burgess, 2003] Lowe, R. and Burgess, D. (2003). The properties and causes of rippling in quasi-perpendicular collisionless shock fronts. In *Annales Geophysicae*, volume 21, pages 671–679. Copernicus GmbH.

[Lu et al., 2020] Lu, S., Wang, R., Lu, Q., Angelopoulos, V., Nakamura, R., Artemyev, A., Pritchett, P., Liu, T., Zhang, X.-J., Baumjohann, W., et al. (2020). Magnetotail reconnection onset caused by electron kinetics with a strong external driver. *Nature communications*, 11(1):1–7.

[Lucek et al., 2005] Lucek, E., Constantinescu, D., Goldstein, M., Pickett, J., Pincon, J.-L., Sahraoui, F., Treumann, R., and Walker, S. (2005). The magnetosheath. *Space Science Reviews*, 118(1):95–152.

[Luhmann et al., 1986] Luhmann, J., Russell, C., and Elphic, R. (1986). Spatial distributions of magnetic field fluctuations in the dayside magnetosheath. *Journal of Geophysical Research: Space Physics*, 91(A2):1711–1715.

[Madanian et al., 2021] Madanian, H., Desai, M., Schwartz, S., Wilson, L., Fuselier, S., Burch, J., Le Contel, O., Turner, D., Ogasawara, K., Brosius, A. L., et al. (2021). The dynamics of a high mach number quasi-perpendicular shock: Mms observations. *The Astrophysical Journal*, 908(1):40.

[Marcowith et al., 2016] Marcowith, A., Bret, A., Bykov, A., Dieckman, M. E., Drury, L. O., Lembège, B., Lemoine, M., Morlino, G., Murphy, G., Pelletier, G., et al. (2016). The microphysics of collisionless shock waves. *Reports on Progress in Physics*, 79(4):046901.

[Markidis, 2021] Markidis, S. (2021). The old and the new: Can physics-informed deep-learning replace traditional linear solvers? *Frontiers in big Data*, page 92.

[Markidis et al., 2010] Markidis, S., Lapenta, G., et al. (2010). Multi-scale simulations of plasma with ipic3d. *Mathematics and Computers in Simulation*, 80(7):1509–1519.

[Mazelle et al., 2010] Mazelle, C., Lembège, B., Morgenthaler, A., Meziane, K., Horbury, T., Génot, V., Lucek, E., and Dandouras, I. (2010). Self-reformation of the quasi-perpendicular shock: Cluster observations. In *AIP Conference Proceedings*, volume 1216, pages 471–474. American Institute of Physics.

[McFadden et al., 2008] McFadden, J., Carlson, C., Larson, D., Ludlam, M., Abiad, R., Elliott, B., Turin, P., Marckwordt, M., and Angelopoulos, V. (2008). The themis esa plasma instrument and in-flight calibration. *Space Science Reviews*, 141(1):277–302.

[Merka et al., 2003] Merka, J., Szabo, A., Narock, T., King, J., Paularena, K., and Richardson, J. (2003). A comparison of imp 8 observed bow shock positions with model predictions. *Journal of Geophysical Research: Space Physics*, 108(A2).

[Millas et al., 2020] Millas, D., Innocenti, M. E., Laperre, B., Raeder, J., Poedts, S., and Lapenta, G. (2020). Domain of influence analysis: implications for data assimilation in space weather forecasting. *Frontiers in Astronomy and Space Sciences*, 7:571286.

[Mohri et al., 2018] Mohri, M., Rostamizadeh, A., and Talwalkar, A. (2018). *Foundations of machine learning*. MIT press.

[Morlet et al., 1982] Morlet, J., Arens, G., Fourgeau, E., and Glard, D. (1982). Wave propagation and sampling theory—part i: Complex signal and scattering in multilayered media. *Geophysics*, 47(2):203–221.

[Morlino and Caprioli, 2012] Morlino, G. and Caprioli, D. (2012). Strong evidence for hadron acceleration in tycho's supernova remnant. *Astronomy & Astrophysics*, 538:A81.

[Morse et al., 1972] Morse, D., Destler, W., and Auer, P. (1972). Nonstationary behavior of collisionless shocks. *Physical Review Letters*, 28(1):13.

[Müller et al., 2020] Müller, D., Cyr, O. S., Zouganelis, I., Gilbert, H. R., Marsden, R., Nieves-Chinchilla, T., Antonucci, E., Auchère, F., Berghmans, D., Horbury, T., et al. (2020). The solar orbiter mission-science overview. *Astronomy & Astrophysics*, 642:A1.

[Němeček et al., 1998] Němeček, Z., Šafránková, J., Přech, L., Sibeck, D., Kokubun, S., and Mukai, T. (1998). Transient flux enhancements in the magnetosheath. *Geophysical Research Letters*, 25(8):1273–1276.

[Ng et al., 2022] Ng, J., Chen, L.-J., Bessho, N., Shuster, J., Burkholder, B., and Yoo, J. (2022). Electron-scale reconnection in three-dimensional shock turbulence. *Geophysical Research Letters*, 49(15):e2022GL099544. e2022GL099544 2022GL099544.

[Ng et al., 2021] Ng, J., Chen, L.-J., and Omelchenko, Y. (2021). Bursty magnetic reconnection at the earth's magnetopause triggered by high-speed jets. *Physics of Plasmas*, 28(9):092902.

[Norenius et al., 2021] Norenius, L., Hamrin, M., Goncharov, O., Gunell, H., Opgenoorth, H., Pitkänen, T., Chong, S., Partamies, N., and Baddeley, L. (2021). Ground-based magnetometer response to impacting magnetosheath jets. *Journal of Geophysical Research: Space Physics*, 126(8):e2021JA029115.

[Nykyri et al., 2019] Nykyri, K., Bengtson, M., Angelopoulos, V., Nishimura, Y., and Wing, S. (2019). Can enhanced flux loading by high-speed jets lead to a substorm? multipoint detection of the christmas day substorm onset at 08: 17 ut, 2015. *Journal of Geophysical Research: Space Physics*, 124(6):4314–4340.

[Odelstad et al., 2022] Odelstad, E., Karlsson, T., Eriksson, A., Bergman, S., and Wieser, G. S. (2022). Ion-ion cross-field instability of lower hybrid waves in the inner coma of comet 67p. *Journal of Geophysical Research: Space Physics*, page e2022JA030535.

[Olshevsky et al., 2021] Olshevsky, V., Khotyaintsev, Y. V., Lalti, A., Divin, A., Delzanno, G. L., Anderzén, S., Herman, P., Chien, S. W., Avanov, L., Dimmock, A. P., et al. (2021). Automated classification of plasma regions using 3d particle energy distributions. *Journal of Geophysical Research: Space Physics*, 126(10):e2021JA029620.

[Omelchenko et al., 2021] Omelchenko, Y., Chen, L.-J., and Ng, J. (2021). 3d space-time adaptive hybrid simulations of magnetosheath high-speed jets. *Journal of Geophysical Research: Space Physics*, 126(7):e2020JA029035.

[Paganini et al., 2018] Paganini, M., de Oliveira, L., and Nachman, B. (2018). Accelerating science with generative adversarial networks: an application to 3d particle showers in multilayer calorimeters. *Physical review letters*, 120(4):042003.

[Palmroth, 2022] Palmroth, M. (2022). Daring to think of the impossible: The story of vlasiator. *Frontiers in Astronomy and Space Sciences*, 9.

[Palmroth et al., 2015] Palmroth, M., Archer, M., Vainio, R., Hietala, H., Pfau-Kempf, Y., Hoilijoki, S., Hannuksela, O., Ganse, U., Sandroos, A., Alfthan, S. v., et al. (2015). Ulf foreshock under radial imf: Themis observations and global kinetic simulation vlasiator results compared. *Journal of Geophysical Research: Space Physics*, 120(10):8782–8798.

[Palmroth et al., 2018a] Palmroth, M., Ganse, U., Pfau-Kempf, Y., Battarbee, M., Turc, L., Brito, T., Grandin, M., Hoilijoki, S., Sandroos, A., and von Alfthan, S. (2018a). Vlasov methods in space physics and astrophysics. *Living Reviews in Computational Astrophysics*, 4(1):1–54.

[Palmroth et al., 2018b] Palmroth, M., Hietala, H., Plaschke, F., Archer, M., Karlsson, T., Blanco-Cano, X., Sibeck, D., Kajdič, P., Ganse, U., Pfau-Kempf, Y., et al. (2018b). Magnetosheath jet properties and evolution as determined by a global hybrid-vlasov simulation. In *Annales Geophysicae*, volume 36, pages 1171–1182. Copernicus GmbH.

[Palmroth et al., 2013] Palmroth, M., Honkonen, I., Sandroos, A., Kempf, Y., von Alfthan, S., and Pokhotelov, D. (2013). Preliminary testing of global hybrid-vlasov simulation: Magnetosheath and cusps under northward interplanetary magnetic field. *Journal of Atmospheric and Solar-Terrestrial Physics*, 99:41–46.

[Palmroth et al., 2021] Palmroth, M., Raptis, S., Suni, J., Karlsson, T., Turc, L., Johlander, A., Ganse, U., Pfau-Kempf, Y., Blanco-Cano, X., Akhavan-Tafti, M., et al. (2021). Magnetosheath jet evolution as a function of lifetime: global

hybrid-vlasov simulations compared to mms observations. In *Annales Geophysicae*, volume 39, pages 289–308. Copernicus GmbH.

[Paschmann and Daly, 1998] Paschmann, G. and Daly, P. W. (1998). Analysis methods for multi-spacecraft data. issi scientific reports series sr-001, esa/issi, vol. 1. isbn 1608-280x, 1998. *ISSI Scientific Reports Series*, 1.

[Paschmann and Daly, 2008] Paschmann, G. and Daly, P. W. (2008). *Multi-Spacecraft Analysis Methods Revisited*. ISSI Scientific Report.

[Paschmann et al., 1998] Paschmann, G., Fazakerley, A. N., and Schwartz, S. J. (1998). Moments of plasma velocity distributions. *Analysis methods for multi-spacecraft data*, 1:125–157.

[Paschmann and Schwartz, 2000] Paschmann, G. and Schwartz, S. (2000). Issi book on analysis methods for multi-spacecraft data. In *Cluster-II workshop multiscale/multipoint plasma measurements*, volume 449, page 99.

[Pfau-Kempf et al., 2020] Pfau-Kempf, Y., Palmroth, M., Johlander, A., Turc, L., Alho, M., Battarbee, M., Dubart, M., Grandin, M., and Ganse, U. (2020). Hybrid-vlasov modeling of three-dimensional dayside magnetopause reconnection. *Physics of Plasmas*, 27(9):092903.

[Plaschke et al., 2013] Plaschke, F., Hietala, H., and Angelopoulos, V. (2013). Anti-sunward high-speed jets in the subsolar magnetosheath. In *Annales Geophysicae*, volume 31, pages 1877–1889. Copernicus GmbH.

[Plaschke et al., 2018] Plaschke, F., Hietala, H., Archer, M., Blanco-Cano, X., Kajdič, P., Karlsson, T., Lee, S. H., Omidi, N., Palmroth, M., Roytershteyn, V., et al. (2018). Jets downstream of collisionless shocks. *Space Science Reviews*, 214(5):1–77.

[Plaschke et al., 2020] Plaschke, F., Jernej, M., Hietala, H., and Vuorinen, L. (2020). On the alignment of velocity and magnetic fields within magnetosheath jets. In *Annales geophysicae*, volume 38, pages 287–296. Copernicus GmbH.

[Plaschke et al., 2017] Plaschke, F., Karlsson, T., Hietala, H., Archer, M., Vörös, Z., Nakamura, R., Magnes, W., Baumjohann, W., Torbert, R., Russell, C., et al. (2017). Magnetosheath high-speed jets: Internal structure and interaction with ambient plasma. *Journal of Geophysical Research: Space Physics*, 122(10):10–157.

[Pollock et al., 2016] Pollock, C., Moore, T., Jacques, A., Burch, J., Gliese, U., Saito, Y., Omoto, T., Avanov, L., Barrie, A., Coffey, V., et al. (2016). Fast plasma investigation for magnetospheric multiscale. *Space Science Reviews*, 199(1):331–406.

[Porth et al., 2014] Porth, O., Xia, C., Hendrix, T., Moschou, S., and Keppens, R. (2014). Mpi-amrvac for solar and astrophysics. *The Astrophysical Journal Supplement Series*, 214(1):4.

[Preisser et al., 2020] Preisser, L., Blanco-Cano, X., Kajdič, P., Burgess, D., and Trotta, D. (2020). Magnetosheath jets and plasmoids: Characteristics and formation mechanisms from hybrid simulations. *The Astrophysical Journal Letters*, 900(1):L6.

[Raab et al., 2016] Raab, W., Branduardi-Raymont, G., Wang, C., Dai, L., Donovan, E., Enno, G., Escoubet, P., Holland, A., Jing, L., Kataria, D., et al. (2016). Smile: A joint esa/cas mission to investigate the interaction between the solar wind and earth's magnetosphere. In *Space telescopes and instrumentation 2016: Ultraviolet to gamma ray*, volume 9905, page 990502. SPIE.

[Raissi et al., 2019] Raissi, M., Perdikaris, P., and Karniadakis, G. E. (2019). Physics-informed neural networks: A deep learning framework for solving forward and inverse problems involving nonlinear partial differential equations. *Journal of Computational physics*, 378:686–707.

[Raptis, 2022] Raptis, S. (2022). Magnetosheath Jets MMS1 (5/2015 - 6/2020) - Classified.

[Raptis et al., 2018] Raptis, S., Amaya, J., Shamash, A., Depypere, G., and Lapenta, G. (2018). Processing solar images to forecast coronal mass ejections using artificial intelligence. Master's thesis, KU Leuven.

[Raptis et al., 2020a] Raptis, S., Aminalragia-Giamini, S., Karlsson, T., and Lindberg, M. (2020a). Classification of magnetosheath jets using neural networks and high resolution omni (hro) data. *Frontiers in Astronomy and Space Sciences*, 7:24.

[Raptis et al., 2020b] Raptis, S., Karlsson, T., Plaschke, F., Kullen, A., and Lindqvist, P.-A. (2020b). Classifying magnetosheath jets using mms: Statistical properties. *Journal of Geophysical Research: Space Physics*, 125(11):e2019JA027754.

[Raptis et al., 2022] Raptis, S., Karlsson, T., Vaivads, A., Pollock, C., Plaschke, F., Johlander, A., Trollvik, H., and Lindqvist, P. (2022). Downstream high-speed plasma jet generation as a direct consequence of shock reformation. *Nature Communications*, 13(1):598–598.

[Runov et al., 2021] Runov, A., Grandin, M., Palmroth, M., Battarbee, M., Ganse, U., Hietala, H., Hoilijoki, S., Kilpua, E., Pfau-Kempf, Y., Toledo-Redondo, S., et al. (2021). Ion distribution functions in magnetotail reconnection: global hybrid-vlasov simulation results. In *Annales Geophysicae*, volume 39, pages 599–612. Copernicus GmbH.

[Russell et al., 2016] Russell, C., Anderson, B., Baumjohann, W., Bromund, K., Dearborn, D., Fischer, D., Le, G., Leinweber, H., Leneman, D., Magnes, W., et al. (2016). The magnetospheric multiscale magnetometers. *Space Science Reviews*, 199(1):189–256.

[Samtaney et al., 2009] Samtaney, R., Loureiro, N., Uzdensky, D., Schekochihin, A., and Cowley, S. (2009). Formation of plasmoid chains in magnetic reconnection. *Physical review letters*, 103(10):105004.

[Savin et al., 2012] Savin, S., Amata, E., Zelenyi, L., Lutsenko, V., Safrankova, J., Nemecek, Z., Borodkova, N., Buechner, J., Daly, P., Kronberg, E., et al. (2012). Super fast plasma streams as drivers of transient and anomalous magnetospheric dynamics. In *Annales Geophysicae*, volume 30, pages 1–7. Copernicus GmbH.

[Schwartz and Burgess, 1991] Schwartz, S. J. and Burgess, D. (1991). Quasi-parallel shocks: A patchwork of three-dimensional structures. *Geophysical Research Letters*, 18(3):373–376.

[Schwartz et al., 1992] Schwartz, S. J., Burgess, D., Wilkinson, W. P., Kessel, R. L., Dunlop, M., and Lühr, H. (1992). Observations of short large-amplitude magnetic structures at a quasi-parallel shock. *Journal of Geophysical Research: Space Physics*, 97(A4):4209–4227.

[Schwartz et al., 2022] Schwartz, S. J., Goodrich, K. A., Wilson III, L. B., Turner, D. L., Trattner, K. J., Kucharek, H., Gingell, I., Fuselier, S. A., Cohen, I. J., Madanian, H., Ergun, R. E., Gershman, D. J., and Strangeway, R. J. (2022). Energy partition at collisionless supercritical quasiperpendicular shocks. *Journal of Geophysical Research: Space Physics*, 127. e2022JA030637 2022JA030637.

[Sibeck et al., 2021] Sibeck, D., Lee, S.-H., Omidi, N., and Angelopoulos, V. (2021). Foreshock cavities: Direct transmission through the bow shock. *Journal of Geophysical Research: Space Physics*, 126(5):e2021JA029201.

[Sitnov et al., 2021a] Sitnov, M., Motoba, T., and Swisdak, M. (2021a). Multiscale nature of the magnetotail reconnection onset. *Geophysical Research Letters*, 48(10):e2021GL093065.

[Sitnov et al., 2021b] Sitnov, M., Stephens, G., Motoba, T., and Swisdak, M. (2021b). Data mining reconstruction of magnetotail reconnection and implications for its first-principle modeling. *Frontiers in Physics*, 9:644884.

[Slavin and Holzer, 1981] Slavin, J. A. and Holzer, R. E. (1981). Solar wind flow about the terrestrial planets 1. modeling bow shock position and shape. *Journal of Geophysical Research: Space Physics*, 86(A13):11401–11418.

[Sonnerup and Scheible, 1998] Sonnerup, B. U. and Scheible, M. (1998). Minimum and maximum variance analysis. *Analysis methods for multi-spacecraft data*, 1:185–220.

[Stone et al., 1998] Stone, E. C., Frandsen, A., Mewaldt, R., Christian, E., Margolies, D., Ormes, J., and Snow, F. (1998). The advanced composition explorer. *Space Science Reviews*, 86(1):1–22.

[Strang and Nguyen, 1996] Strang, G. and Nguyen, T. (1996). *Wavelets and filter banks*. SIAM.

[Sulaiman et al., 2015] Sulaiman, A., Masters, A., Dougherty, M., Burgess, D., Fujimoto, M., and Hospodarsky, G. (2015). Quasiperpendicular high mach number shocks. *Physical review letters*, 115(12):125001.

[Suni et al., 2021] Suni, J., Palmroth, M., Turc, L., Battarbee, M., Johlander, A., Tarvus, V., Alho, M., Bussov, M., Dubart, M., Ganse, U., et al. (2021). Connection between foreshock structures and the generation of magnetosheath jets: Vlasiator results. *Geophysical Research Letters*, 48(20):e2021GL095655.

[Svenningsson et al., 2022] Svenningsson, I., Yordanova, E., Cozzani, G., Khotyaintsev, Y. V., and André, M. (2022). Kinetic generation of whistler waves in the turbulent magnetosheath. *Geophysical Research Letters*, 49(15):e2022GL099065. e2022GL099065 2022GL099065.

[Swanson, 2012] Swanson, D. G. (2012). *Plasma waves*. Elsevier.

[Torbert et al., 2016] Torbert, R., Russell, C., Magnes, W., Ergun, R., Lindqvist, P.-A., LeContel, O., Vaith, H., Macri, J., Myers, S., Rau, D., et al. (2016). The fields instrument suite on mms: Scientific objectives, measurements, and data products. *Space Science Reviews*, 199(1):105–135.

[Torrence and Compo, 1998] Torrence, C. and Compo, G. P. (1998). A practical guide to wavelet analysis. *Bulletin of the American Meteorological society*, 79(1):61–78.

[Treumann, 2009] Treumann, R. (2009). Fundamentals of collisionless shocks for astrophysical application, 1. non-relativistic shocks. *The Astronomy and Astrophysics Review*, 17(4):409–535.

[Treumann and Baumjohann, 1997] Treumann, R. A. and Baumjohann, W. (1997). *Advanced space plasma physics*, volume 30. Imperial College Press London.

[Trotta and Burgess, 2019] Trotta, D. and Burgess, D. (2019). Electron acceleration at quasi-perpendicular shocks in sub-and supercritical regimes: 2d and 3d simulations. *Monthly Notices of the Royal Astronomical Society*, 482(1):1154–1162.

[Trotta et al., 2022] Trotta, D., Pecora, F., Settino, A., Perrone, D., Hietala, H., Horbury, T., Matthaeus, W., Burgess, D., Servidio, S., and Valentini, F. (2022). On the transmission of turbulent structures across the earth's bow shock. *arXiv preprint arXiv:2202.14029*.

[Turc et al., 2018] Turc, L., Ganse, U., Pfau-Kempf, Y., Hoilijoki, S., Battarbee, M., Juusola, L., Jarvinen, R., Brito, T., Grandin, M., and Palmroth, M. (2018). Foreshock properties at typical and enhanced interplanetary magnetic field strengths: Results from hybrid-vlasov simulations. *Journal of Geophysical Research: Space Physics*, 123(7):5476–5493.

[Turner et al., 2018] Turner, D., Wilson, L., Liu, T., Cohen, I., Schwartz, S., Osmane, A., Fennell, J., Clemmons, J., Blake, J., Westlake, J., et al. (2018). Autogenous and efficient acceleration of energetic ions upstream of earth's bow shock. *Nature*, 561(7722):206–210.

[Turner et al., 2021] Turner, D. L., Wilson, L., Goodrich, K., Madanian, H., Schwartz, S. J., Liu, T. Z., Johlander, A., Caprioli, D., Cohen, I., Gershman, D., et al. (2021). Direct multipoint observations capturing the reformation of a supercritical fast magnetosonic shock. *The Astrophysical journal letters*, 911(2):L31.

[Von Alfthan et al., 2014] Von Alfthan, S., Pokhotelov, D., Kempf, Y., Hoilijoki, S., Honkonen, I., Sandroos, A., and Palmroth, M. (2014). Vlasiator: First global hybrid-vlasov simulations of earth's foreshock and magnetosheath. *Journal of Atmospheric and Solar-Terrestrial Physics*, 120:24–35.

[Vörös et al., 2017] Vörös, Z., Yordanova, E., Varsani, A., Genestreti, K., Khotyaintsev, Y. V., Li, W., Graham, D. B., Norgren, C., Nakamura, R., Narita, Y., et al. (2017). Mms observation of magnetic reconnection in the turbulent magnetosheath. *Journal of Geophysical Research: Space Physics*, 122(11):11–442.

[Vuorinen et al., 2019] Vuorinen, L., Hietala, H., and Plaschke, F. (2019). Jets in the magnetosheath: Imf control of where they occur. In *Annales geophysicae*, volume 37, pages 689–697. Copernicus GmbH.

[Vuorinen et al., 2021] Vuorinen, L., Hietala, H., Plaschke, F., and LaMoury, A. T. (2021). Magnetic field in magnetosheath jets: A statistical study of bz near the magnetopause. *Journal of Geophysical Research: Space Physics*, 126(9):e2021JA029188.

[Vuorinen et al., 2022] Vuorinen, L., Vainio, R., Hietala, H., and Liu, T. Z. (2022). Monte carlo simulations of electron acceleration at bow waves driven by fast jets in the earth's magnetosheath. *The Astrophysical Journal*, 934(2):165.

[Wang et al., 2018] Wang, B., Nishimura, Y., Hietala, H., Lyons, L., Angelopoulos, V., Plaschke, F., Ebihara, Y., and Weatherwax, A. (2018). Impacts of magnetosheath high-speed jets on the magnetosphere and ionosphere measured by optical imaging and satellite observations. *Journal of Geophysical Research: Space Physics*, 123(6):4879–4894.

[Wang et al., 2022] Wang, B., Wang, Y., Liu, T. Z., and Angelopoulos, V. (2022). The geoeffectiveness of solar wind current sheets and its modulation by foreshock ions. *Geophysical Research Letters*, 49(12):e2022GL098918. e2022GL098918 2022GL098918.

[Wang et al., 2019] Wang, S., Chen, L.-J., Bessho, N., Hesse, M., Wilson III, L. B., Giles, B., Moore, T. E., Russell, C. T., Torbert, R. B., and Burch, J. L. (2019). Observational evidence of magnetic reconnection in the terrestrial bow shock transition region. *Geophysical Research Letters*, 46(2):562–570.

[Wilson III et al., 2013] Wilson III, L., Koval, A., Sibeck, D., Szabo, A., Cattell, C., Kasper, J., Maruca, B., Pulupa, M., Salem, C., and Wilber, M. (2013). Shocklets, slams, and field-aligned ion beams in the terrestrial foreshock. *Journal of Geophysical Research: Space Physics*, 118(3):957–966.

[Wilson III, 2016] Wilson III, L. B. (2016). Low frequency waves at and upstream of collisionless shocks. *Low-frequency waves in space plasmas*, pages 269–291.

[Yamazaki et al., 2022] Yamazaki, R., Matsukiyo, S., Morita, T., Tanaka, S. J., Umeda, T., Aihara, K., Edamoto, M., Egashira, S., Hatsuyama, R., Higuchi, T., Hihara, T., Horie, Y., Hoshino, M., Ishii, A., Ishizaka, N., Itadani, Y., Izumi, T., Kambayashi, S., Kakuchi, S., Katsuki, N., Kawamura, R., Kawamura, Y., Kisaka, S., Kojima, T., Konuma, A., Kumar, R., Minami, T., Miyata, I., Moritaka, T., Murakami, Y., Nagashima, K., Nakagawa, Y., Nishimoto, T., Nishioka, Y., Ohira, Y., Ohnishi, N., Ota, M., Ozaki, N., Sano, T., Sakai, K., Sei, S., Shiota, J., Shoji, Y., Sugiyama, K., Suzuki, D., Takagi, M., Toda, H., Tomita, S., Tomiya, S., Yoneda, H., Takezaki, T., Tomita, K., Kuramitsu, Y., and Sakawa, Y. (2022). High-power laser experiment forming a supercritical collisionless shock in a magnetized uniform plasma at rest. *Phys. Rev. E*, 105:025203.

[Yao et al., 2021] Yao, W., Fazzini, A., Chen, S., Burdonov, K., Antici, P., Béard, J., Bolaños, S., Ciardi, A., Diab, R., Filippov, E., et al. (2021). Laboratory evidence for proton energization by collisionless shock surfing. *Nature Physics*, 17(10):1177–1182.

[Yeakel et al., 2022] Yeakel, K. L., Vandegriff, J. D., Garton, T. M., Jackman, C. M., Clark, G., Vines, S. K., Smith, A. W., and Kollmann, P. (2022). Classification of cassini's orbit regions as magnetosphere, magnetosheath, and solar wind via machine learning. *Frontiers in Astronomy and Space Sciences*, 9.

[Yordanova et al., 2020] Yordanova, E., Vörös, Z., Raptis, S., and Karlsson, T. (2020). Current sheet statistics in the magnetosheath. *Frontiers in Astronomy and Space Sciences*, 7:2.

[Yordanova et al., 2016] Yordanova, E., Vörös, Z., Varsani, A., Graham, D. B., Norgren, C., Khotyaintsev, Y. V., Vaivads, A., Eriksson, E., Nakamura, R.,

Lindqvist, P.-A., et al. (2016). Electron scale structures and magnetic reconnection signatures in the turbulent magnetosheath. *Geophysical Research Letters*, 43(12):5969–5978.

[Zhang et al., 2022] Zhang, H., Zong, Q., Connor, H., Delamere, P., Facskó, G., Han, D., Hasegawa, H., Kallio, E., Kis, Á., Le, G., et al. (2022). Dayside transient phenomena and their impact on the magnetosphere and ionosphere. *Space Science Reviews*, 218(5):1–146.

[Zhelavskaya et al., 2021] Zhelavskaya, I. S., Aseev, N. A., and Shprits, Y. (2021). A combined neural network-and physics-based approach for modeling plasmasphere dynamics. *Journal of Geophysical Research: Space Physics*, 126(3):e2020JA028077.